Copy 5
RM L51I25

NACA RM L51I25

NACA

RESEARCH MEMORANDUM

PRESSURE DISTRIBUTION AT LOW SPEED ON A $\frac{1}{4}$-SCALE BELL X-5 AIRPLANE MODEL

By William B. Kemp, Jr., and Albert G. Few, Jr.

Langley Aeronautical Laboratory
Langley Field, Va.

NATIONAL ADVISORY COMMITTEE
FOR AERONAUTICS

WASHINGTON

December 4, 1951

NATIONAL ADVISORY COMMITTEE FOR AERONAUTICS

RESEARCH MEMORANDUM

PRESSURE DISTRIBUTION AT LOW SPEED ON A $\frac{1}{4}$-SCALE BELL X-5 AIRPLANE MODEL

By William B. Kemp, Jr., and Albert G. Few, Jr.

SUMMARY

This paper contains the results of measurements at 20° and 60° wing sweep of the low-speed pressure distribution on the wing, wing slat, wing leading-edge fillet, and fuselage of a $\frac{1}{4}$-scale model of a preliminary Bell X-5 airplane design. The pressure-distribution measurements were made to obtain specific aerodynamic load information for application to the Bell X-5 airplane. Some of the results, however, are useful for application to swept-wing airplanes in general.

INTRODUCTION

An investigation of the low-speed pressure distribution on a $\frac{1}{4}$-scale model of a Bell X-5 airplane design has been conducted in the Langley 300 MPH 7- by 10-foot tunnel. The X-5 airplane is a proposed research airplane incorporating wings having a sweepback angle that can be varied continuously between 20° and 60°. Provision for longitudinal translation of the wing with respect to the fuselage is also made. Results of longitudinal and lateral stability and control investigations of the $\frac{1}{4}$-scale model are given in references 1 and 2, respectively.

The pressure-distribution investigation reported herein was directed toward obtaining specific aerodynamic load information for application to the Bell X-5 airplane. Measurements of pressure distribution were made at two stations on the right wing and slat, on the wing leading-edge fillet, and on the forward part of the fuselage with wing sweep angles of 20° and 60°. The wing and slat pressures were integrated to determine

the section characteristics at the two measurement stations. Fuselage pressure distributions were determined for several values of nose-inlet velocity ratio.

SYMBOLS

The system of axes employed for plotting slat pressure coefficients is given in figure 1. The symbols used in this paper are defined as follows:

P	pressure coefficient $\left(\frac{p_l - p}{q}\right)$
p_l	local static pressure, pounds per square foot
p	free-stream static pressure, pounds per square foot
q	dynamic pressure, pounds per square foot $\left(\frac{\rho V^2}{2}\right)$
ρ	mass density of air, slugs per cubic foot
V	free-stream velocity, feet per second
V_j	average velocity in jet duct, feet per second
V_j/V	nose-inlet velocity ratio
c	local wing chord, normal to 0.40 chord of unswept wing at all wing sweeps, feet
ψ	angle of yaw, positive when nose is to the right, degrees
α	angle of attack of thrust line, degrees
Λ	angle of sweepback of quarter-chord line of unswept wing, degrees
x	distance behind local wing leading edge measured in the wing chord plane on a line normal to the 0.40 chord of unswept wing at all wing sweeps
z	distance above wing chord plane

[redacted]

x_p distance behind local leading edge of wing fillet parallel to plane of symmetry

x_n distance behind local leading edge of nose inlet measured parallel to nose-inlet center line

δ_f flap deflection, degrees

c_n section normal-force coefficient $\left(-\oint Pd\frac{x}{c}\right)$

c_c section chord-force coefficient $\left(\oint Pd\frac{z}{c}\right)$

c_{m_s} slat section pitching-moment coefficient, referred to leading edge of local wing chord line $\left(\oint P\frac{x}{c}d\frac{x}{c}+\oint P\frac{z}{c}d\frac{z}{c}\right)$

Subscripts:

s slat

w wing in presence of extended slat

t wing and slat total

APPARATUS AND METHODS

Description of Model

The model used in this investigation was a $\frac{1}{4}$-scale model of a preliminary Bell X-5 design. Physical characteristics of the model are presented in figures 2 and 3, and photographs of the model on the support strut are given as figure 4. Figure 5 includes details of the flap and slat. The model was constructed of wood bonded to steel reinforcing members.

Figure 6 presents a general arrangement of the pressure orifices on the test model. The upper and lower surfaces of the right wing and slat had two spanwise locations of orifices in planes normal to the 0.40 chord of the unswept wing at all wing sweeps. The wing fillet had two spanwise stations of orifices in planes parallel to the plane of symmetry at all wing sweeps. The side, lower, and upper surfaces of the fuselage had orifices in rows parallel to the thrust center line extending from beyond

[redacted]

the wing trailing edge over the nose and into the jet duct inlet. An orifice was located on the fuselage side 22.84 inches rearward of the nose and 2.31 inches above the thrust center line to investigate a probable location for the installation of an accessory air vent.

The wings were pivoted about axes normal to the wing chord planes. The wing incidence measured in a streamwise direction was zero for all wing sweep angles. At all wing sweep angles the wing was located so that the quarter chord of the mean aerodynamic chord fell at a fixed fuselage station.

The jet engine ducting was simulated on the model by the use of an open tube having a constant area from the nose to the jet axis.

Tests

The tests were conducted in the Langley 300 MPH 7- by 10-foot tunnel at a dynamic pressure of 34.15 pounds per square foot which for average test conditions corresponds to a Mach number of 0.152 and a Reynolds number of 2×10^6 based on the mean aerodynamic chord of the wing at 50° sweep.

During the tests, a cone extending into the jet exit (fig. 6) was used to control the air-flow quantity through the jet duct. To determine inlet velocity ratios a survey rake was installed inside the jet duct near the exit. The rake consisted of a series of total-pressure tubes extending over the entire diameter of the jet duct, and a static tube mounted on the center line of the jet duct.

With the model at a given angle of attack, a record was taken of the pressures at the orifices by photographing the multiple-tube manometer to which the orifices were connected.

Corrections

The angle of attack has been corrected for jet-boundary effects computed on the basis of unswept wings by the method of reference 3. Calculations have shown that the effects of sweep on this correction are negligible. All pressure coefficients have been corrected for blocking by the model and its wake by the methods of reference 4. Tunnel air-flow misalinement has been accounted for in the computation of the test data.

[redacted]

RESULTS AND DISCUSSION

Presentation of Results

The result of the pressure-distribution measurements made on various parts of the model are presented in the figures tabulated below:

The data presented are for zero flap deflection unless otherwise noted in the figures. In order to facilitate the determination of the normal and chordwise components of the slat load, the slat pressure coefficients are plotted separately against the x and z coordinates. The pressure measurements were made primarily to obtain information for structural design of the X-5 airplane. Considerable knowledge regarding the flow over the model can be gained, however, from the pressure diagrams presented.

[redacted]

Pressure Distribution on Wing and Slat

Slats retracted.- On the pressure-distribution diagrams of figure 7 for 60° sweep, a region of relatively constant negative pressure near the leading edge of the upper surface is observed at moderate and high angles of attack. This characteristic is indicative of leading-edge separation and is observed to be more extensive on the outboard station than on the inboard station. Pressure distributions on a series of wings having 60° swept leading edges reported in reference 5 showed characteristics very similar to those in figure 7. In reference 5, the pressure distributions were correlated with tuft and smoke observations to show that a leading-edge-separation vortex pattern existed, the core of the vortex being indicated by a negative pressure peak at the downstream end of the separation region. The corresponding negative pressure peaks are evident in figure 7 and indicate that the vortex core was located farther behind the leading edge at the outboard station than at the inboard station and moved rearward with increasing angle of attack. In general, separated flow existed ahead of the vortex core.

The pressure distributions for 20° sweep (fig. 16) indicate that the leading-edge separation vortex which was evident at 60° sweep did not occur when the sweep angle was reduced to 20°. At the higher angles of attack, the data of figure 16 show much more negative pressure peaks on the leading edge at the inboard station than at the outboard station. This is apparently the result of a localized flow separation along the leading edge of the outboard part of the wing.

Effects of slats.- The pressure distributions for 60° sweep with slats extended (figs. 10 and 11) do not show the pronounced effects of the leading-edge separation vortex which were observed with slats retracted at this sweep angle. At the highest angles of attack, the rapid pressure recovery over the rear part of the wing chord at the inboard station, and the flat pressure distribution indicating flow separation at the outboard station may be indicative of a vortex type of flow but the extensive leading-edge separation from the wing was apparently prevented by extension of the slat. Separation did occur, however, from the upper surface of the slat at angles of attack greater than 8.61°.

At 20° sweep, pressure-distribution measurements with slats extended were made at higher angles of attack than with slats retracted because of the action of the slats in delaying stalling of the wing. The slat pressure distributions of figure 20 indicate that the flow on the slat upper surface did not reach the state of complete separation which was observed at 60° sweep.

Effects of flap deflection.- Pressure distributions on the wing and slat at 20° sweep with the partial-span split flaps deflected 50° are presented in figures 25 and 26. It should be noted that the outboard row

[redacted]

of pressure orifices was located very near the outboard tip of the flap and the inboard row was located well within the flap span. Comparison of these results with those of figures 19 and 20 for zero flap deflection shows that deflecting the flap produced an increase in the lifting pressures over the entire wing, particularly in the vicinity of the flap, and also increased appreciably the lifting pressures on the slat.

Effects of yaw.- The effects on the wing pressure distribution of yawing the model with 60° sweep and slats retracted are indicated in figures 8 and 9. Inasmuch as pressure measurements were made on only the right wing, measurements at positive yaw angles yield results for the trailing wing, and conversely, measurements at negative yaw angles provide pressure distributions on the leading wing. At angles of attack near 0° (fig. 8), the effect of yaw was to increase the magnitude of the pressure coefficients on the leading wing and decrease those on the trailing wing. This effect is attributed to the change with yaw angle of the velocity components normal to the leading edge. At 23.52° angle of attack (fig. 9), yawing the model had a pronounced effect on the strength and location of the leading-edge separation vortex. On the leading wing (negative yaw) the vortex was shifted rearward so that flow separation over the entire wing chord was observed at the outboard station. On the trailing wing, the vortex moved toward the leading edge and the pressure recovery downstream from the vortex center became much more pronounced than that observed at zero yaw. With slats extended, the effects on the wing and slat pressure distributions of yawing the model, shown in figures 12 to 15, were considerably less noticeable than those observed with slats retracted.

At 20° sweep with slats retracted, the major effect of yaw angle (figs. 17 and 18) was to increase the magnitude of the peak negative pressure on the leading edge of the leading-wing and reduce it on the trailing wing. This effect is probably associated with an increase in the extent of leading-edge separation on the trailing wing and a decrease on the leading wing. With slats extended at 20° sweep (figs. 21 to 24) yawing the model produced only minor changes in the wing and slat pressure distributions.

Wing fillets.- A comparison of the fillet pressure distributions of figures 27(a) and 27(b) for 20° wing sweep shows that extending the slats had a negligible effect on the pressure distribution at the same angles of attack. Increasing the sweep angle to 60° allowed higher angles of attack to be obtained thus increasing the magnitude of the negative pressure peaks observed on the fillet leading edge. Flow separation from the fillet occurred only at the outboard station at the highest angles of attack with 60° sweep.

[redacted]

Pressure Distribution on Fuselage

The pressure distributions on the upper, side, and lower surfaces of the fuselage are presented in figures 28 to 45. Dashed lines indicate pressures inside the nose inlet. All fuselage pressures measured for the 60° wing sweep configuration were with slats retracted whereas those for 20° sweep were with slats extended to allow the attainment of higher angles of attack before wing stalling occurred. The effect of wing sweep on the fuselage pressure distributions was negligible except for the region on the fuselage side in the vicinity of the wing. (Compare figs. 28 to 30 with figs. 43 to 45.)

The effects of yawing the model are indicated in figures 31 to 36. Only minor changes in the pressure distributions on the top and bottom of the fuselage resulted from changing yaw angle. The fuselage side pressures, however, were much more sensitive to yaw angle; large negative pressure coefficients on the right side of the nose inlet resulted from a positive yaw angle of 5°.

The effects on the fuselage pressure distribution of reducing the inlet velocity ratio by reducing the jet exit area are illustrated by figures 37 to 42. As the inlet velocity ratio was reduced, the magnitude of the negative pressure peaks at the fuselage nose was increased and the pressures inside the nose inlet became more positive.

Aerodynamic Section Characteristics

Figure 46 presents the section normal-force coefficients of the wing with slats retracted for both 20° and 60° sweep. The section normal-force coefficients were essentially the same for the outboard and inboard stations except for the highest angles of attack at 60° sweep in which case the normal-force coefficients at the outboard station were considerably less than at the inboard station.

With slats extended (figs. 47 and 48) the individual contributions of the slat and the wing to the section normal-force coefficient are presented as well as the total section normal-force coefficient of the wing and slat. Section chord-force and pitching-moment coefficients of the slat are also presented. It should be noted that the slat section coefficients are based on the local wing chord. To obtain values based on the local slat chord, the normal-force and chord-force coefficients should be multiplied by 6.67 and the pitching-moment coefficients by 44.4.

With 60° sweep at low and moderate angles of attack, the normal-force coefficients at the outboard station on both the wing and slat were noticeably greater than at the inboard station. At high angles of attack, however, the normal-force coefficients at the outboard station fell below those at the inboard station, probably as a result of the more

[redacted]

severe flow separation previously noted at the outboard station. With 20° sweep, the normal-force coefficients at the outboard station were only slightly greater than those at the inboard station throughout the angle-of-attack range investigated. The effect of sweep angle on the division of load between the wing and slat is indicated in figure 49 in which the portion of the total section normal force carried by the slat is presented as a function of the total section normal-force coefficient. Application of the simple sweep theory, which considers the surface pressures to be independent of the free-stream velocity component parallel to the leading edge, would lead to the conclusion that the division of load between the slat and wing should be independent of sweep angle. Figure 49 shows, however, a considerable effect of sweep on the division of load. It is probable, therefore, that the concepts of the simple sweep theory would not be adequate for predicting the slat loads on swept wings from unswept slat load data.

The effects of angle of yaw on the aerodynamic section characteristics are presented in figures 50 to 52. At angles-of-attack near zero for all model configurations no significant changes in the section characteristics were produced by changing yaw angle. At higher angles of attack, the reduction in the velocity component normal to the leading edge of the right wing with increasing yaw angles would be expected to produce a reduction in the measured normal-force coefficients. With slats retracted (fig. 50) and 60° sweep, the expected reduction was observed at the inboard station. At the outboard station, however, the opposite trend was observed, probably as a result of the extensive separation over the outer portion of the right wing at negative yaw angles which was illustrated by figure 9. With slats extended at high angles of attack for both 20° and 60° sweep, the slat section characteristics were essentially independent of yaw angle. The wing section normal-force coefficient, however, was dependent on yaw angle for both sweep angles.

CONCLUDING REMARKS

Although the tests reported in this paper were conducted primarily to provide specific aerodynamic load information for application to the Bell X-5 airplane, certain observations of more general interest may be made from the pressure distributions obtained. With the wings swept 60° and with slats retracted, a leading-edge-separation vortex pattern existed over the wing at moderate and high angles of attack with resulting separation and loss of lift from the outboard portions of the wing. The strength and location of this vortex was appreciably affected by changing the angle of yaw. Extending the slats prevented separation from the wing leading edge but some of the characteristics of the vortex type of flow were still apparent with slats extended. At 20° sweep, no evidence of a leading-edge-separation vortex was observed with slats either extended

[redacted]

or retracted. With the slats extended at 20° sweep, the maximum aerodynamic load carried by the slat was appreciably increased by deflection of the trailing-edge flap. The effect of sweep on the division of load between the slat and wing was not in agreement with that predicted by using simple sweep theory.

Langley Aeronautical Laboratory
National Advisory Committee for Aeronautics
Langley Field, Va.

REFERENCES

1. Kemp, William B., Jr., Becht, Robert E., and Few, Albert G., Jr.: Stability and Control Characteristics at Low Speeds of a $\frac{1}{4}$-Scale Bell X-5 Airplane Model. Longitudinal Stability and Control. NACA RM L9K08, 1950.

2. Kemp, William B., Jr., Becht, Robert E.: Stability and Control Characteristics at Low Speed of a $\frac{1}{4}$-Scale Bell X-5 Airplane Model. Lateral and Directional Stability and Control. NACA RM L50C17a, 1950.

3. Gillis, Clarence L., Polhamus, Edward C., and Gray, Joseph L., Jr.: Charts for Determining Jet-Boundary Corrections for Complete Models in 7- by 10-Foot Closed Rectangular Wind Tunnels. NACA ARR L5G31, 1945.

4. Herriot, John G.: Blockage Corrections for Three-Dimensional-Flow Closed-Throat Wind Tunnels, with Consideration of the Effect of Compressibility. NACA Rep. 995, 1950. (Formerly NACA RM A7B28.)

5. May, Ralph W., Jr., and Hawes, John G.: Low-Speed Pressure-Distribution and Flow Investigation for a Large Pitch and Yaw Range of Three Low-Aspect-Ratio Pointed Wings Having Leading Edge Swept Back 60° and Biconvex Sections. NACA RM L9J07, 1949.

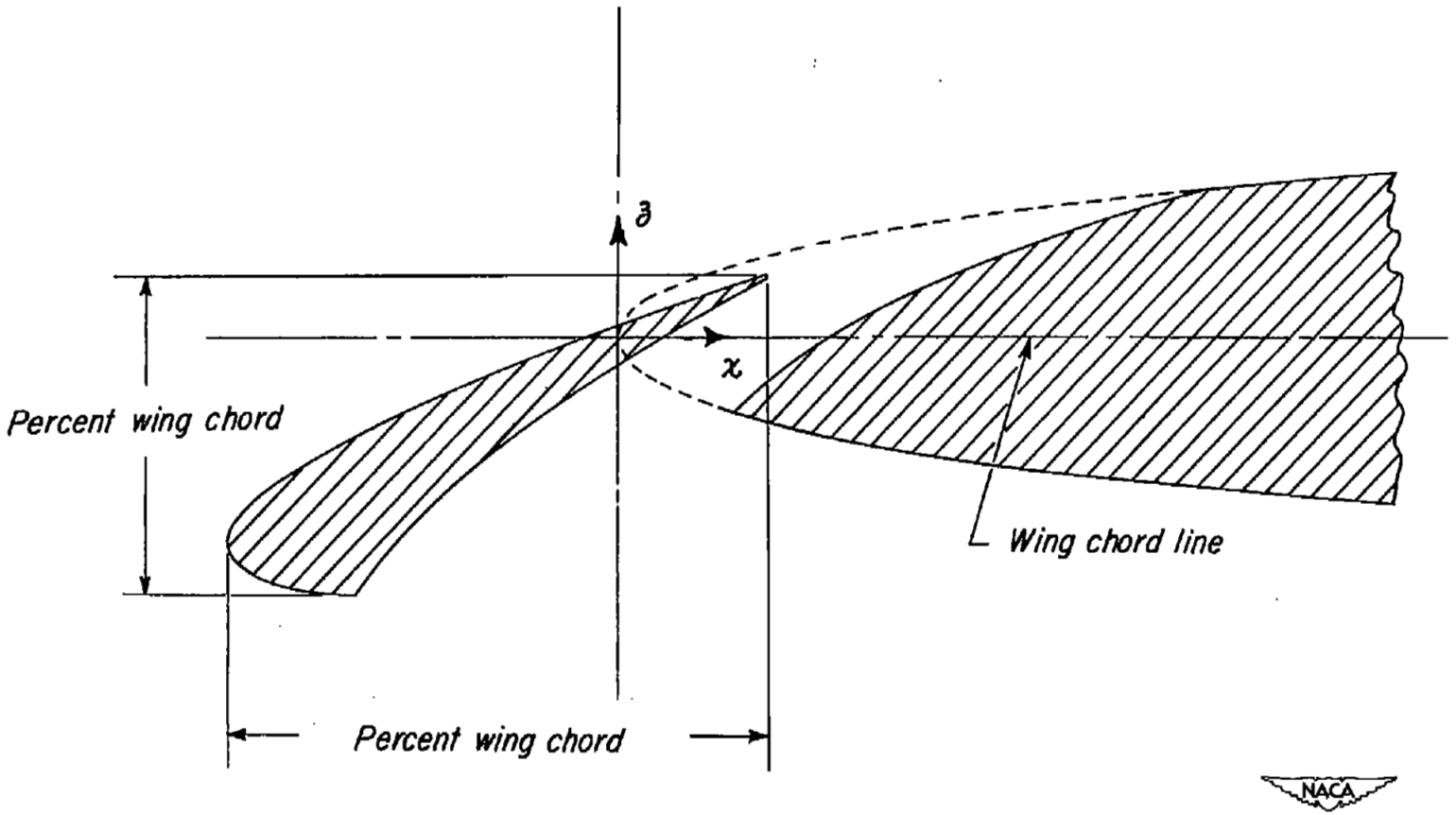

Figure 1.- System of axes for plotting slat pressures. Arrows from origin indicate positive axes.

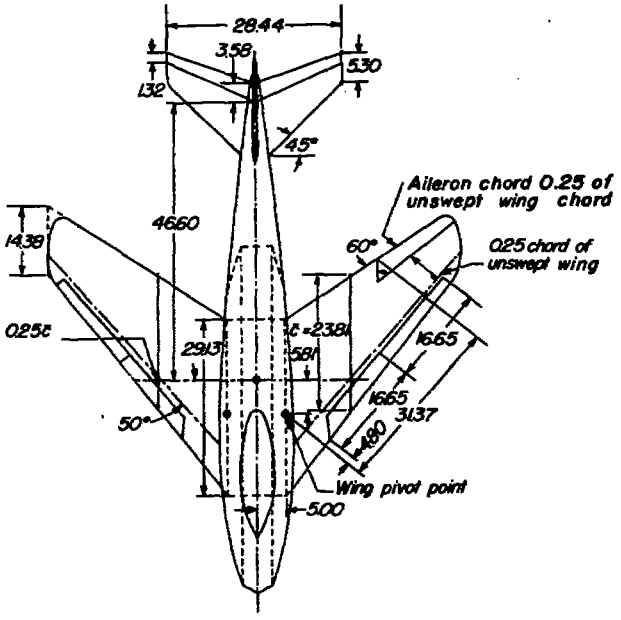

PHYSICAL CHARACTERISTICS

Wing:				
Sweep, deg	20	35	50	60
Area, sq ft	10.33	10.45	10.80	11.33
Aspect ratio	5.76	4.56	2.98	1.92
Span, ft	7.72	6.90	5.67	4.66
Mean aerodynamic chord, ft	1.396	1.579	1.985	2.535
Incidence, deg				0
Dihedral, deg				-2
Airfoil section perpendicular to 0.25c:				
Root				NACA $64_{(10)}$-010.3
Tip				NACA 64-008
Horizontal tail:				
Area, sq ft				1.94
Aspect ratio				2.89
Vertical tail:				
Area, sq ft				1.33
Aspect ratio				1.46

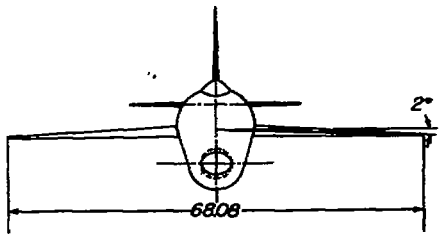

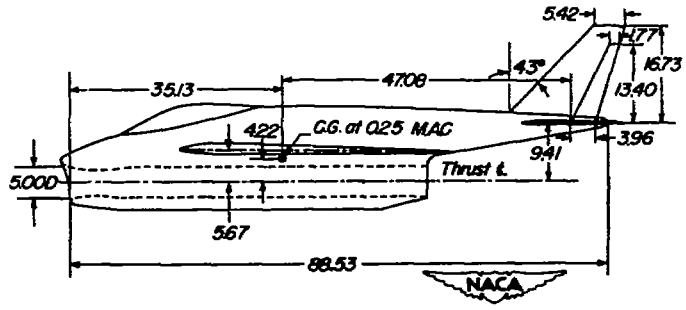

Figure 2.- General arrangement of test model.

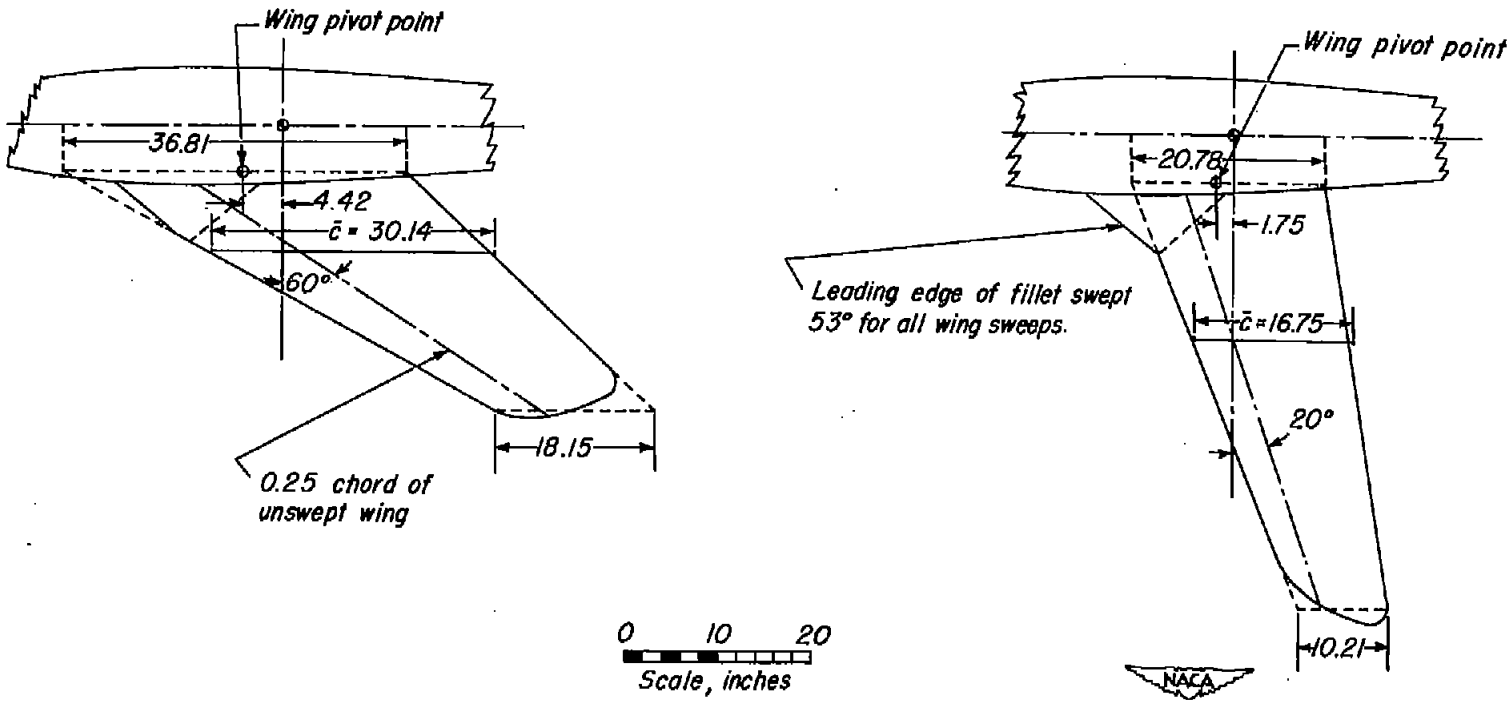

Figure 3.- Wing dimensions at 60° and 20° sweep.

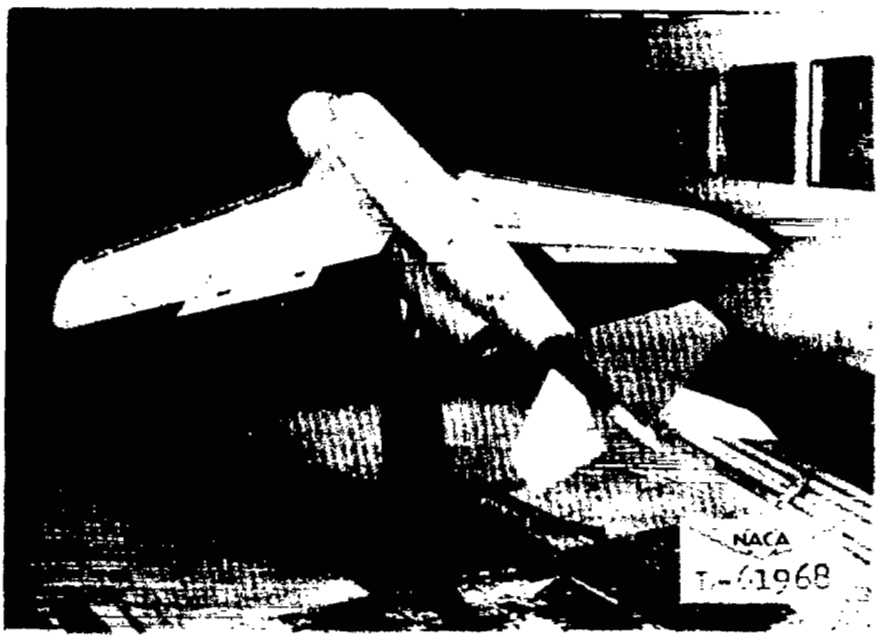

(a) Slat extended; $\delta_f = 50^\circ$; $\Lambda = 20^\circ$.

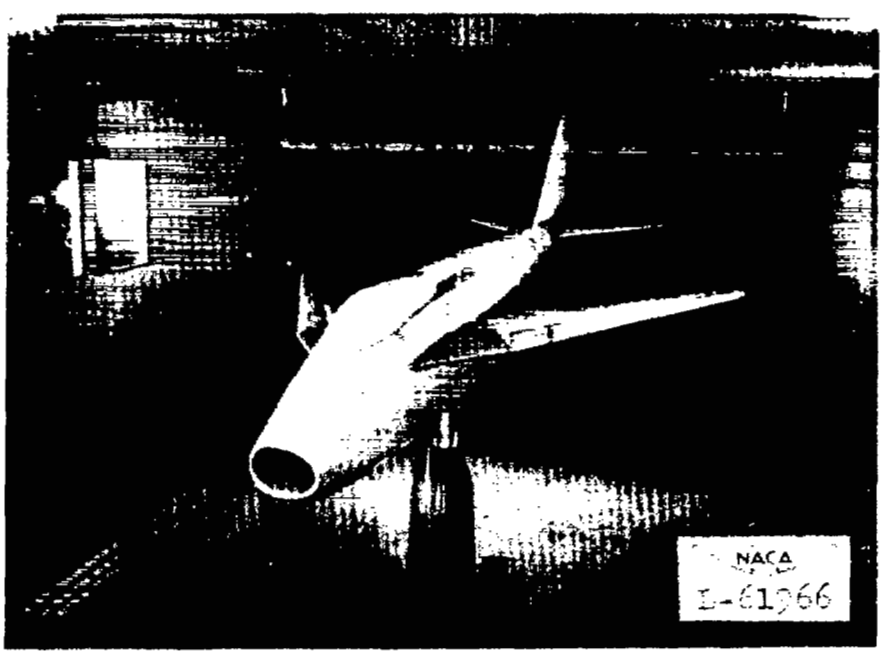

(b) Slats retracted; $\delta_f = 0^\circ$; $\Lambda = 60^\circ$.

Figure 4.- View of test model as mounted in tunnel.

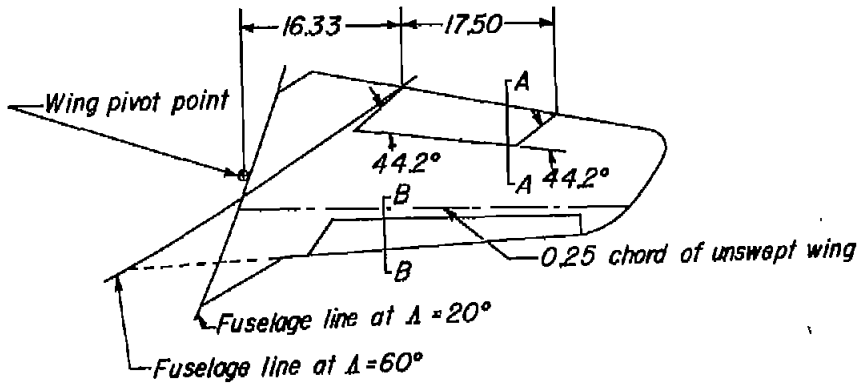

Split flap

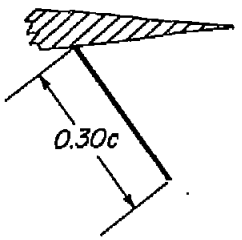

Section A-A

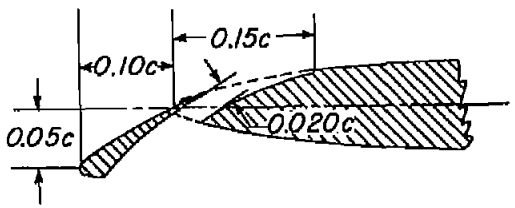

Section B-B

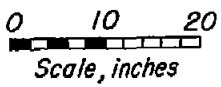

Figure 5.- Details of flap and slat.

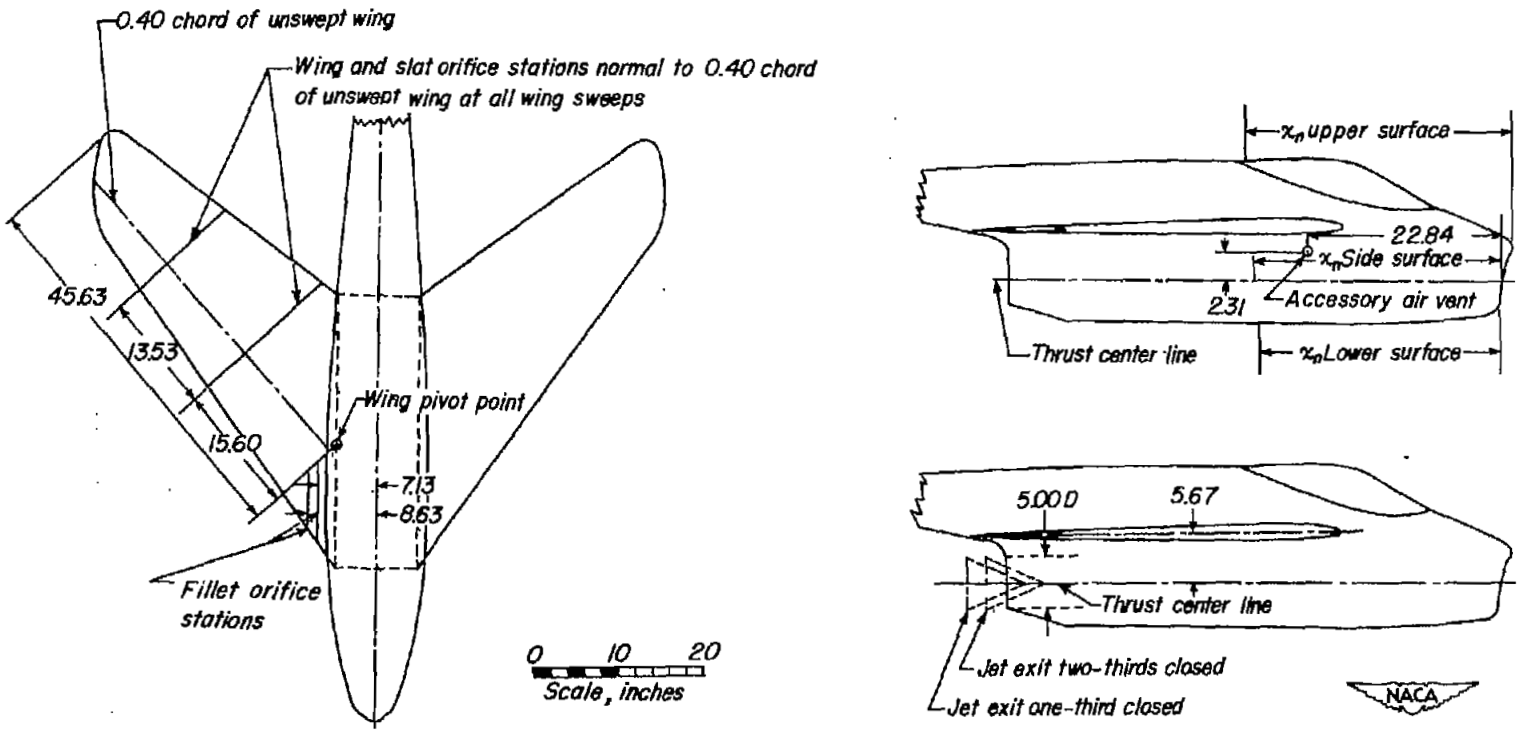

Figure 6.- General arrangement of pressure orifices on test model.

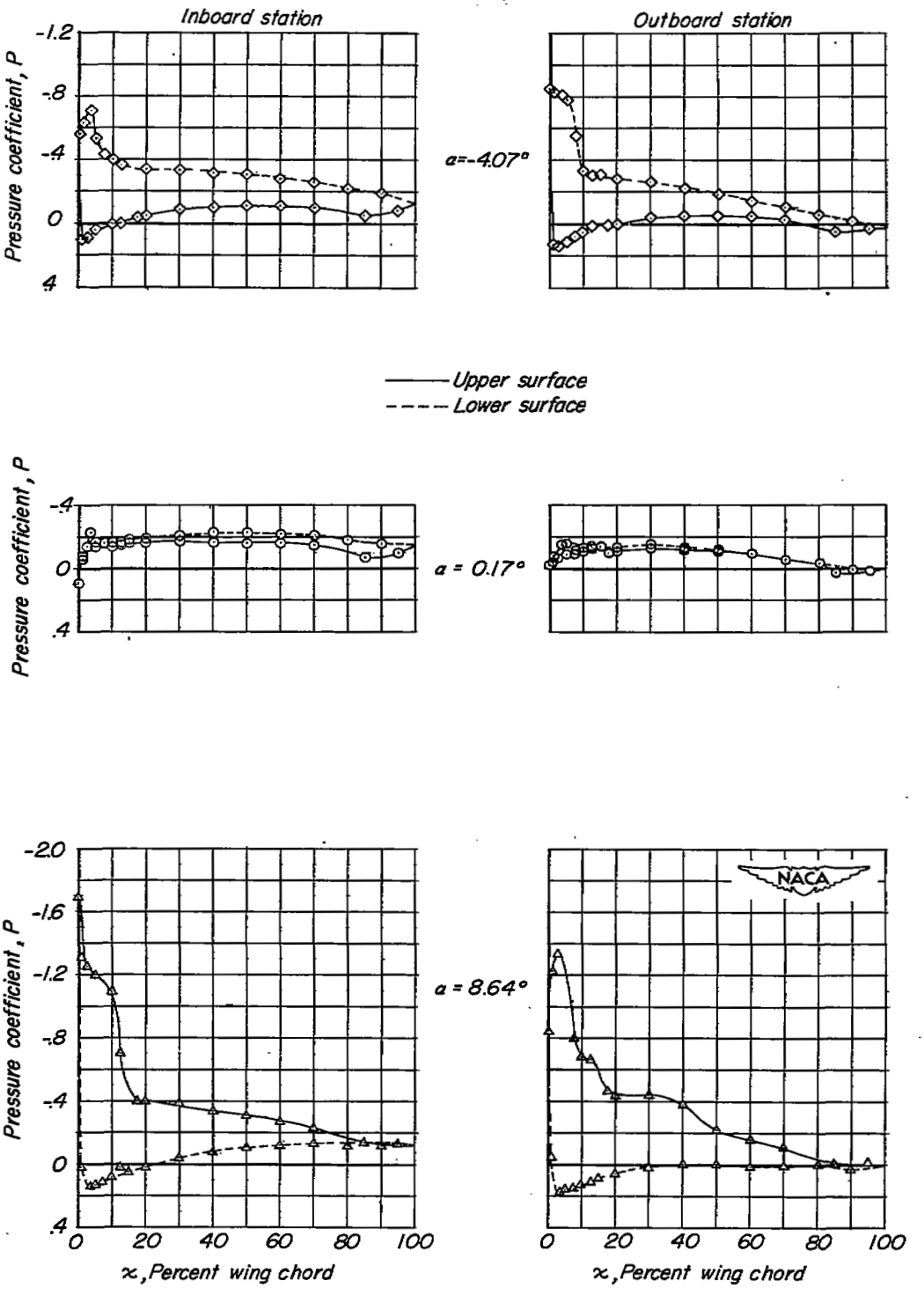

Figure 7.- Pressure distribution on the wing with slats retracted. $\Lambda = 60^{\circ}$; $\psi = 0^{\circ}$.

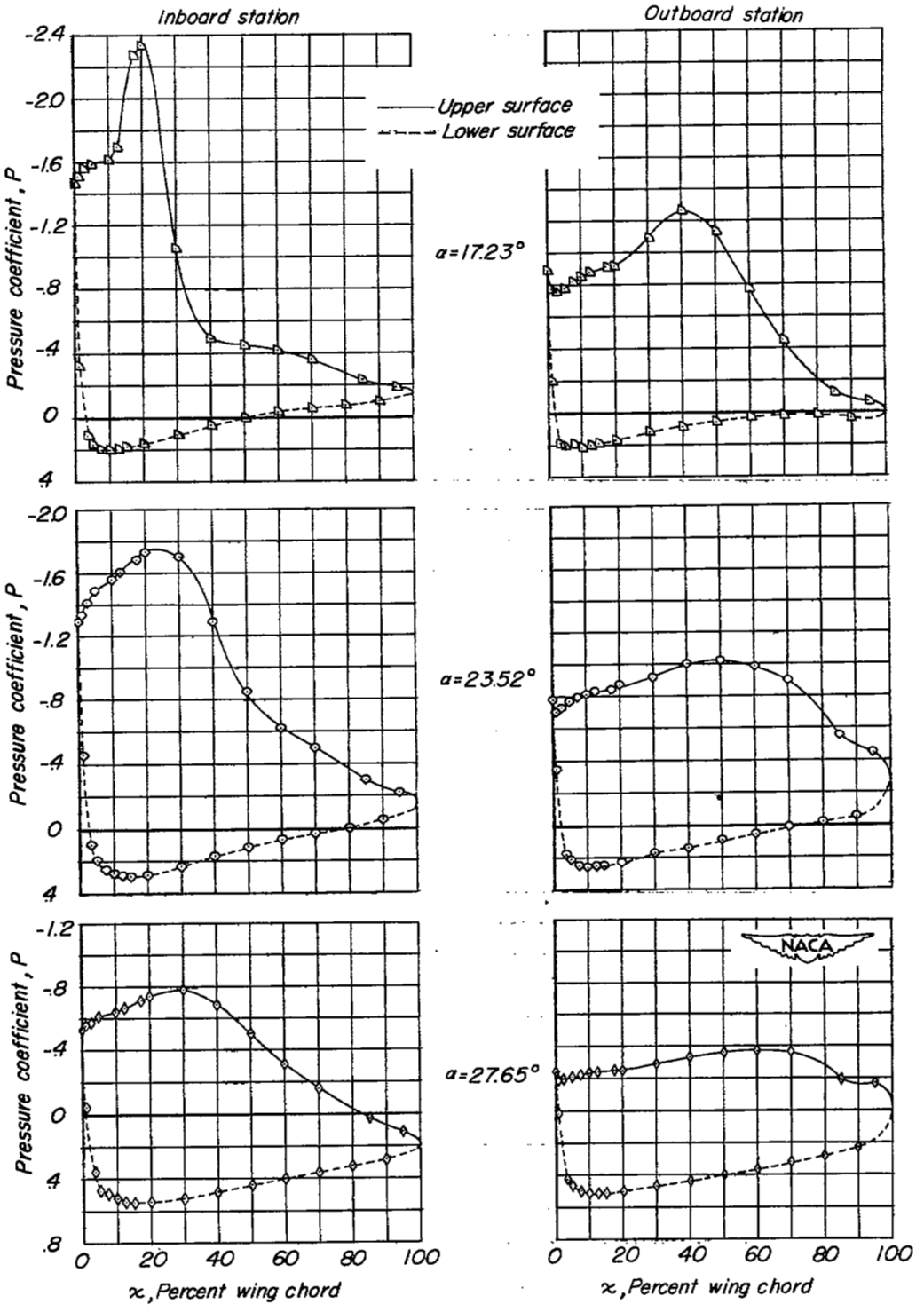

Figure 7.- Concluded.

[redacted]

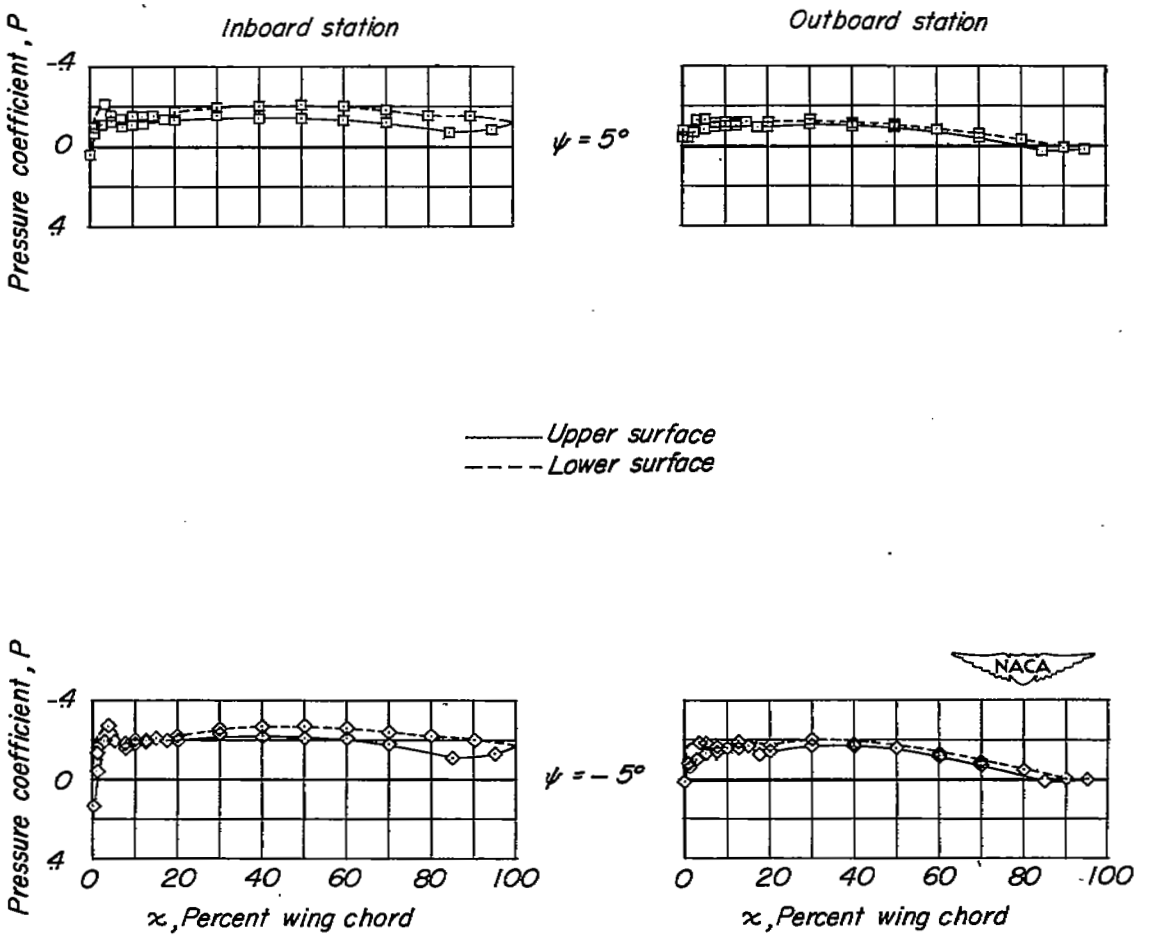

Figure 8.- Pressure distribution on the wing with slats retracted. $\Lambda = 60^\circ$; $\alpha = 0.17^\circ$.

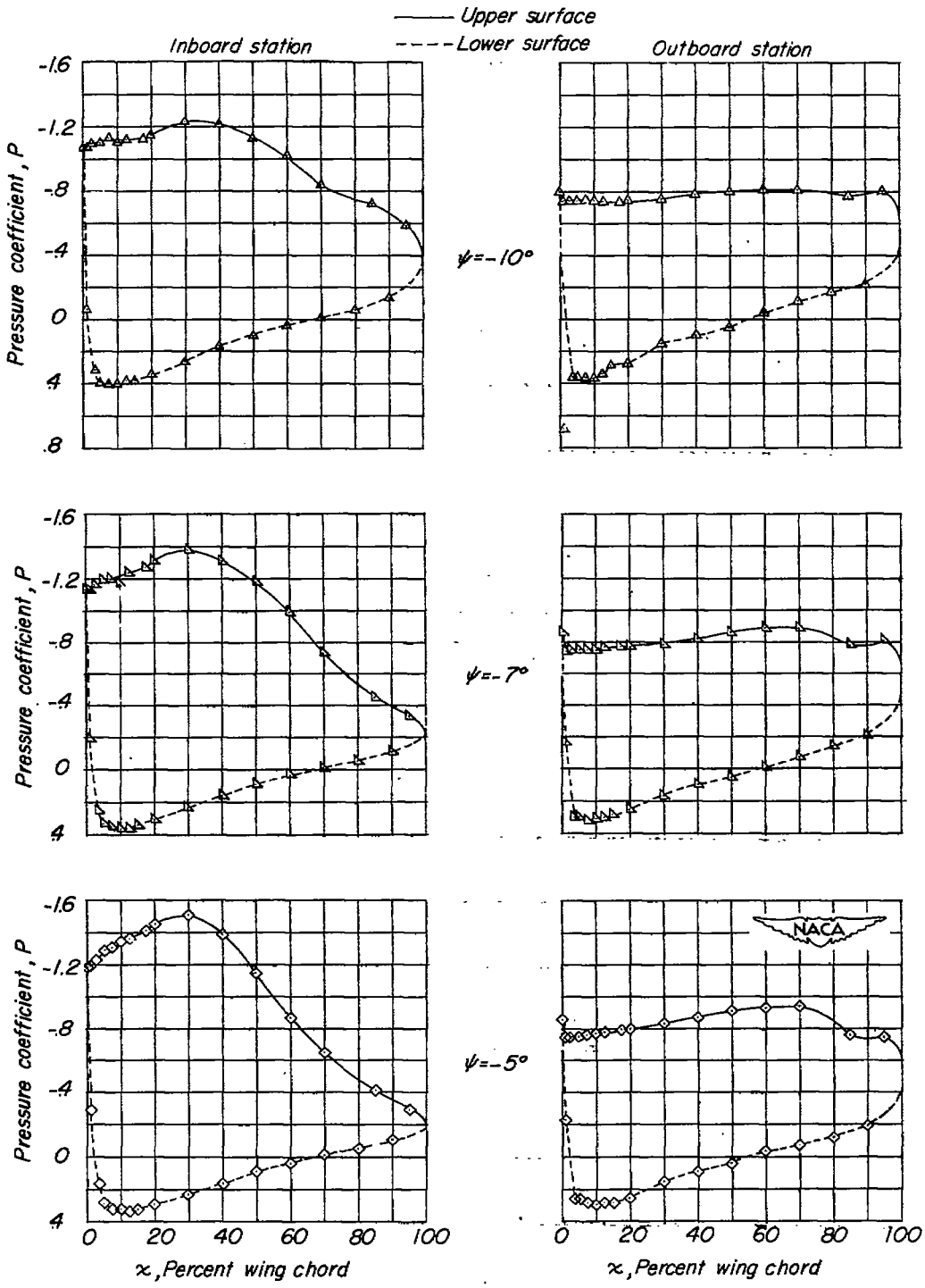

Figure 9.- Pressure distribution on the wing with slats retracted. $\Lambda = 60°$; $\alpha = 23.52°$.

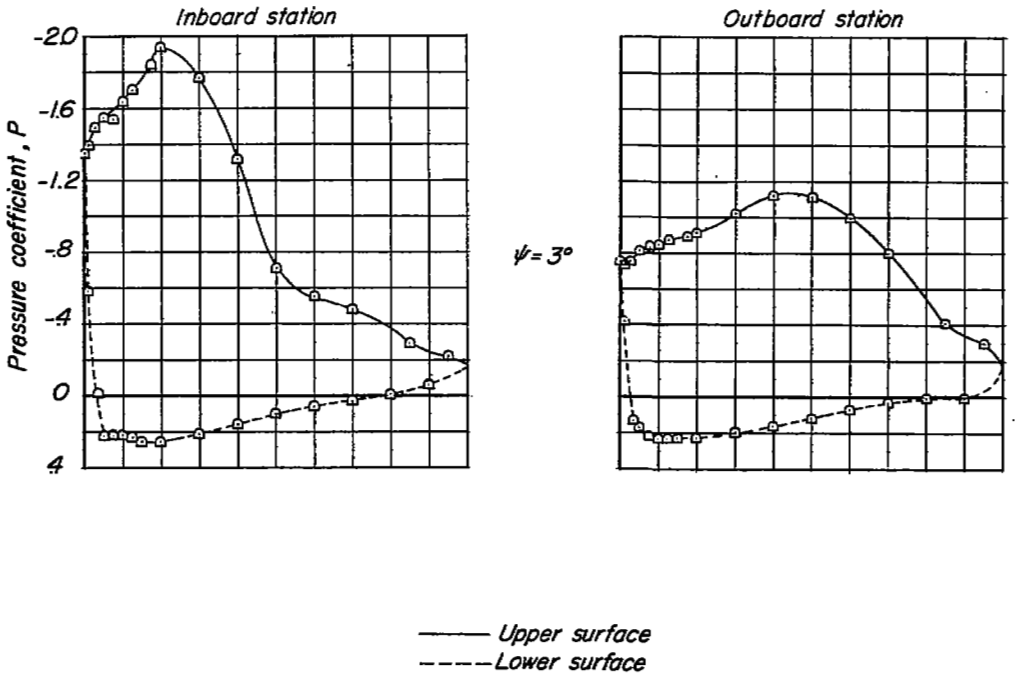

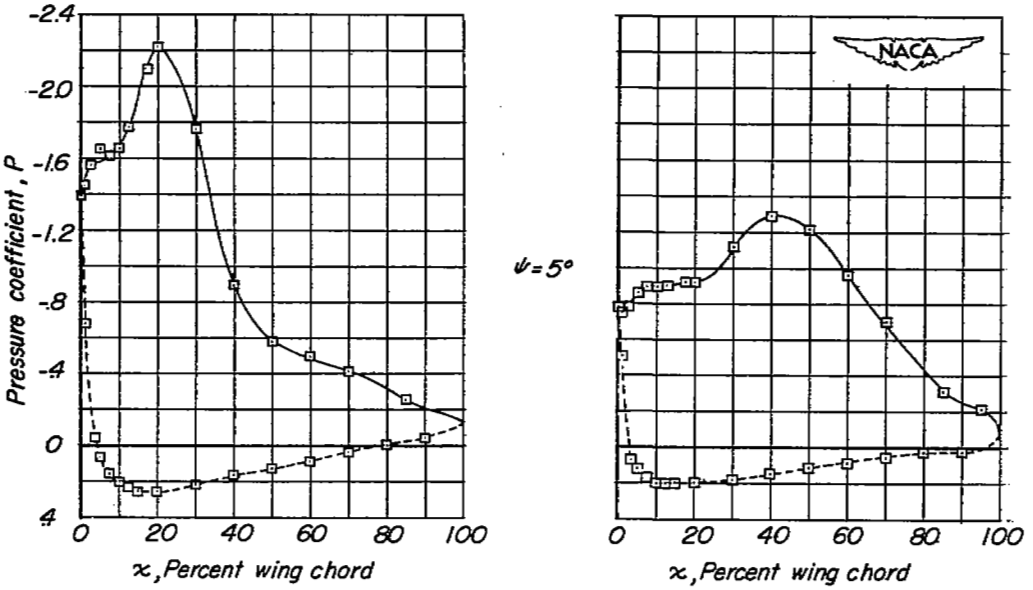

Figure 9.- Continued.

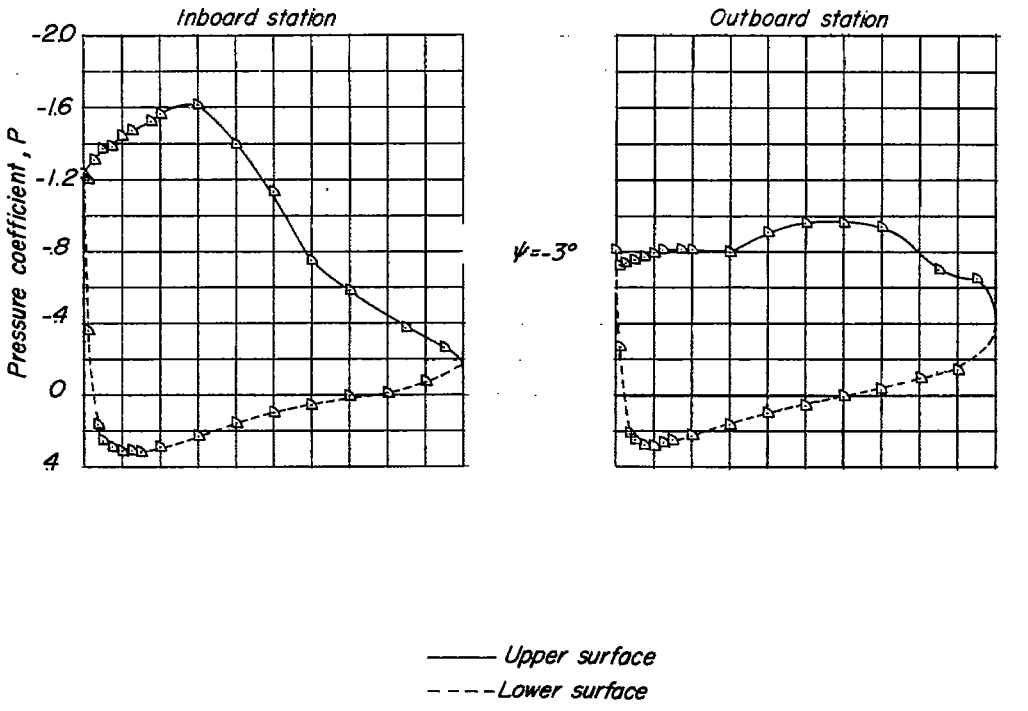

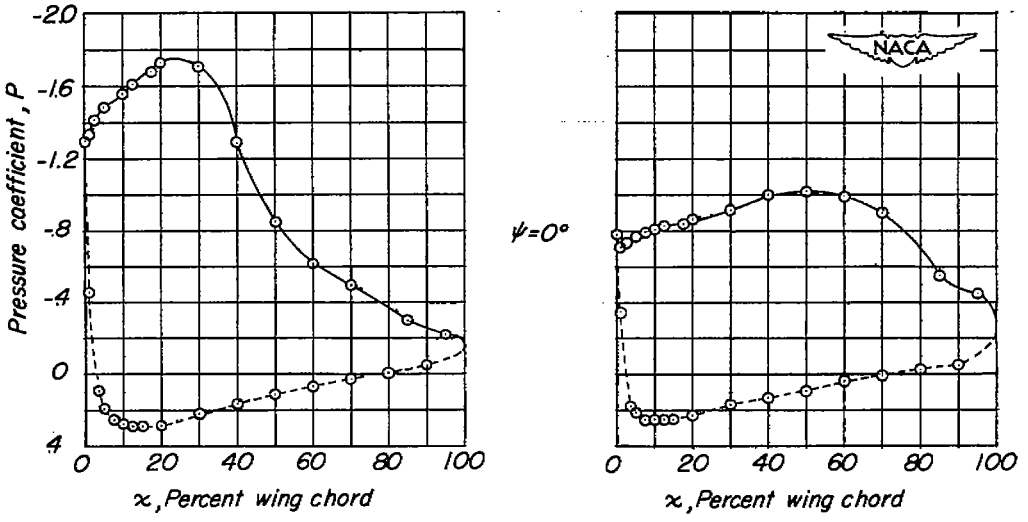

Figure 9.- Continued.

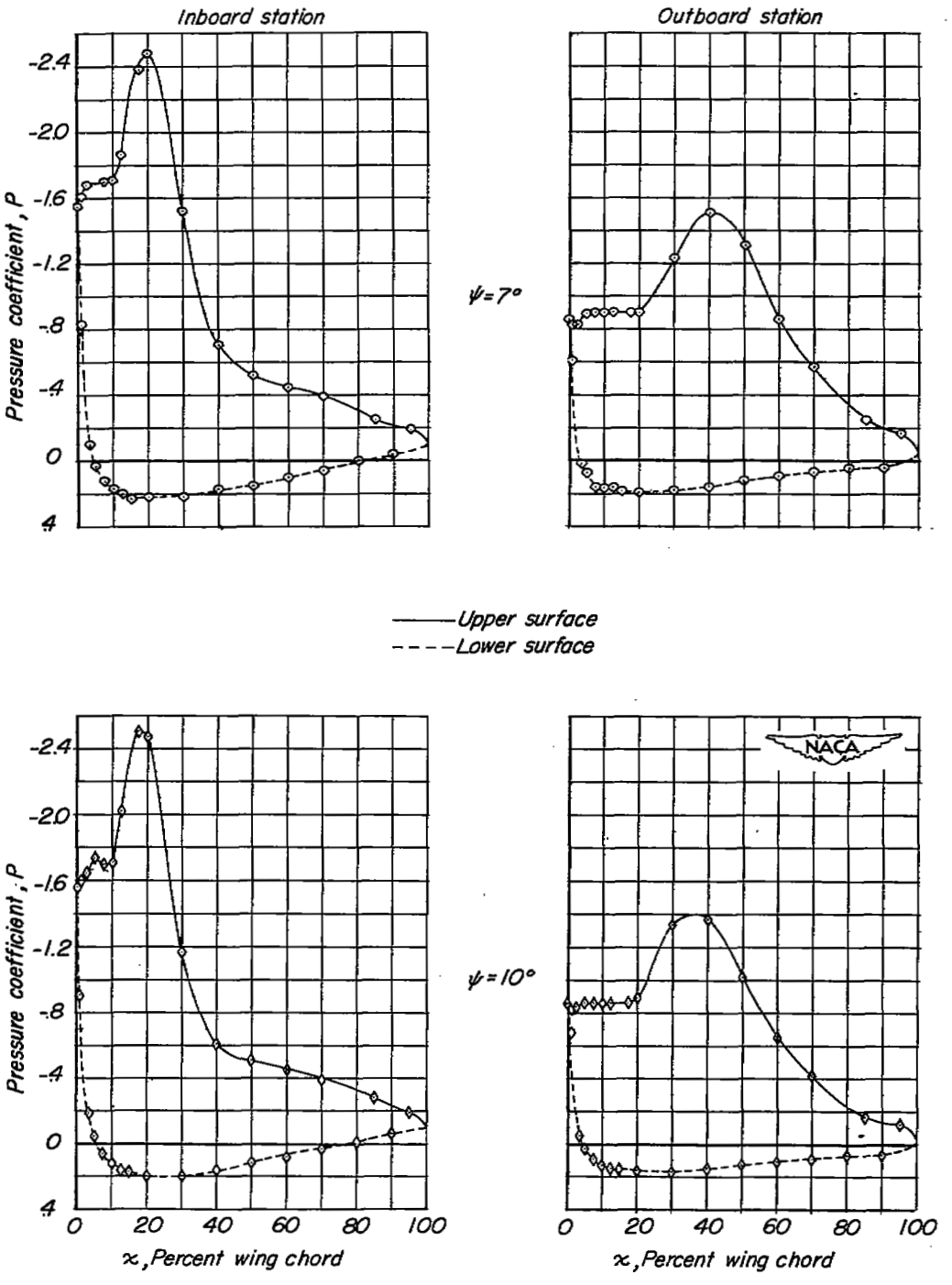

Figure 9.- Concluded.

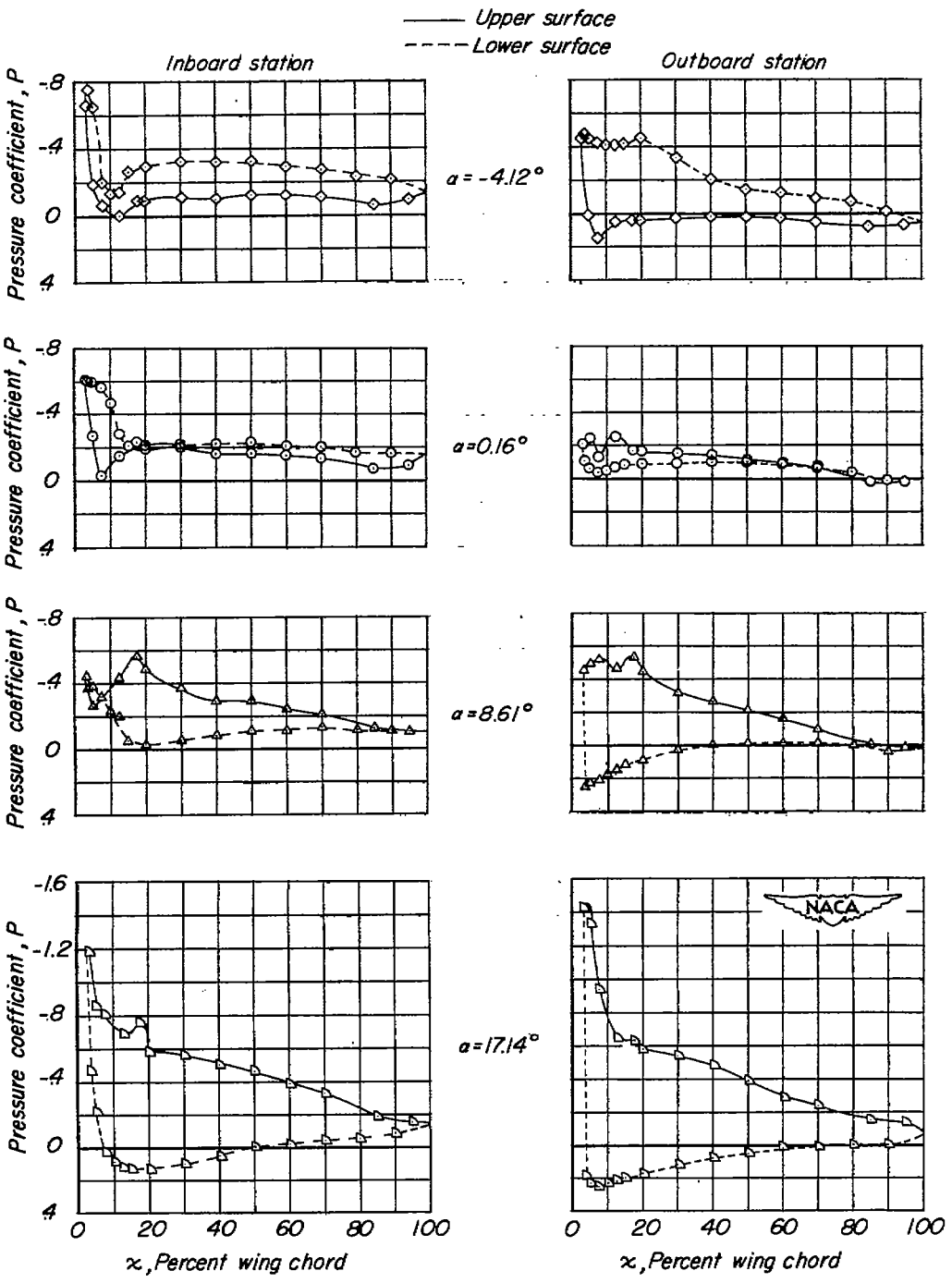

Figure 10.- Pressure distribution on the wing with slats extended. $\Lambda = 60°$; $\psi = 0°$.

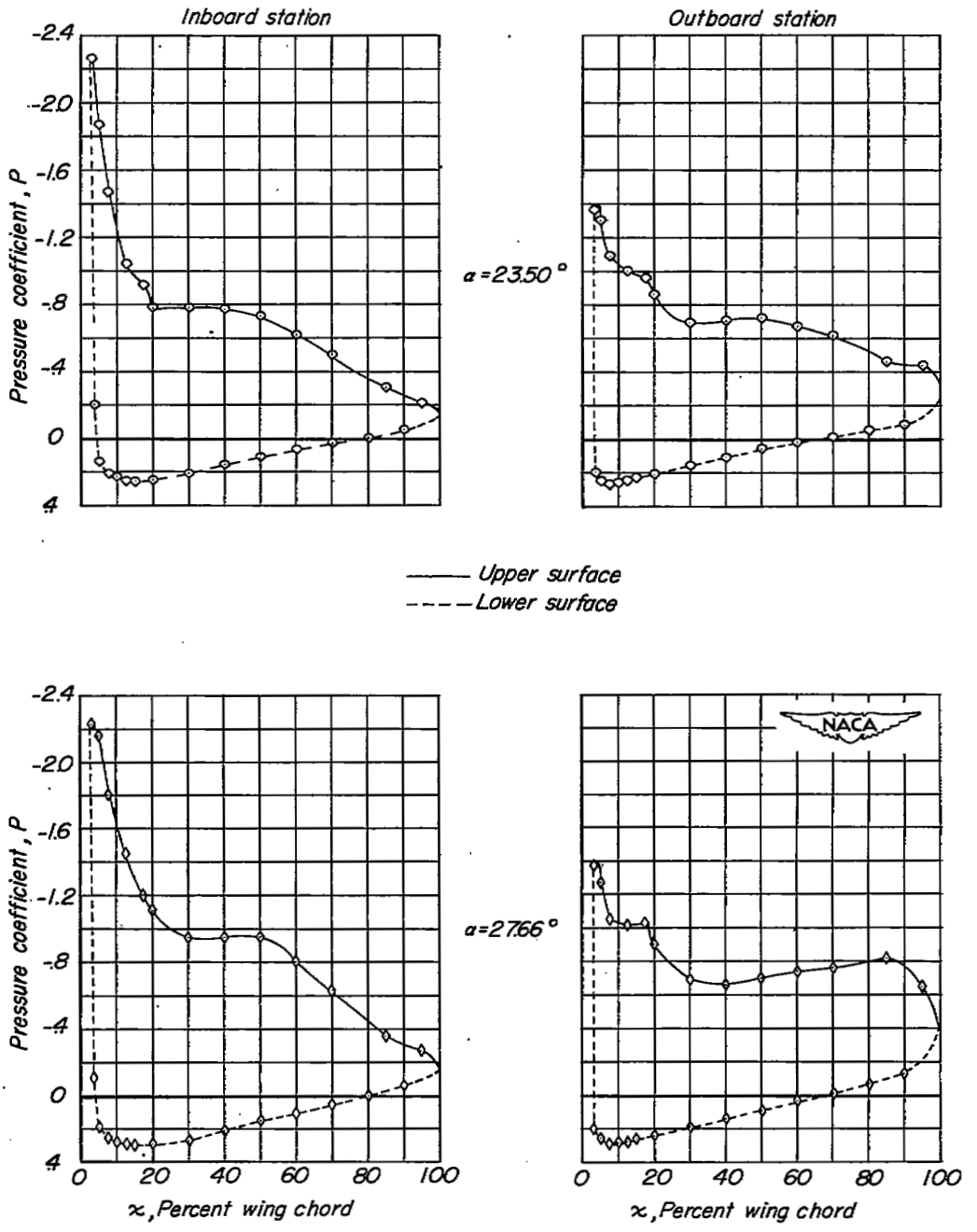

Figure 10.- Concluded.

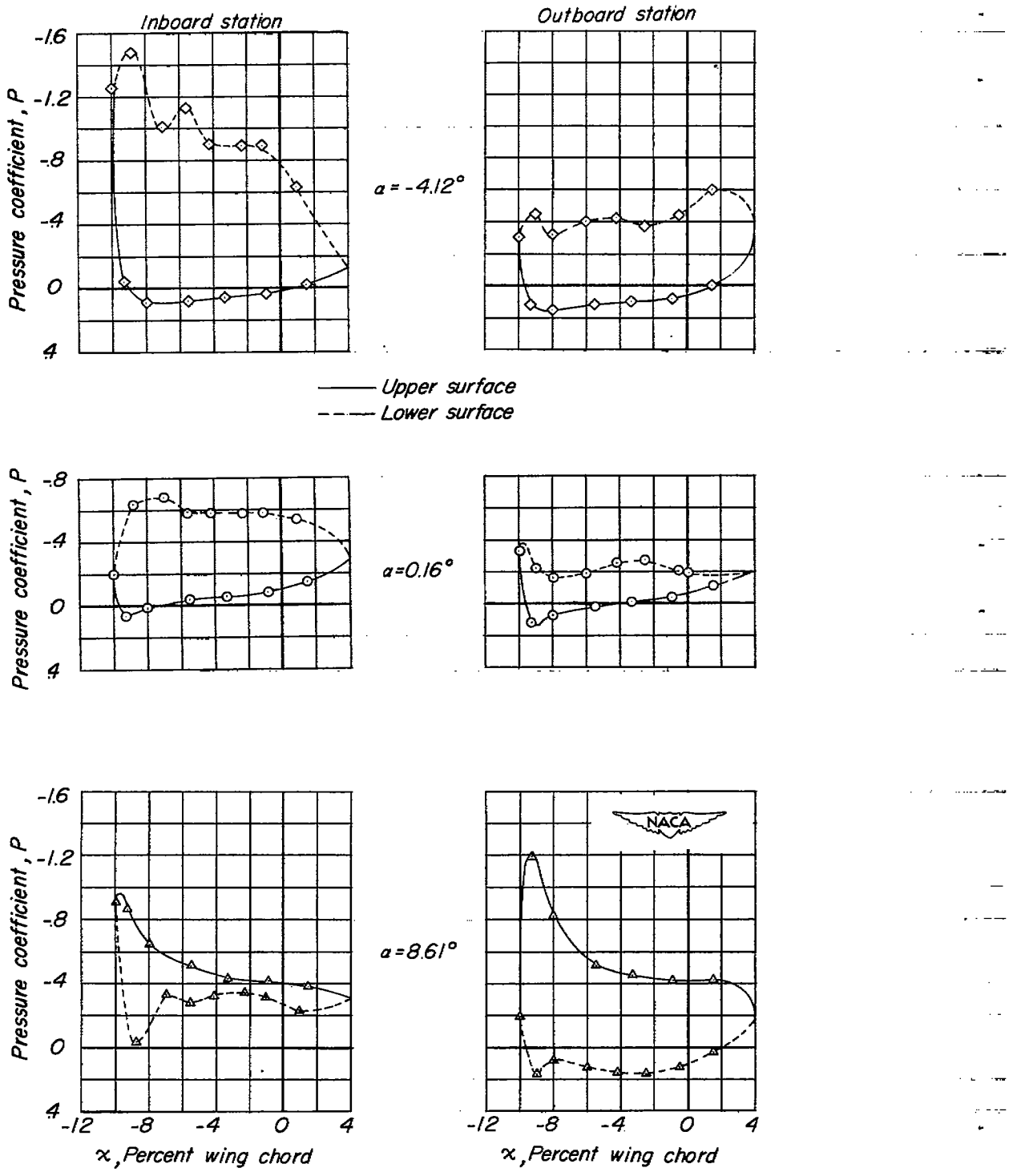

Figure 11.- Pressure distribution on the slat. $\Lambda = 60°$; $\psi = 0°$.

[redacted]

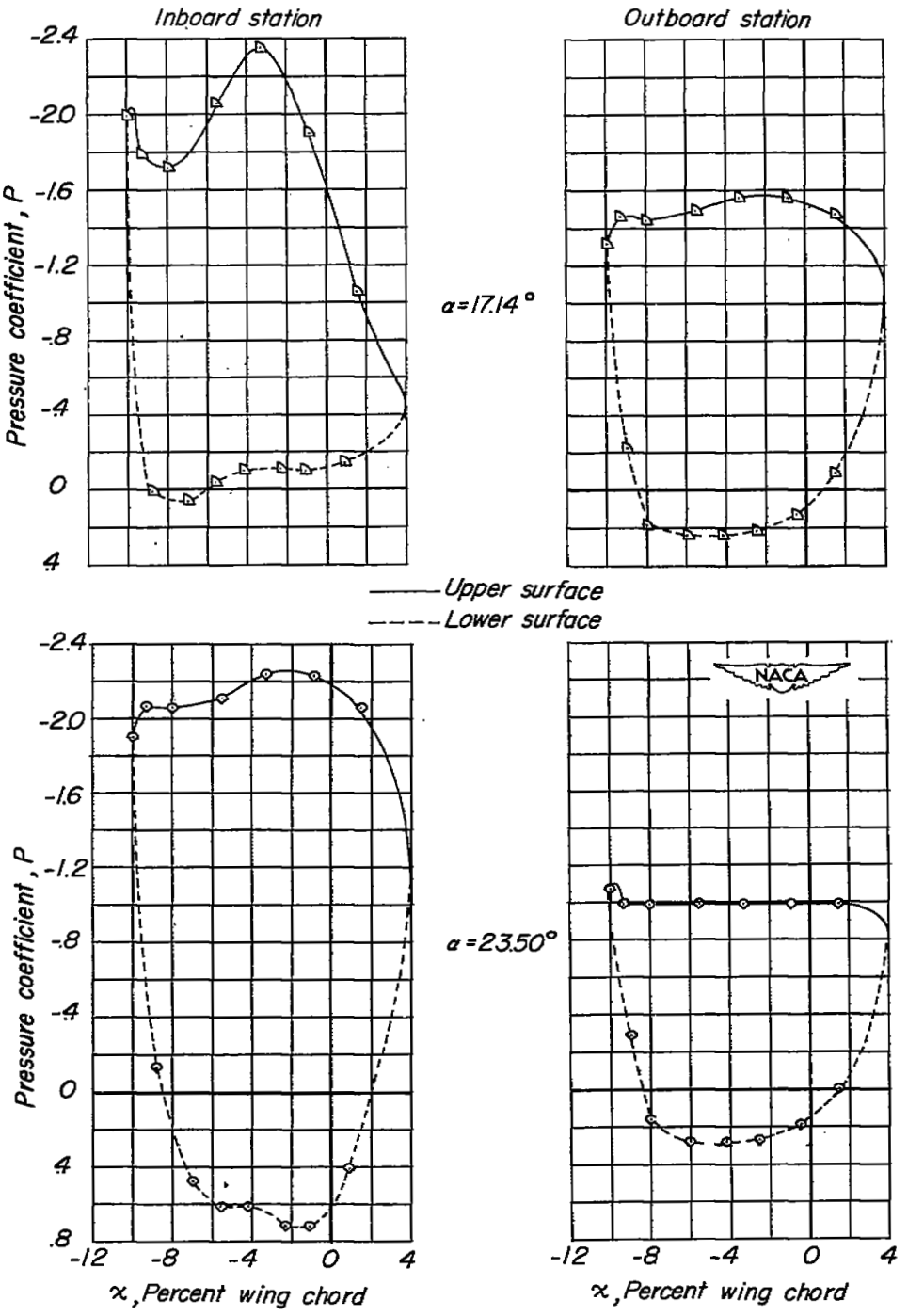

Figure 11.- Continued.

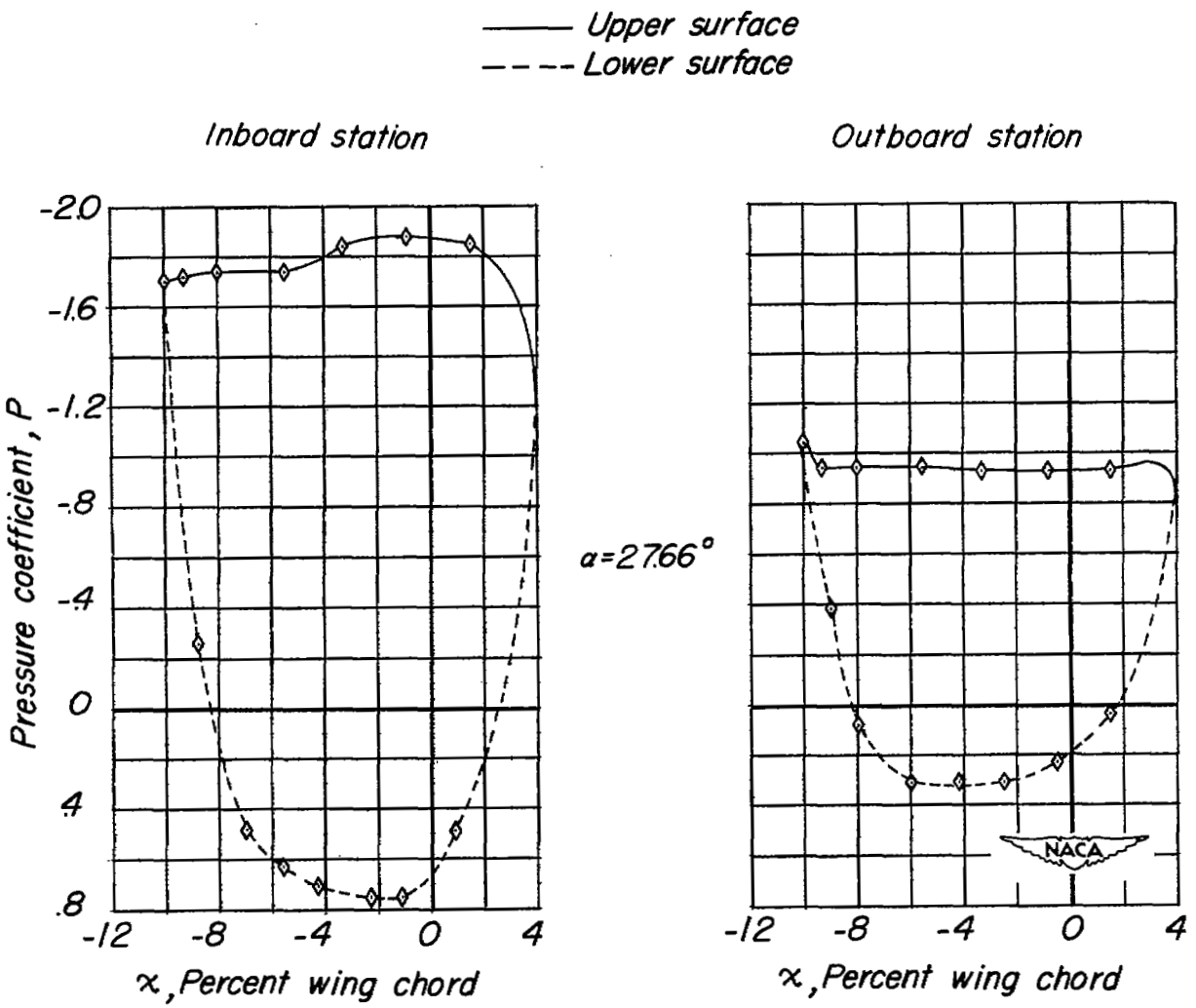

Figure 11.- Continued.

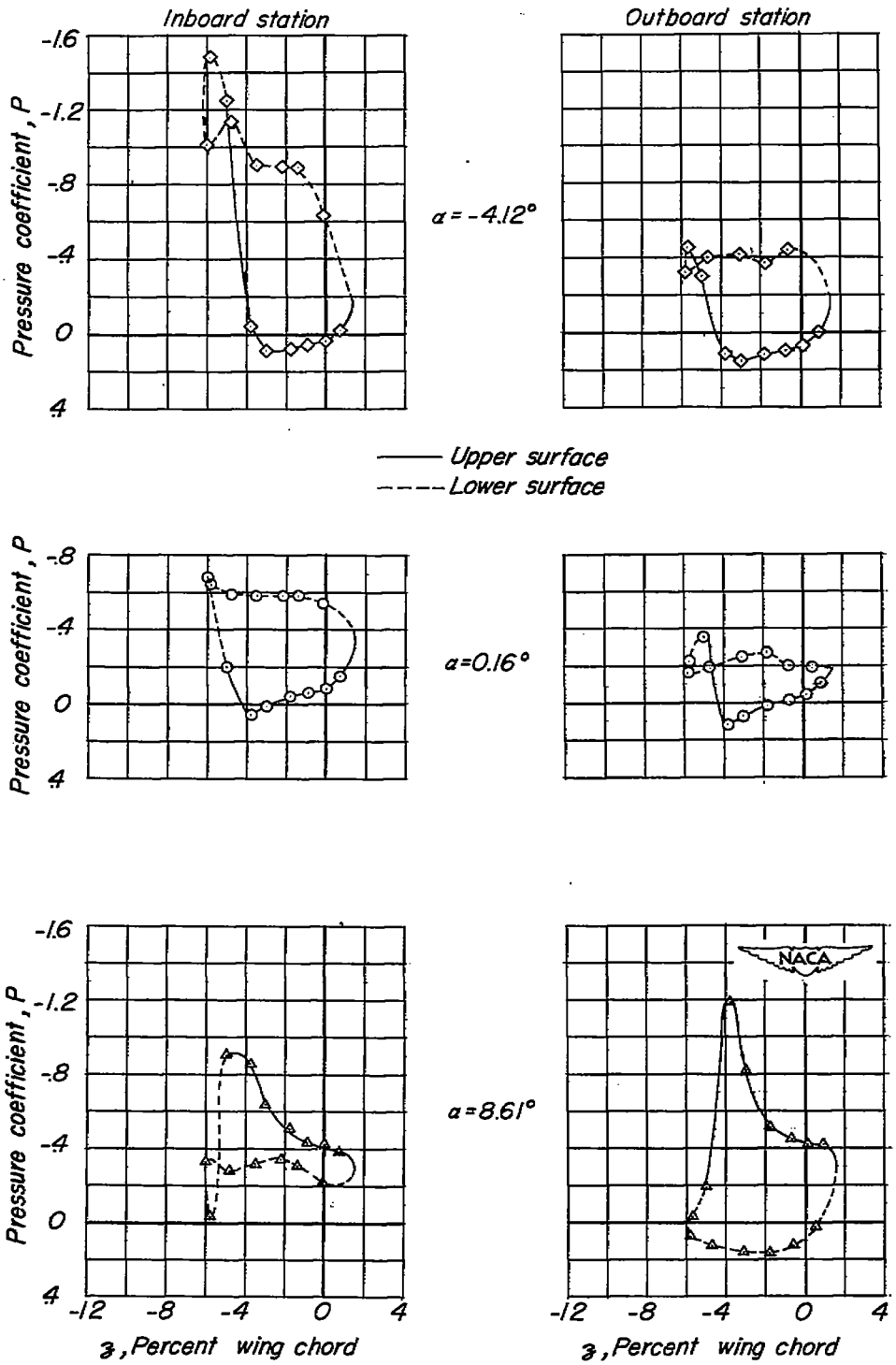

Figure 11.- Continued.

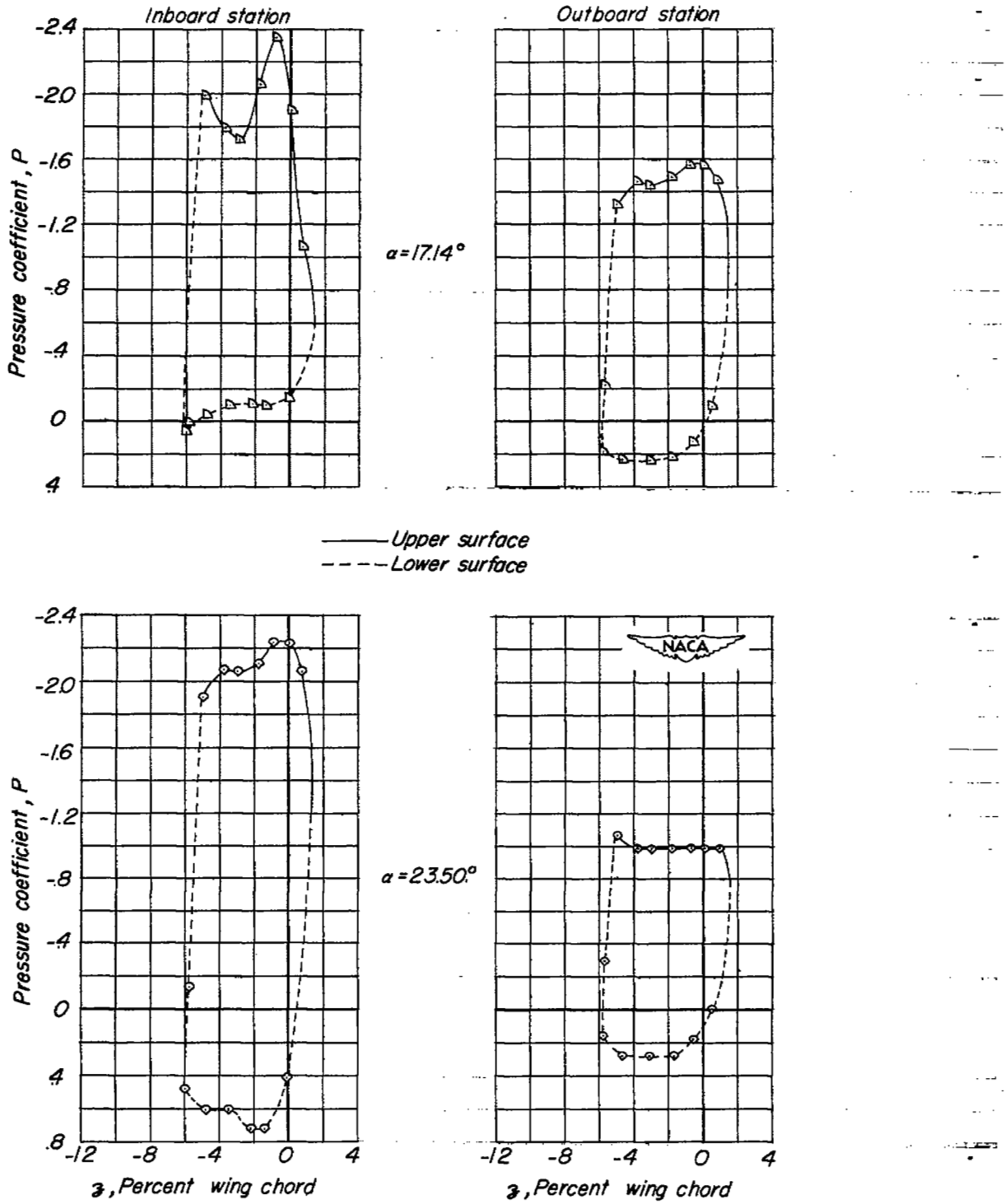

Figure 11.- Continued.

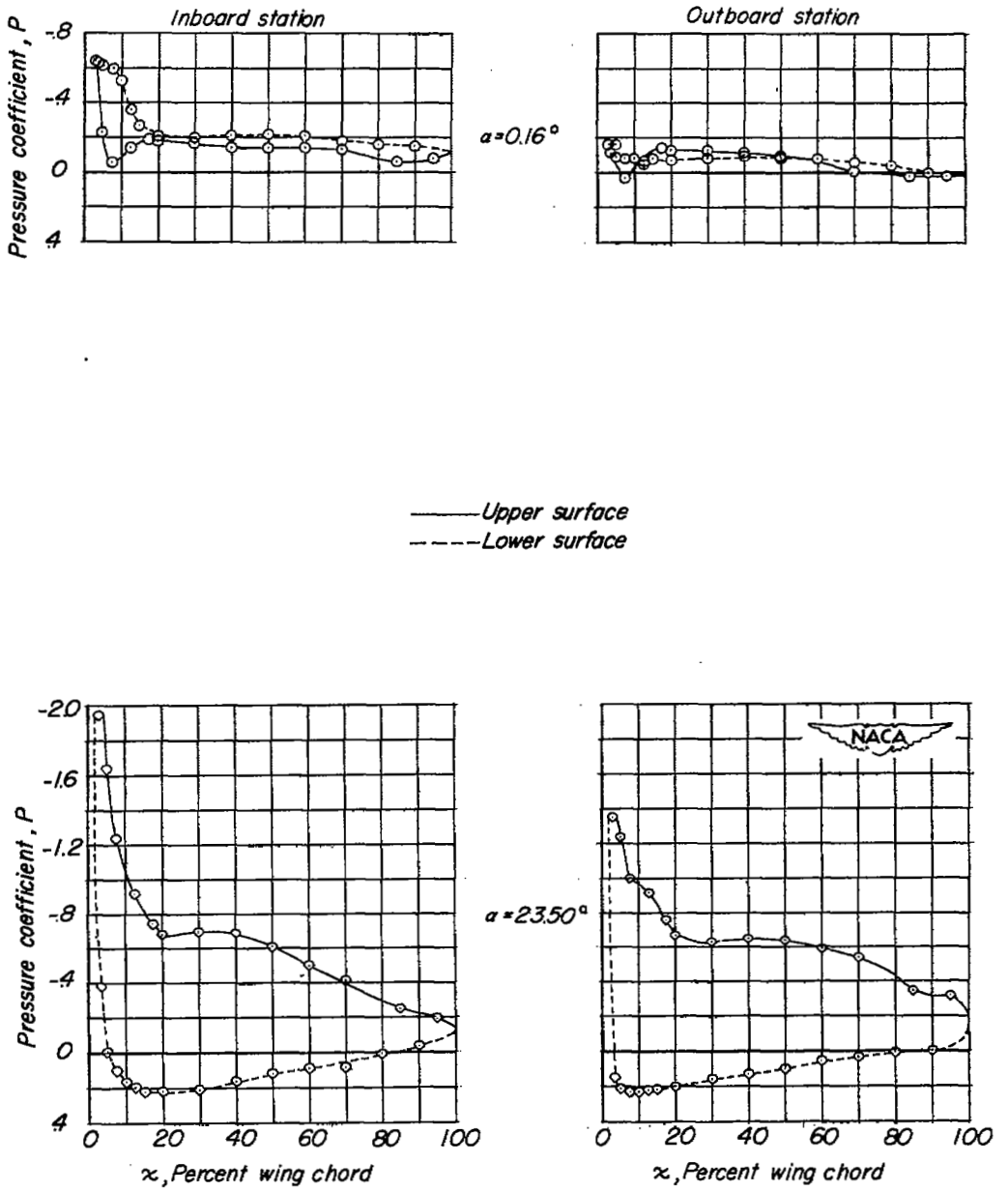

Figure 12.- Pressure distribution on the wing with slats extended. $\Lambda = 60^{\circ}$; $\psi = 5^{\circ}$.

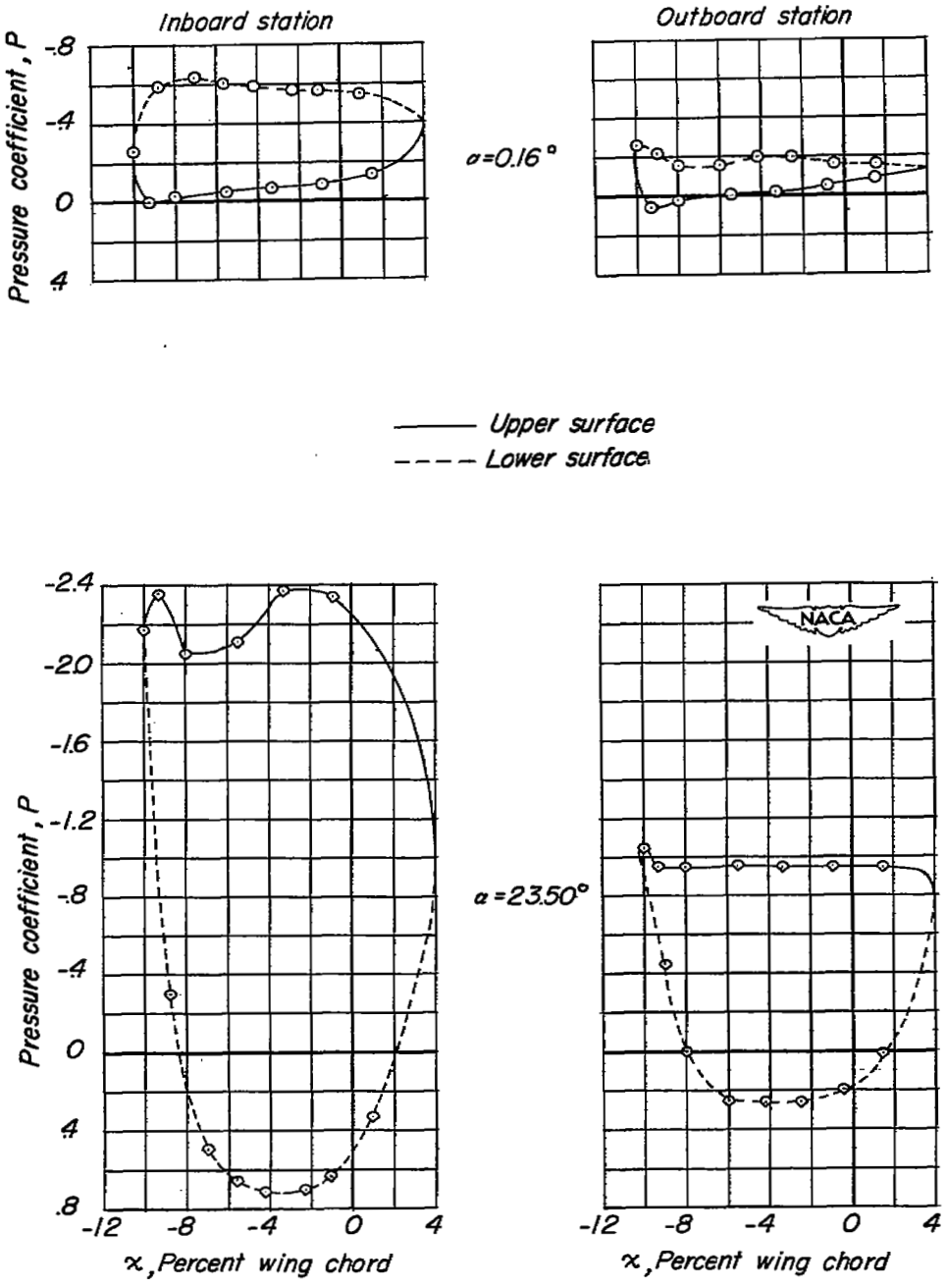

Figure 13.- Pressure distribution on the slat. $\Lambda = 60°$; $\psi = 5°$.

[redacted]

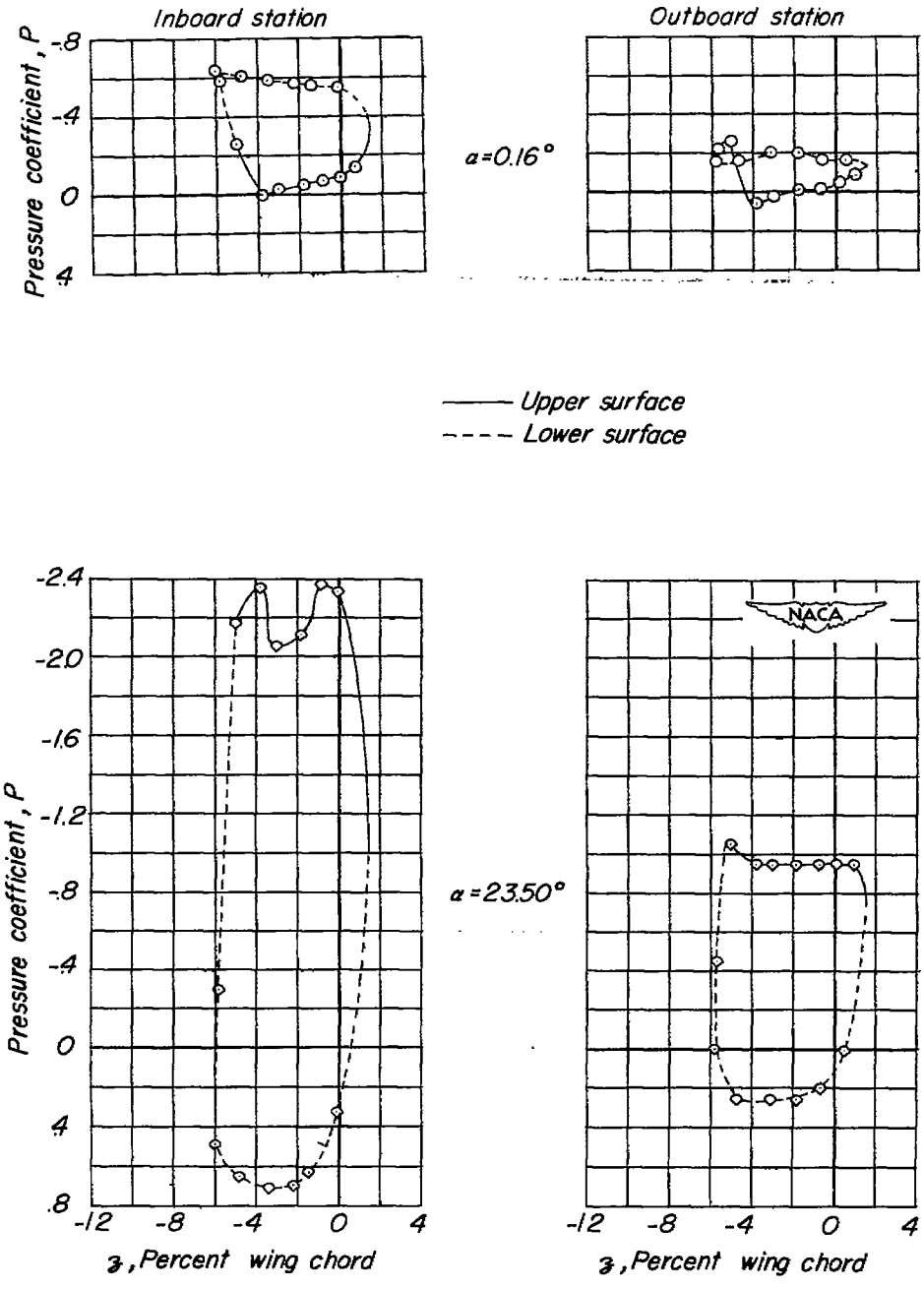

Figure 13.- Concluded.

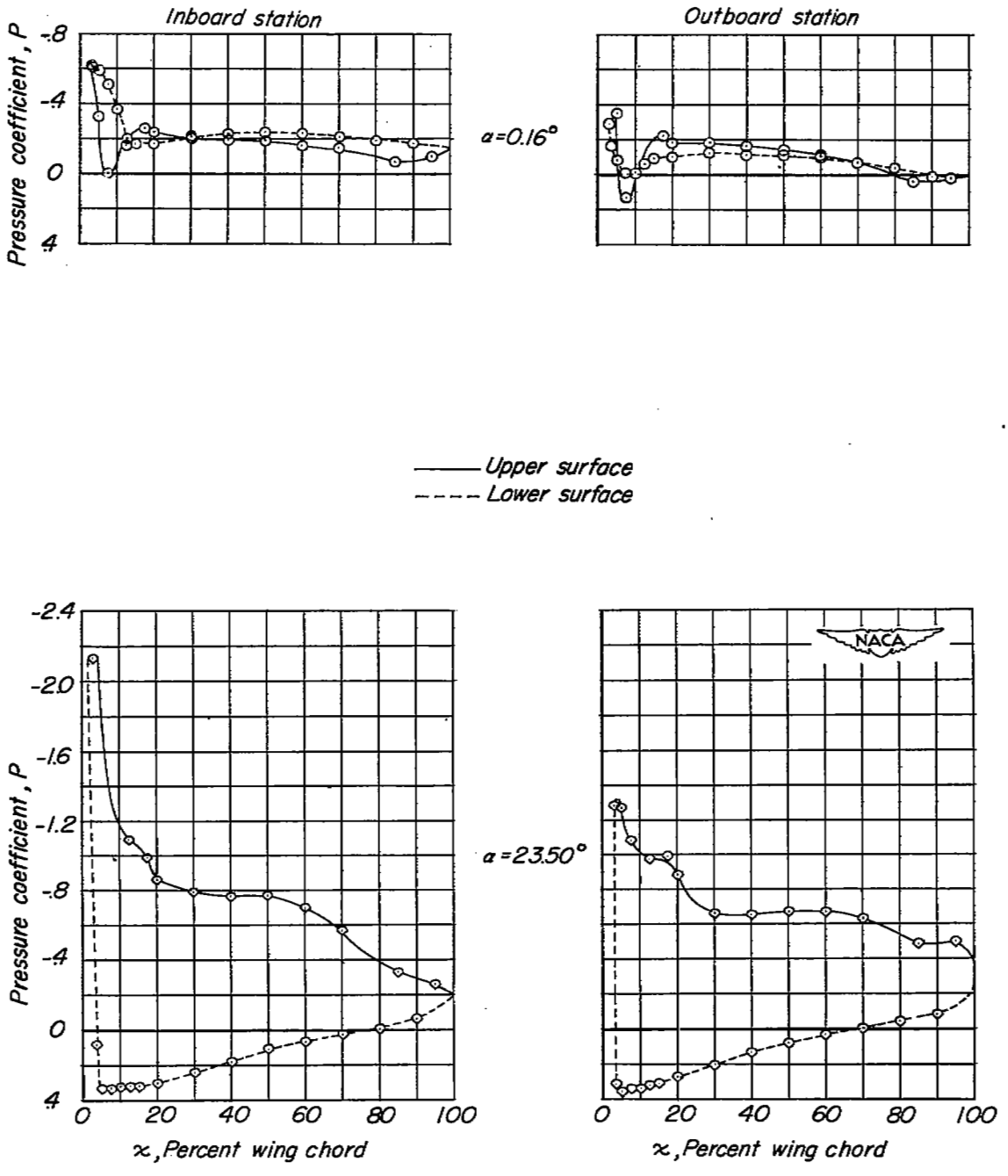

Figure 14.- Pressure distribution on the wing with slats extended. $\Lambda = 60°$; $\psi = -5°$.

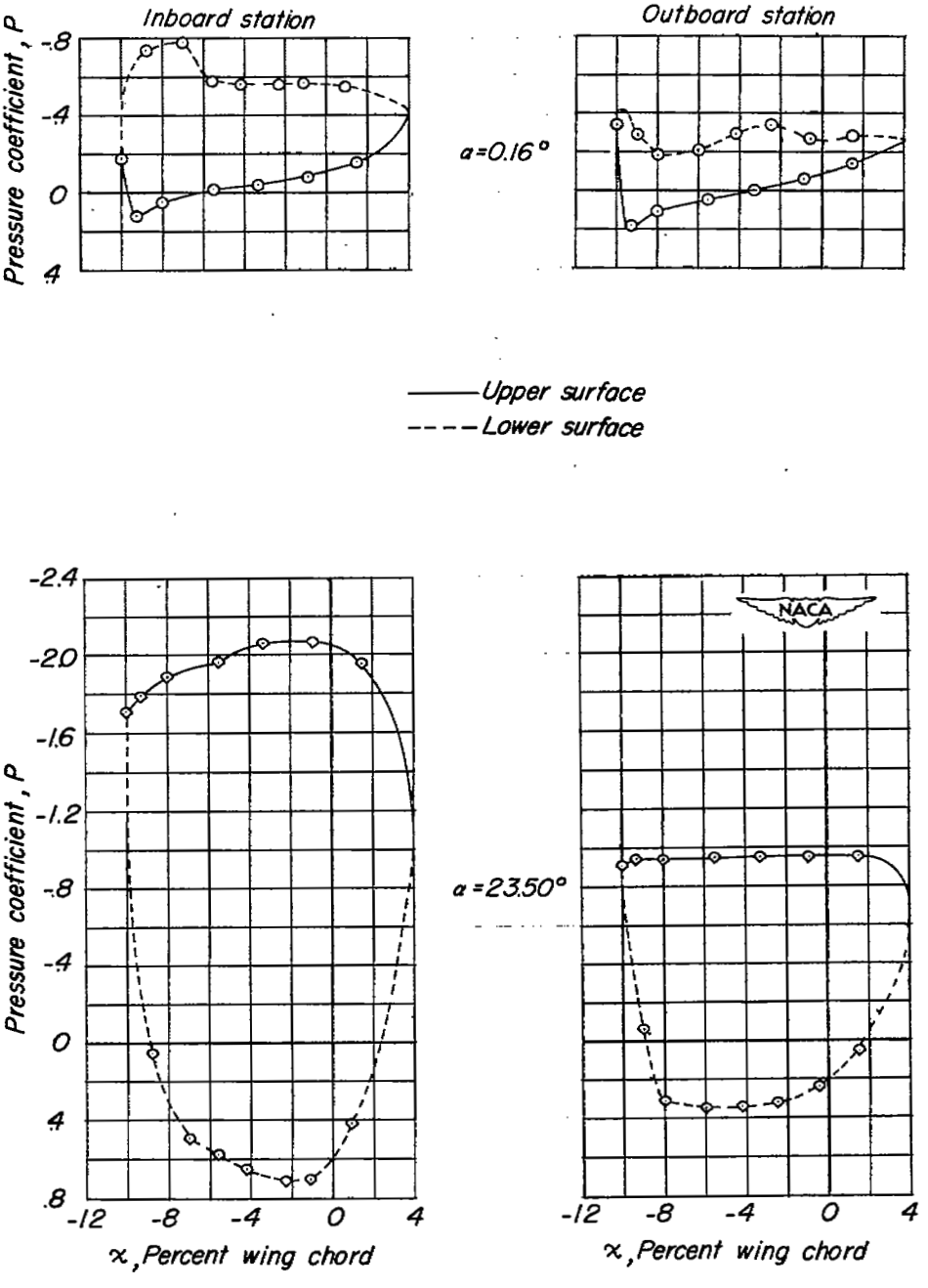

Figure 15.- Pressure distribution on the slat. $\Lambda = 60°$; $\psi = -5°$.

[redacted]

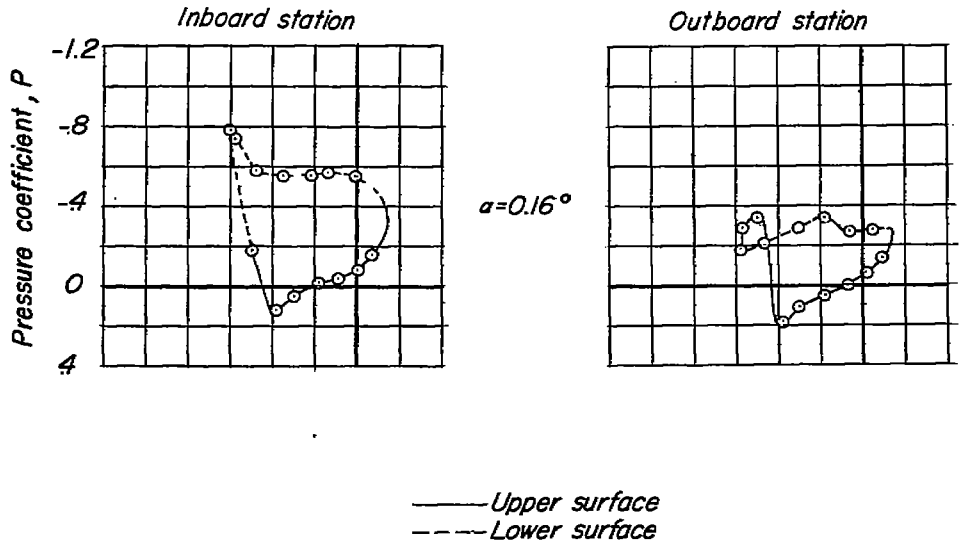

Figure 15.- Concluded.

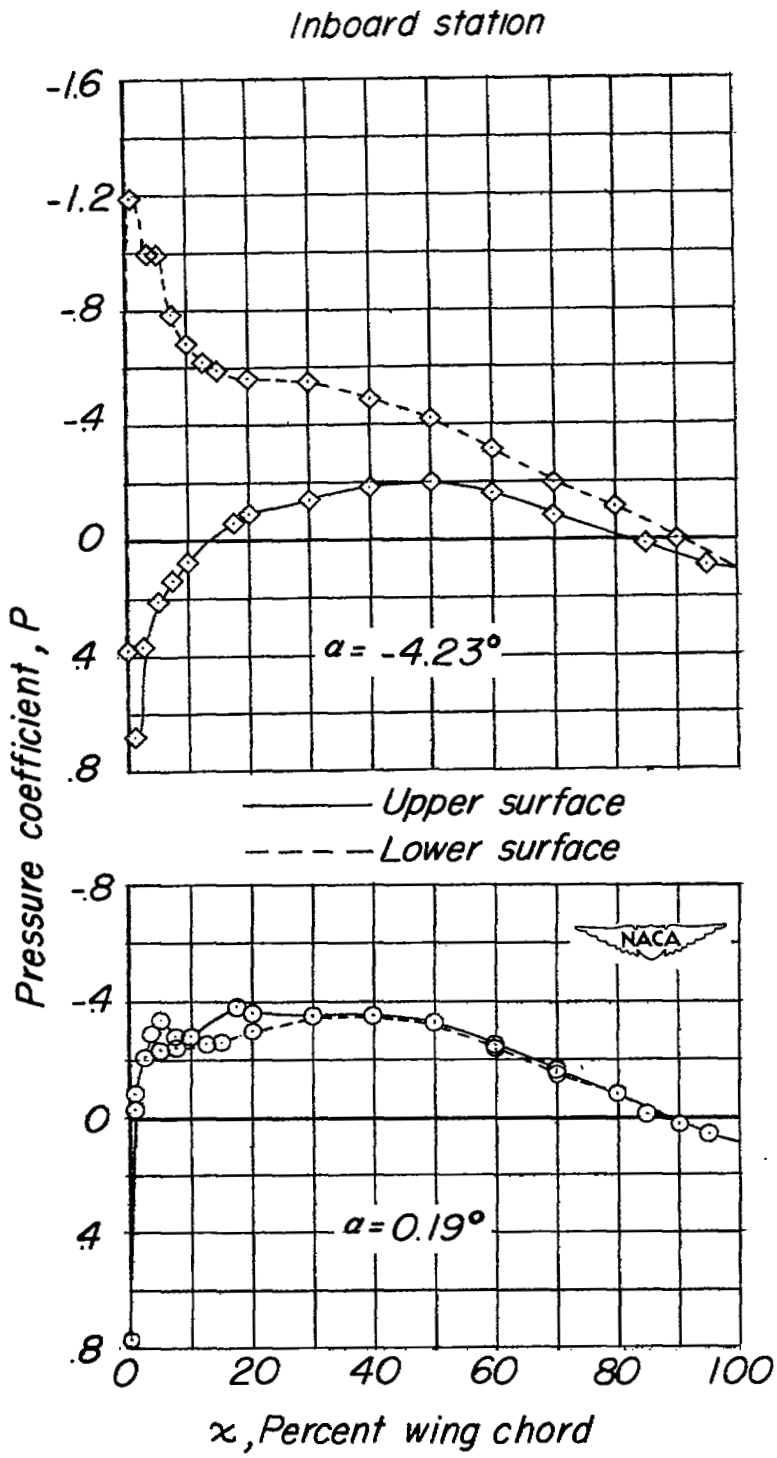

Figure 16.- Pressure distribution on the wing with slats retracted. $\Lambda = 20^\circ$; $\psi = 0^\circ$.

[redacted]

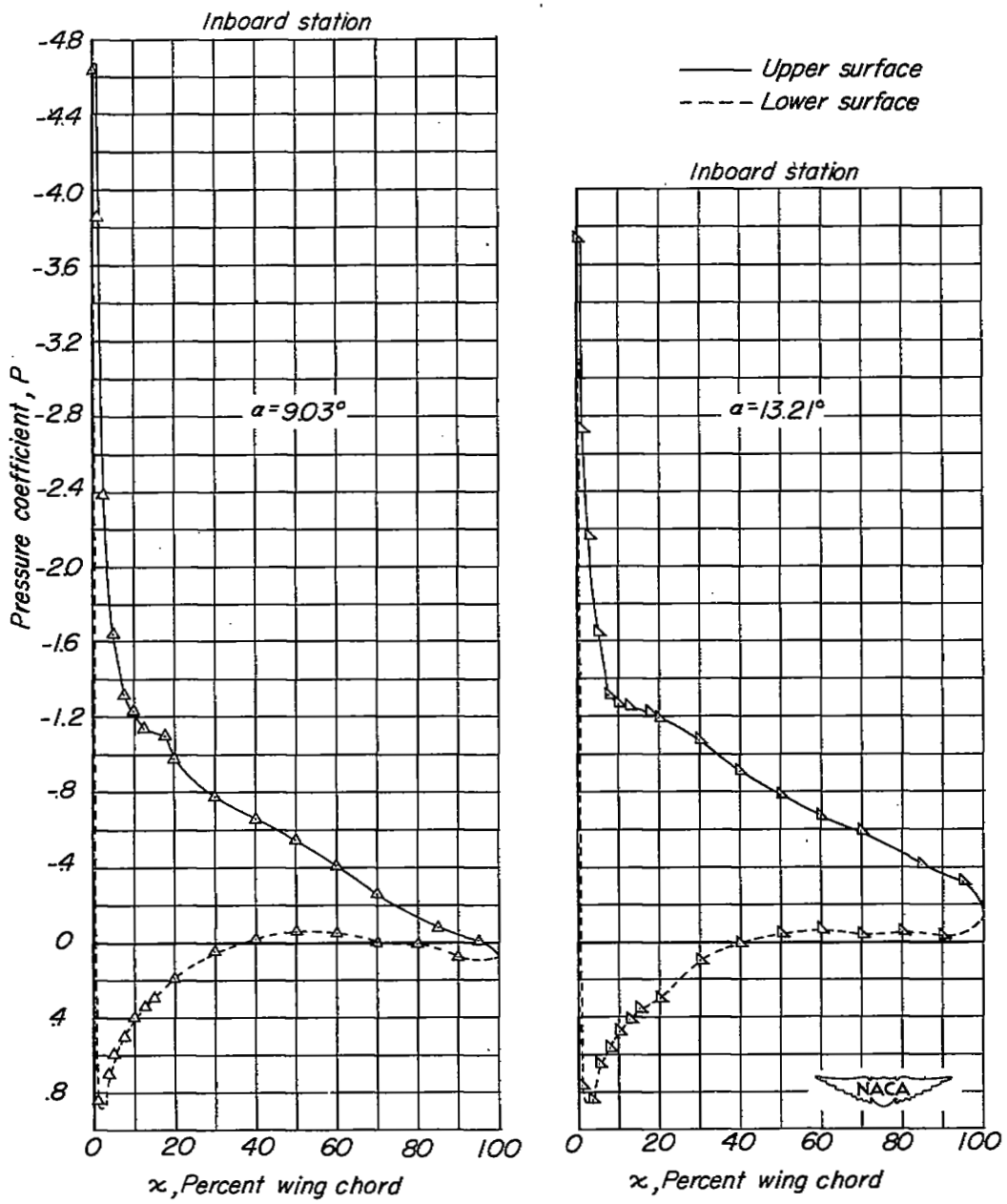

Figure 16.- Continued.

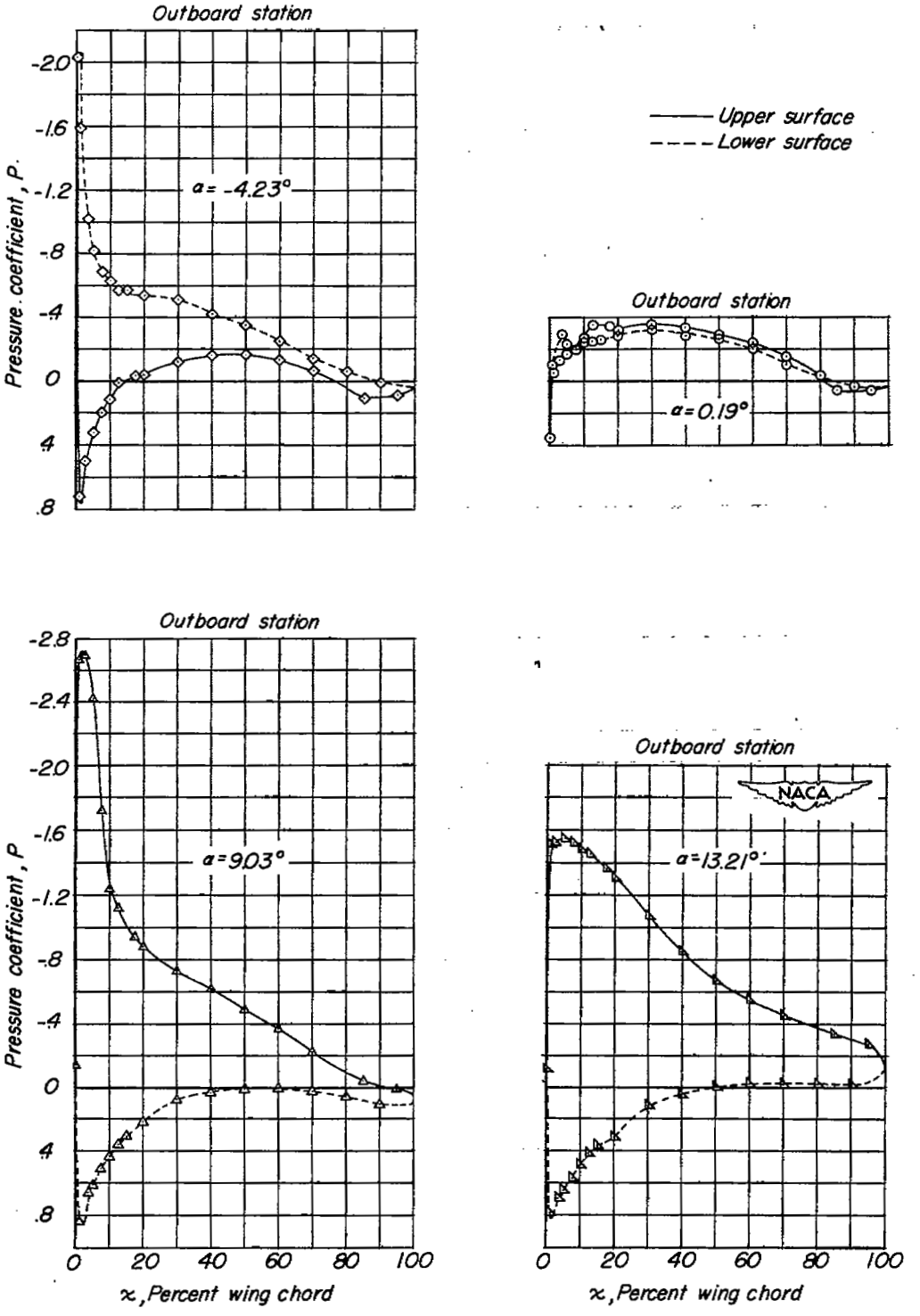

Figure 16.- Concluded.

[redacted]

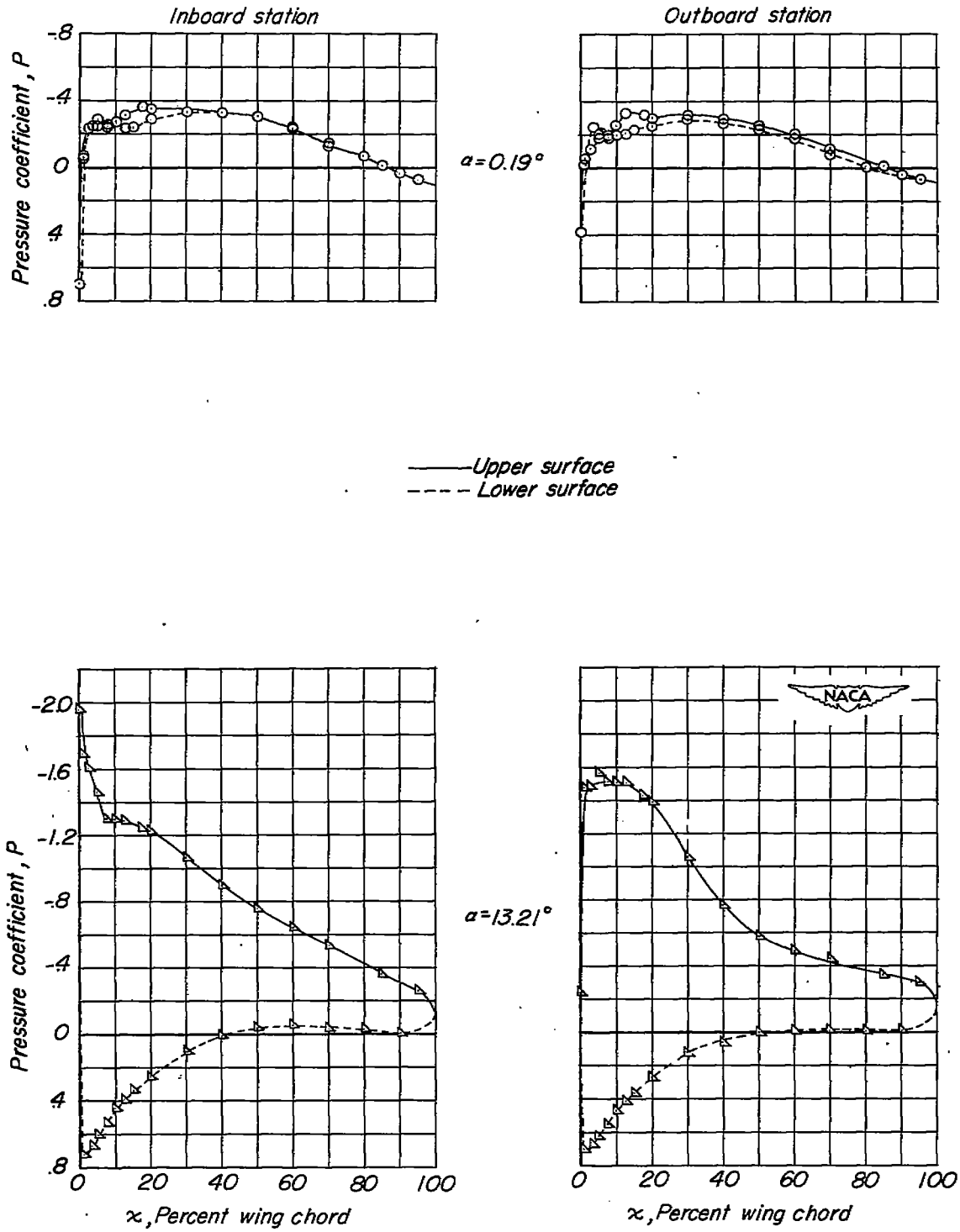

Figure 17.- Pressure distribution on the wing with slats retracted. $\Lambda = 20^{\circ}$; $\psi = 5^{\circ}$.

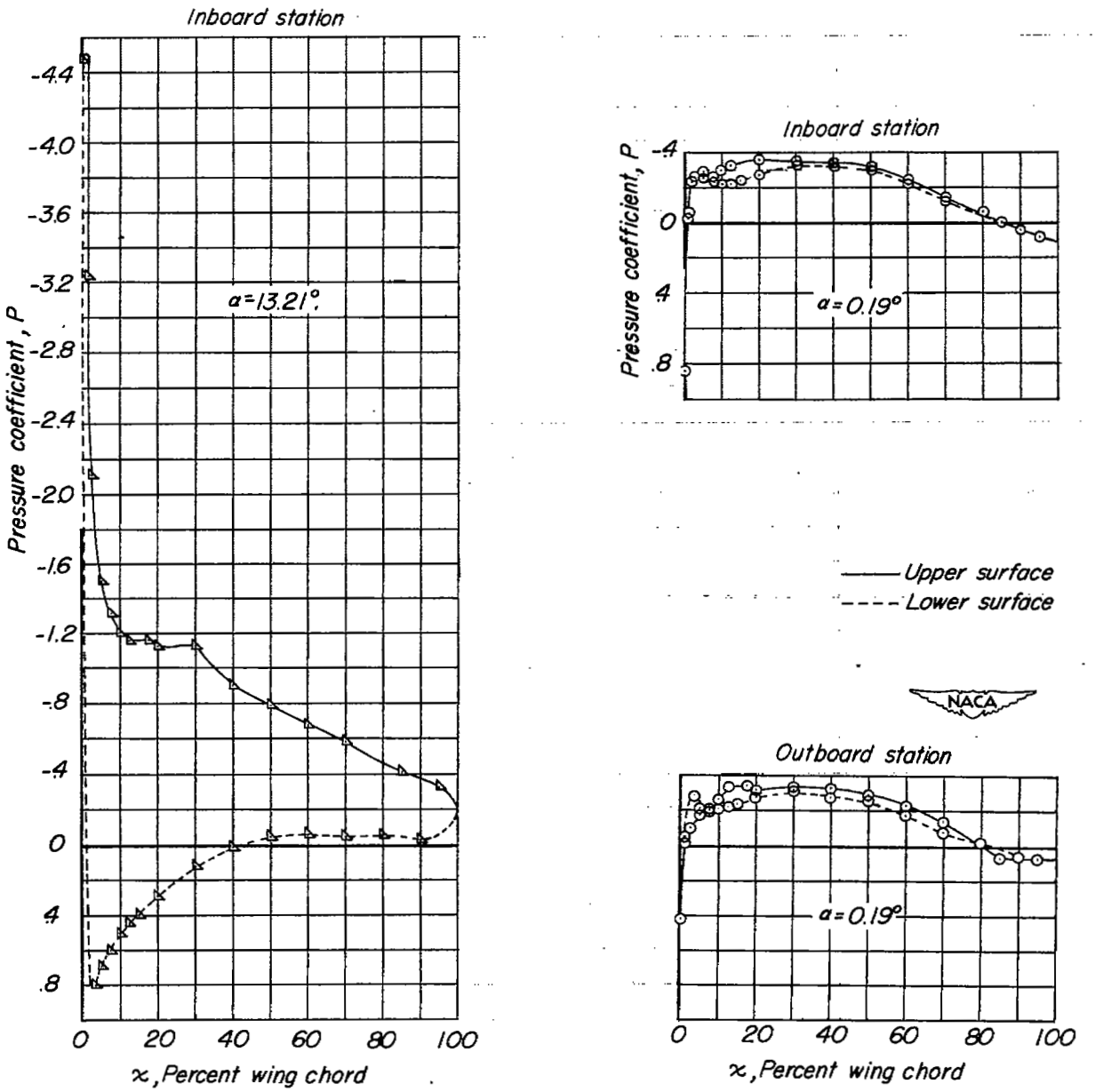

Figure 18.- Pressure distribution on the wing with slats retracted.
$\Lambda = 20^{\circ}$; $\psi = -5^{\circ}$.

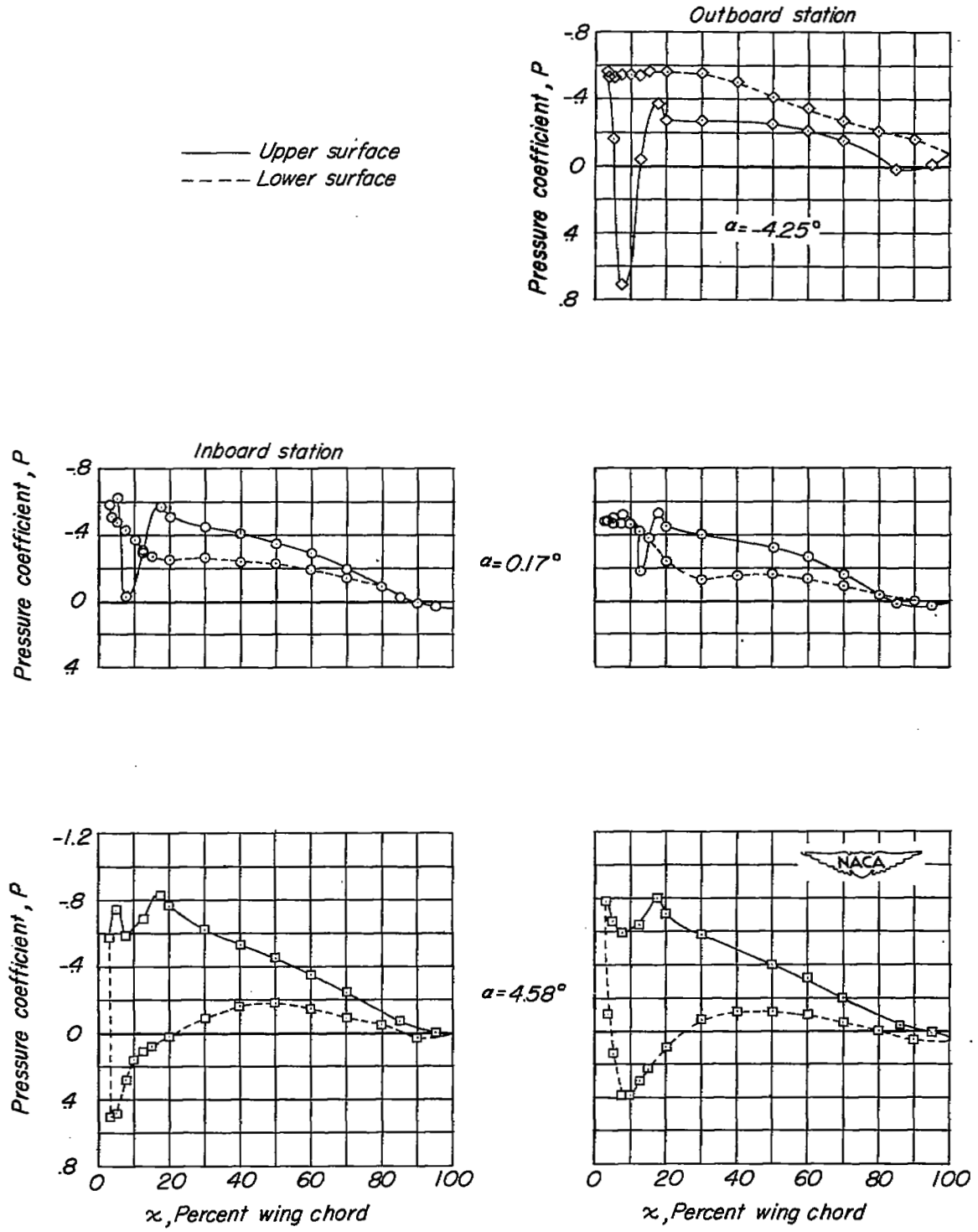

Figure 19.- Pressure distribution on the wing with slats extended. $\Lambda = 20^{\circ}$; $\psi = 0^{\circ}$.

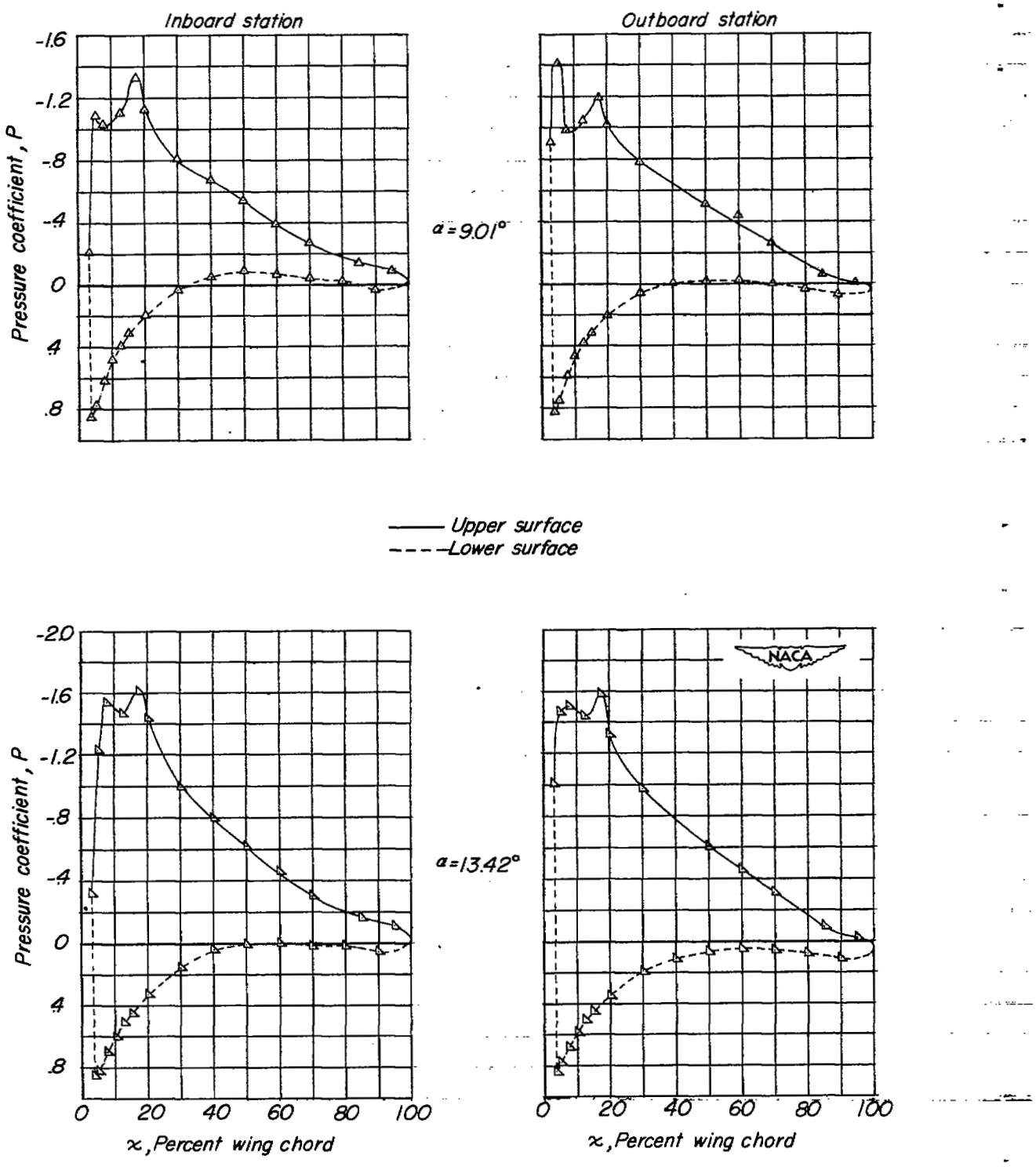

Figure 19.- Continued.

[redacted]

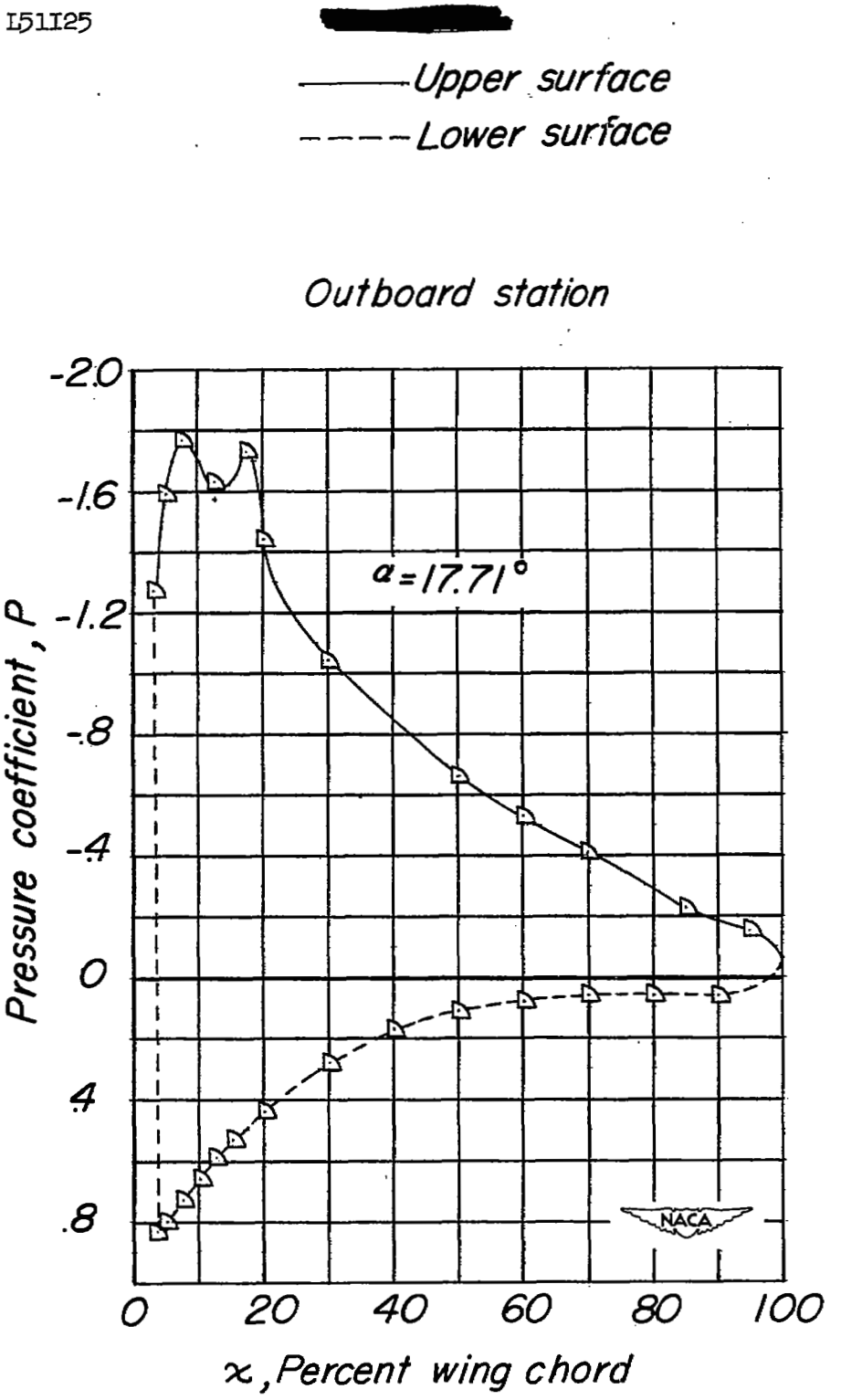

Figure 19.- Concluded.

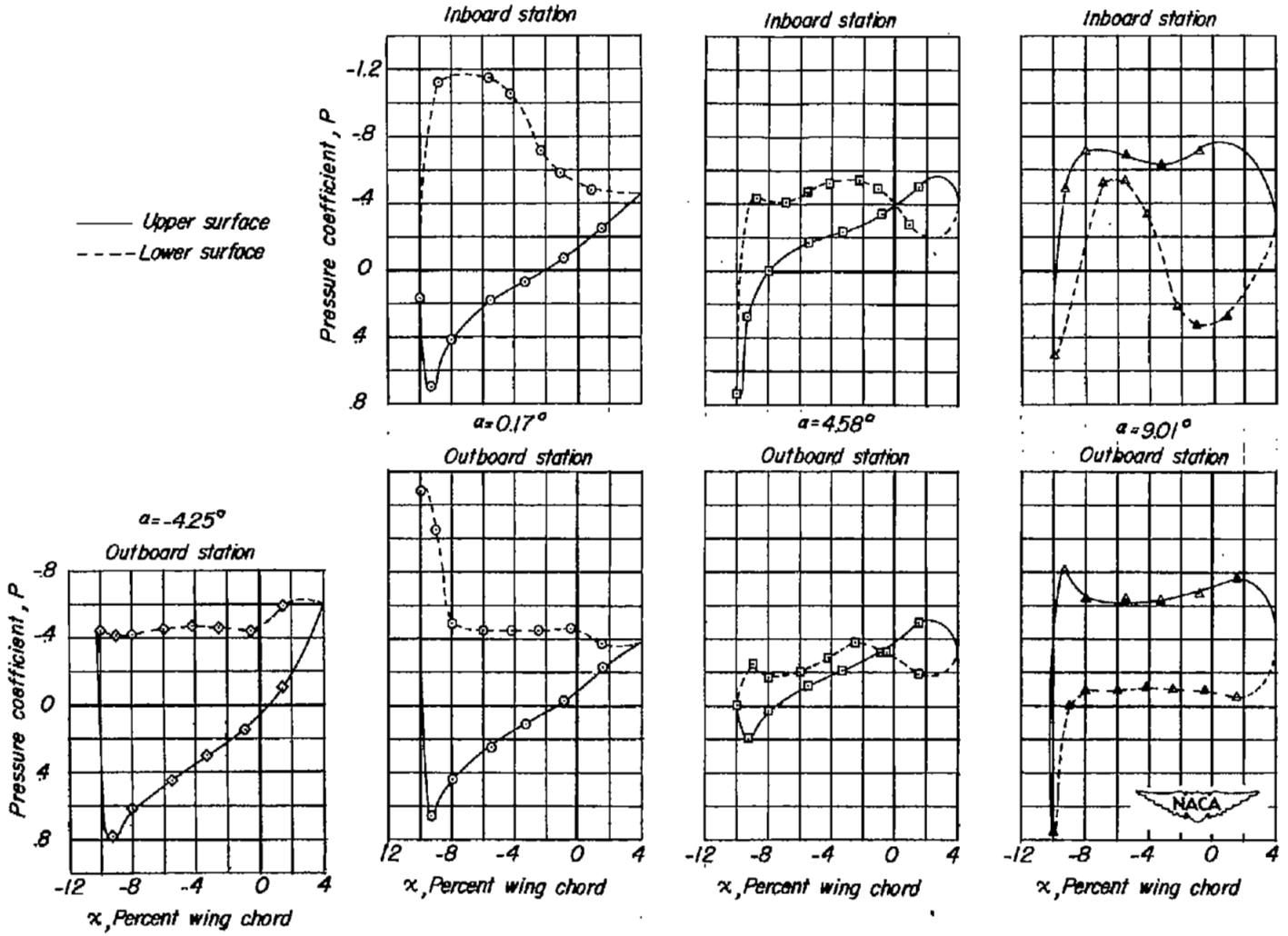

Figure 20.- Pressure distribution on the slat. $\Lambda = 20^{\circ}$; $\psi = 0^{\circ}$.

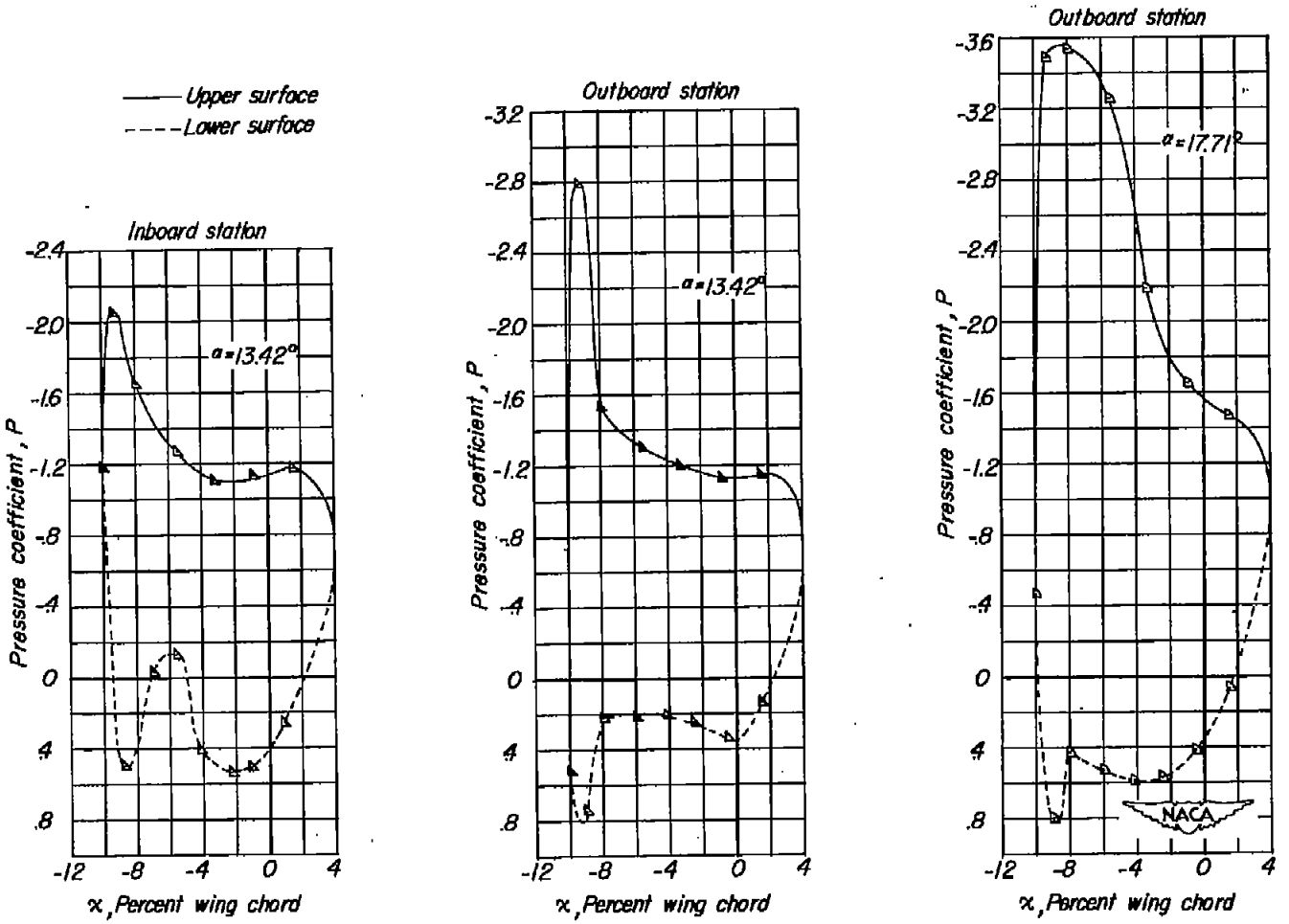

Figure 20.- Continued.

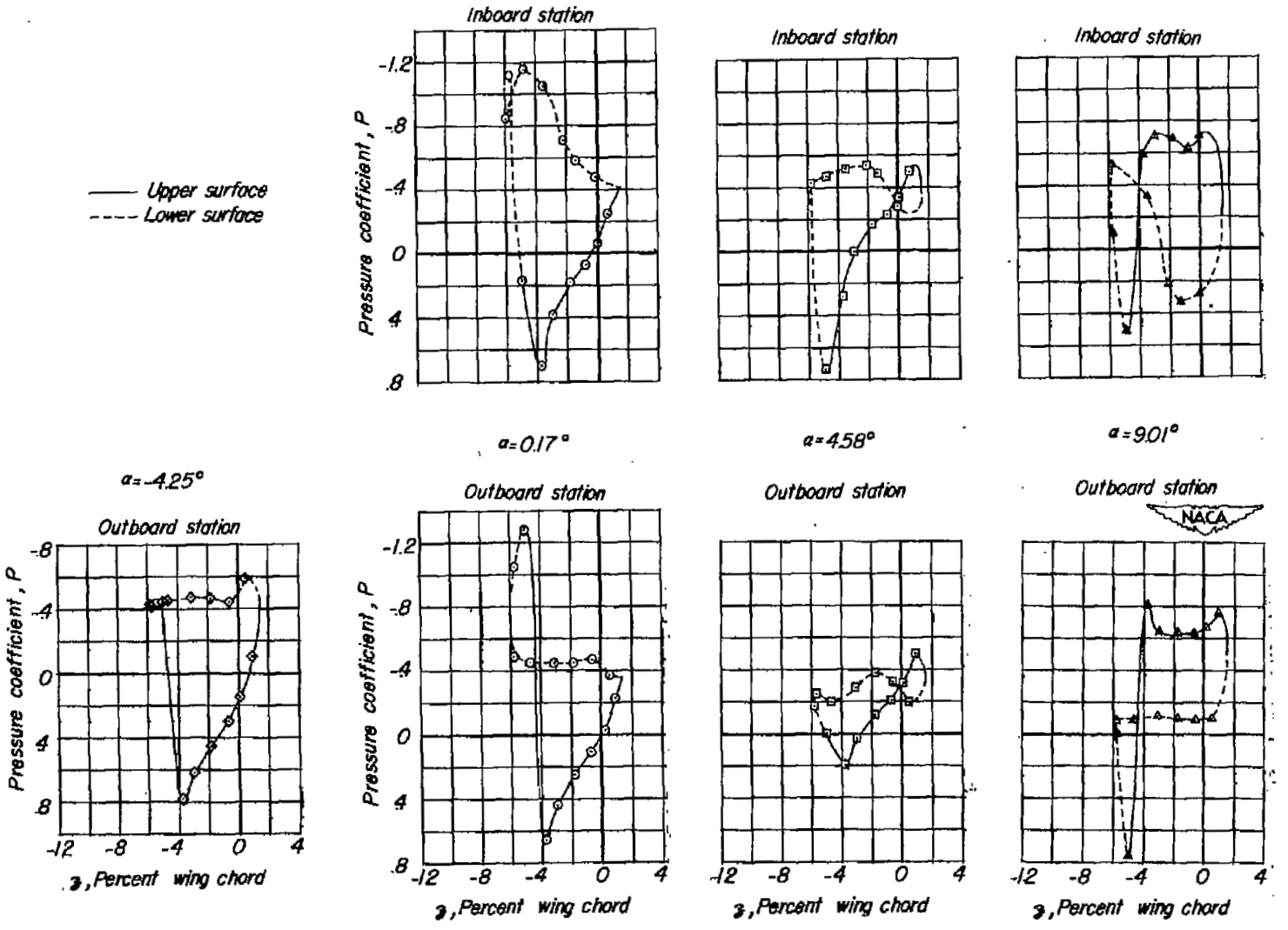

Figure 20.- Continued.

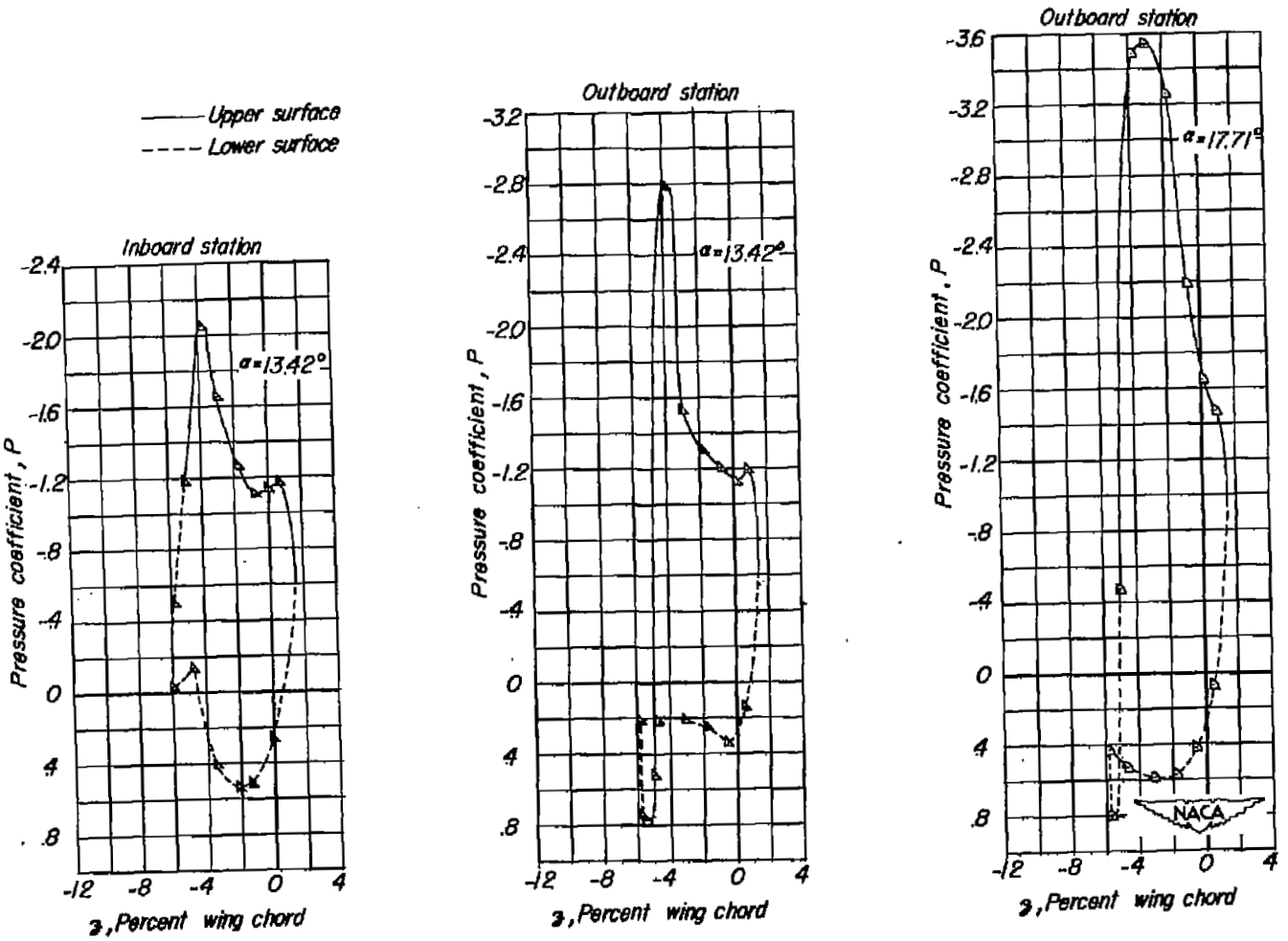

Figure 20.- Concluded.

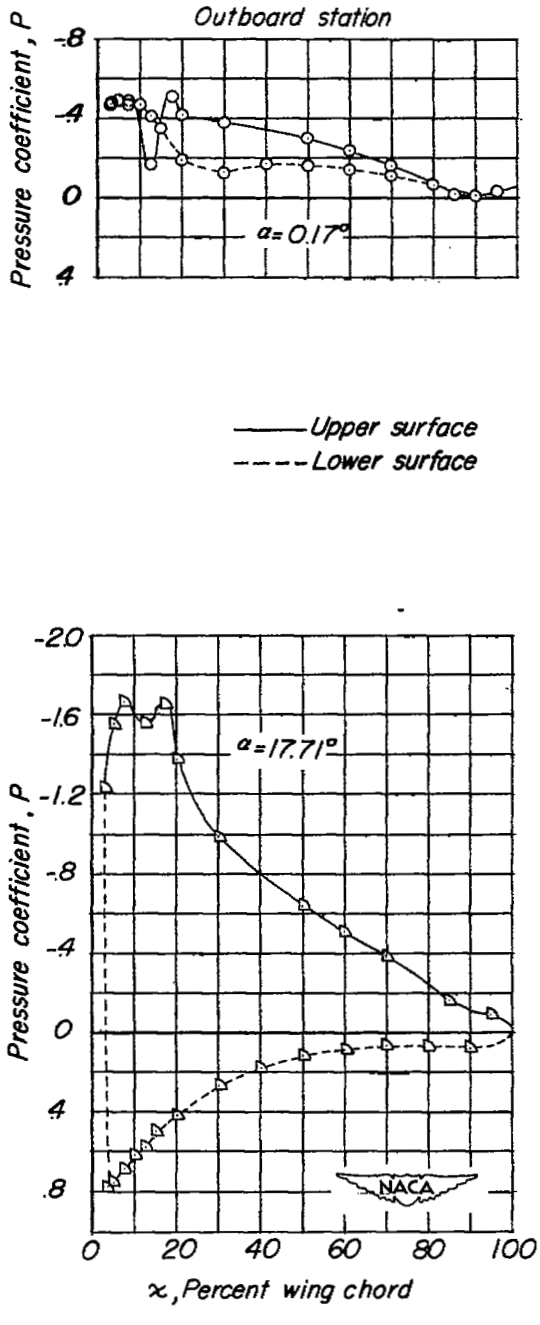

Figure 21.- Pressure distribution on the wing with slats extended. $\Lambda = 20^{\circ}$; $\psi = 5^{\circ}$.

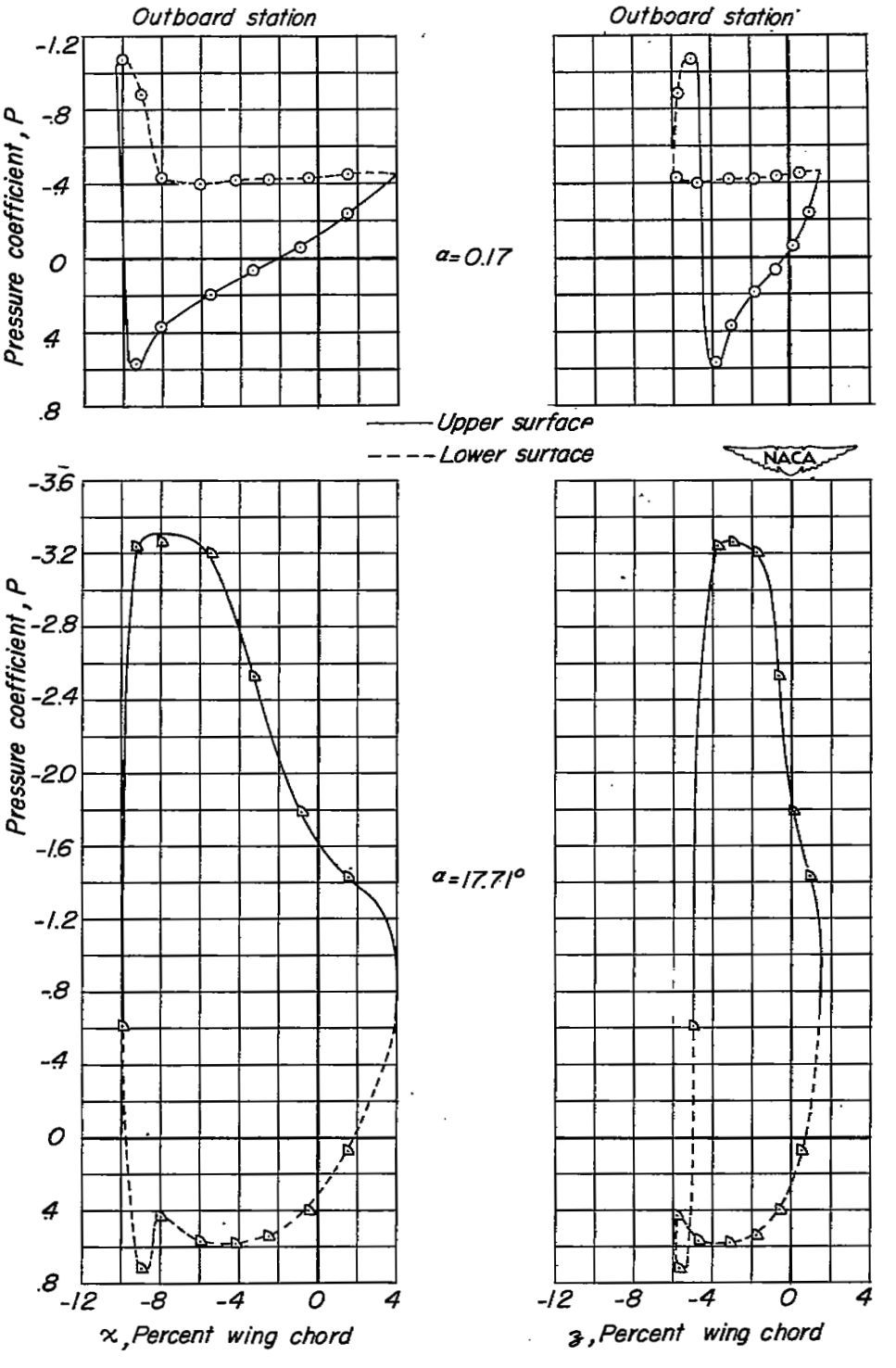

Figure 22.- Pressure distribution on the slat. $\Lambda = 20^{\circ}$; $\psi = 5^{\circ}$.

[redacted]

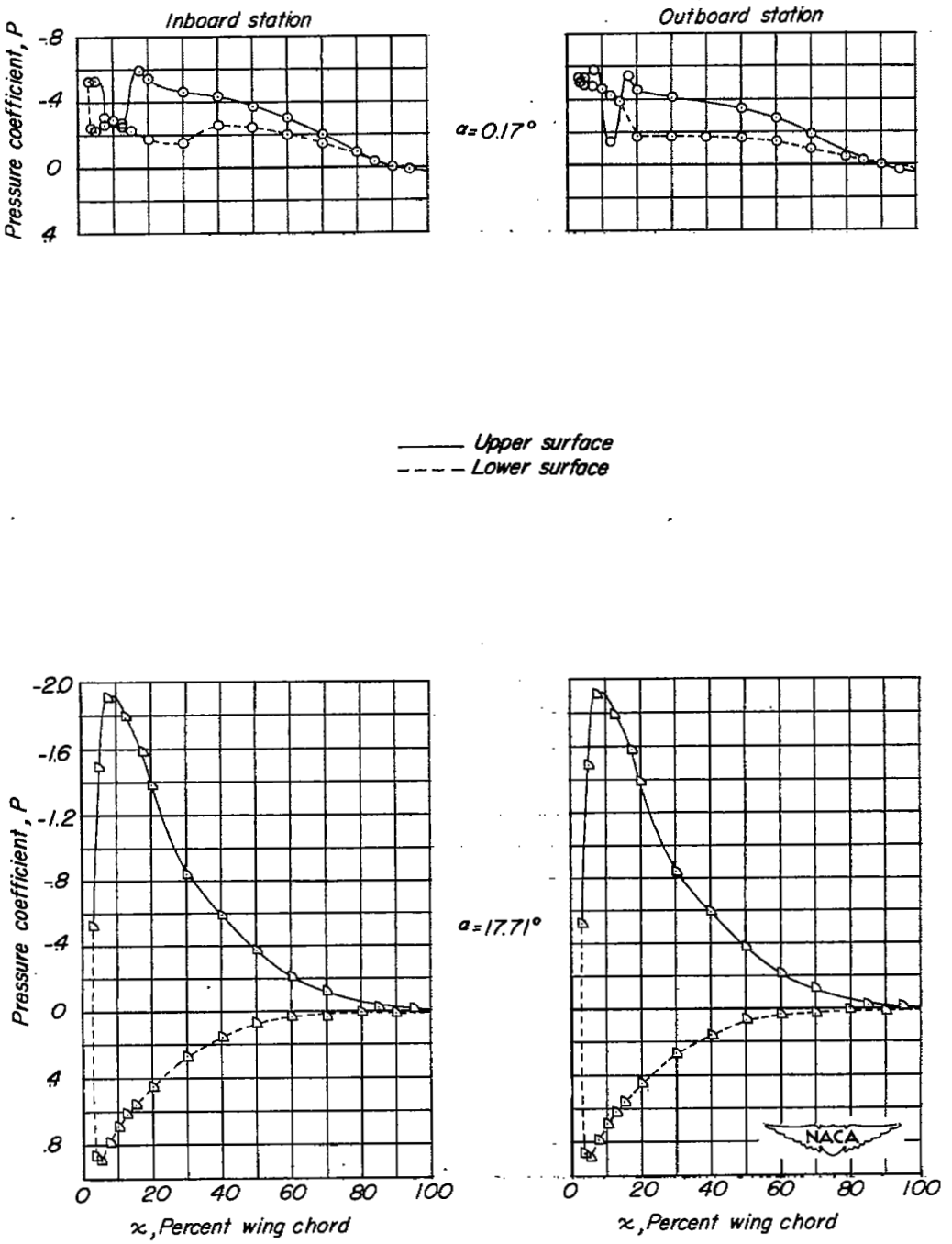

Figure 23.- Pressure distribution on the wing with slats extended. $\Lambda = 20^{\circ}$; $\psi = -5^{\circ}$.

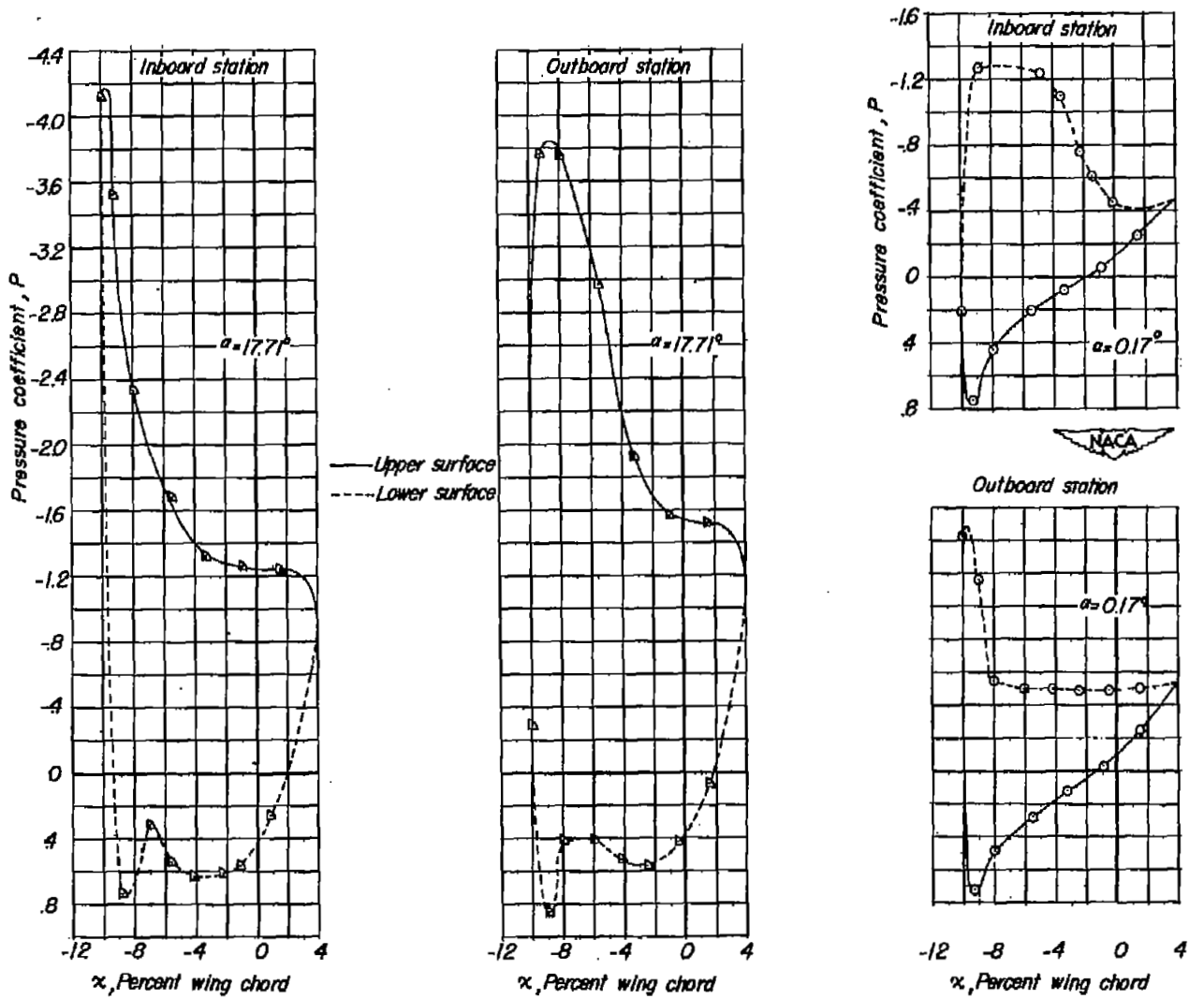

Figure 24.- Pressure distribution on the slat. $\Lambda = 20^{\circ}$; $\psi = -5^{\circ}$.

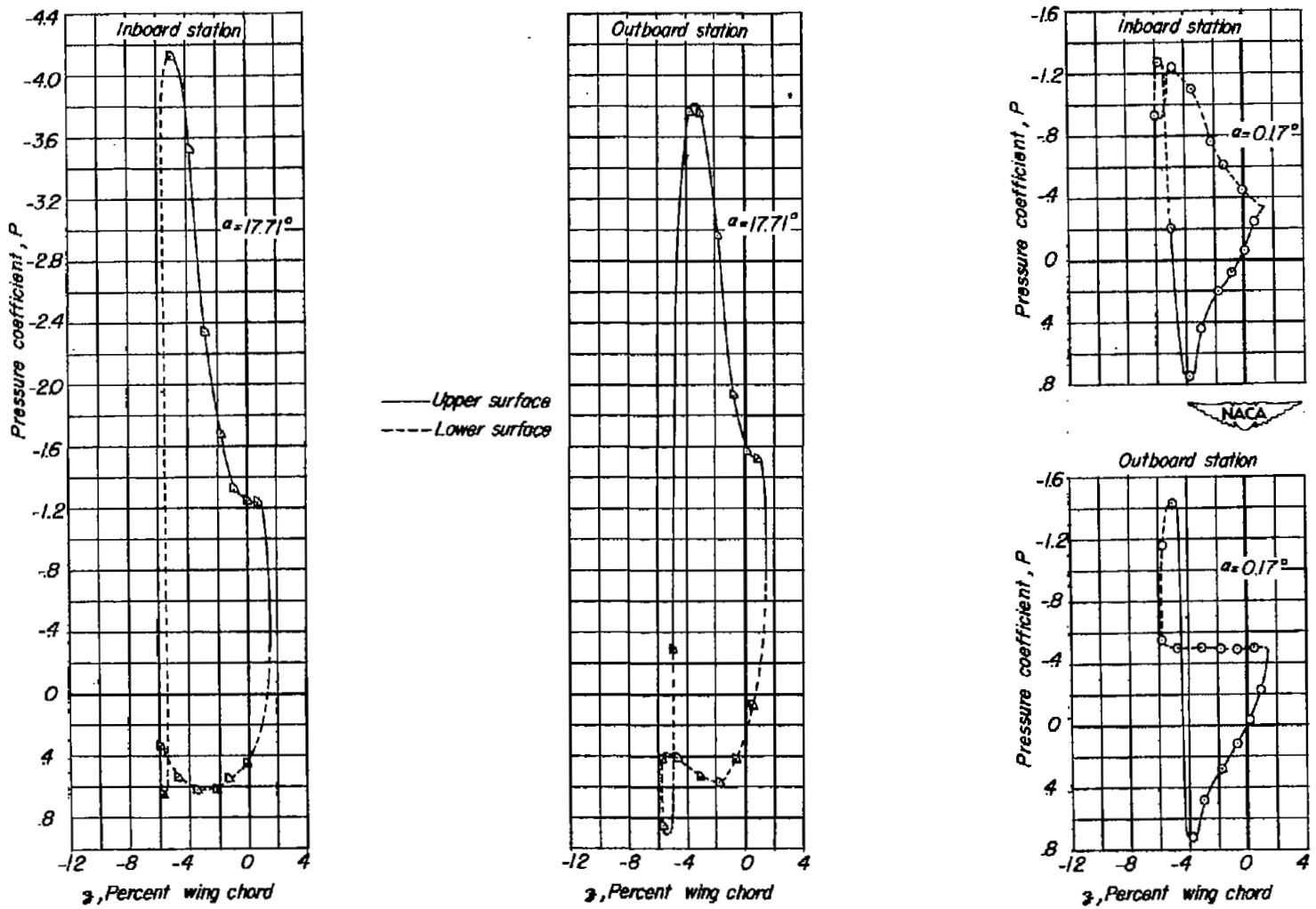

Figure 24.- Concluded.

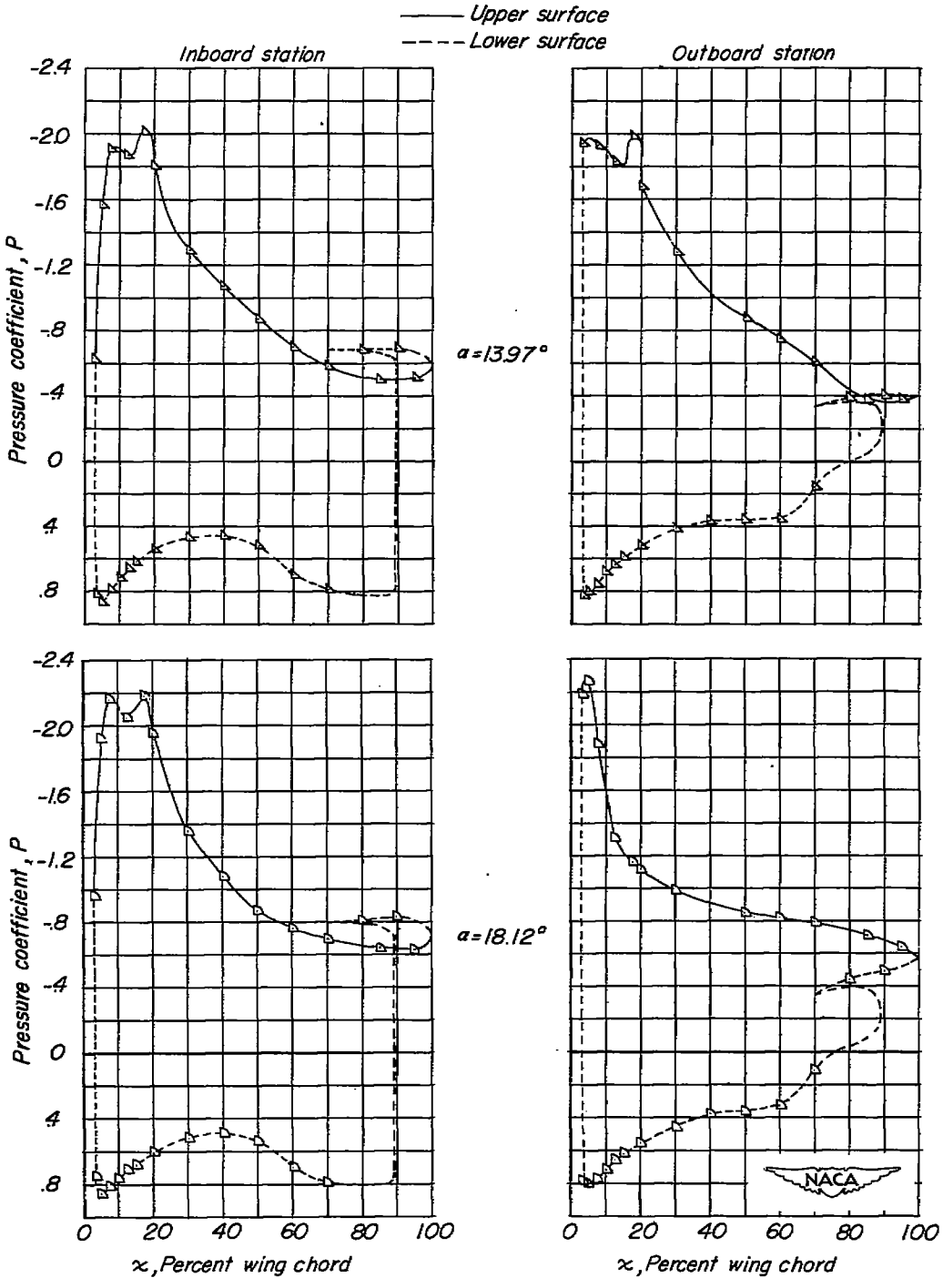

Figure 25.- Pressure distribution on the wing with slats extended. $\Lambda = 20^{\circ}$; $\psi = 0^{\circ}$; $\delta_f = 50^{\circ}$.

[redacted]

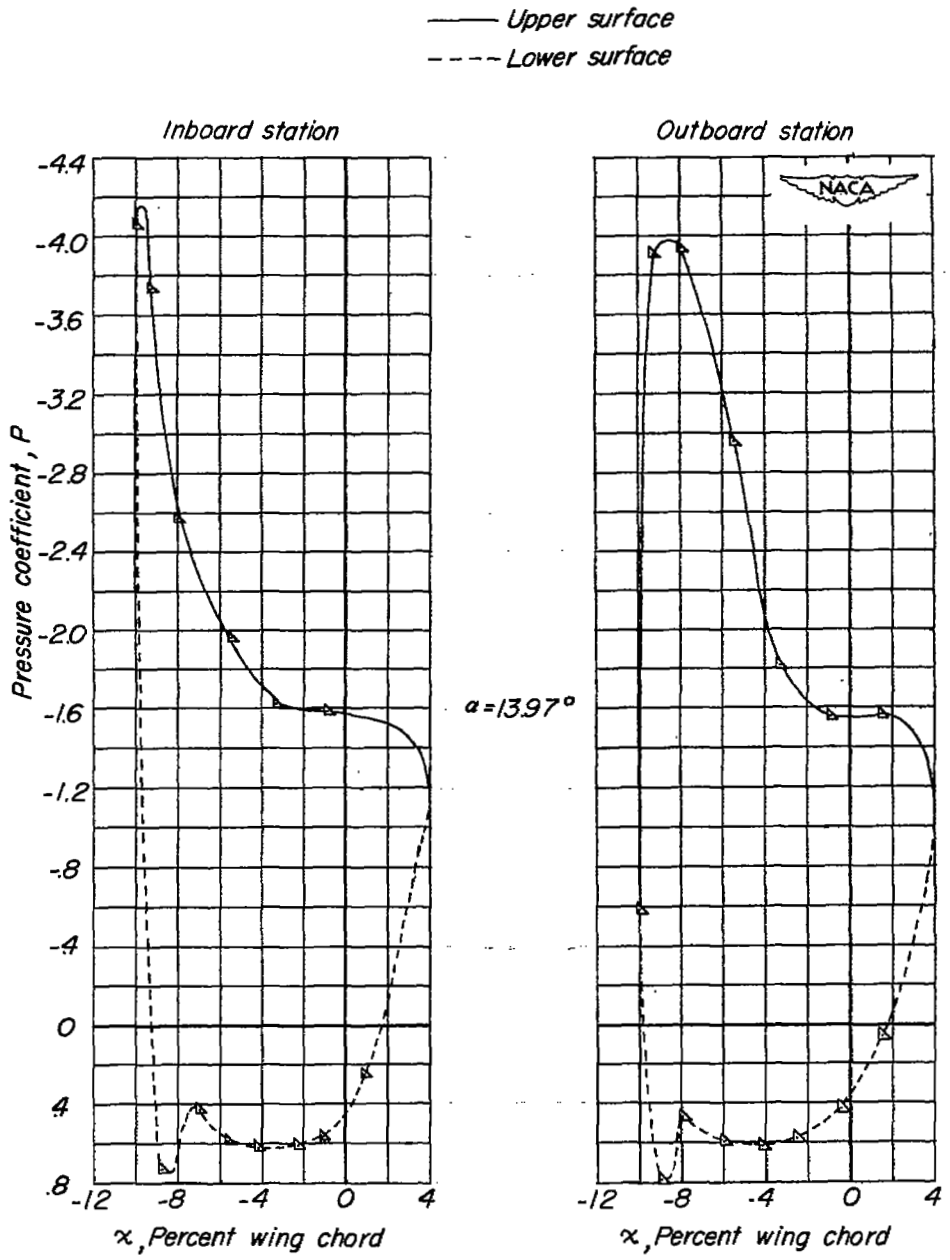

Figure 26.- Pressure distribution on the slat. $\Lambda = 20°$; $\psi = 0°$; $\delta_f = 50°$.

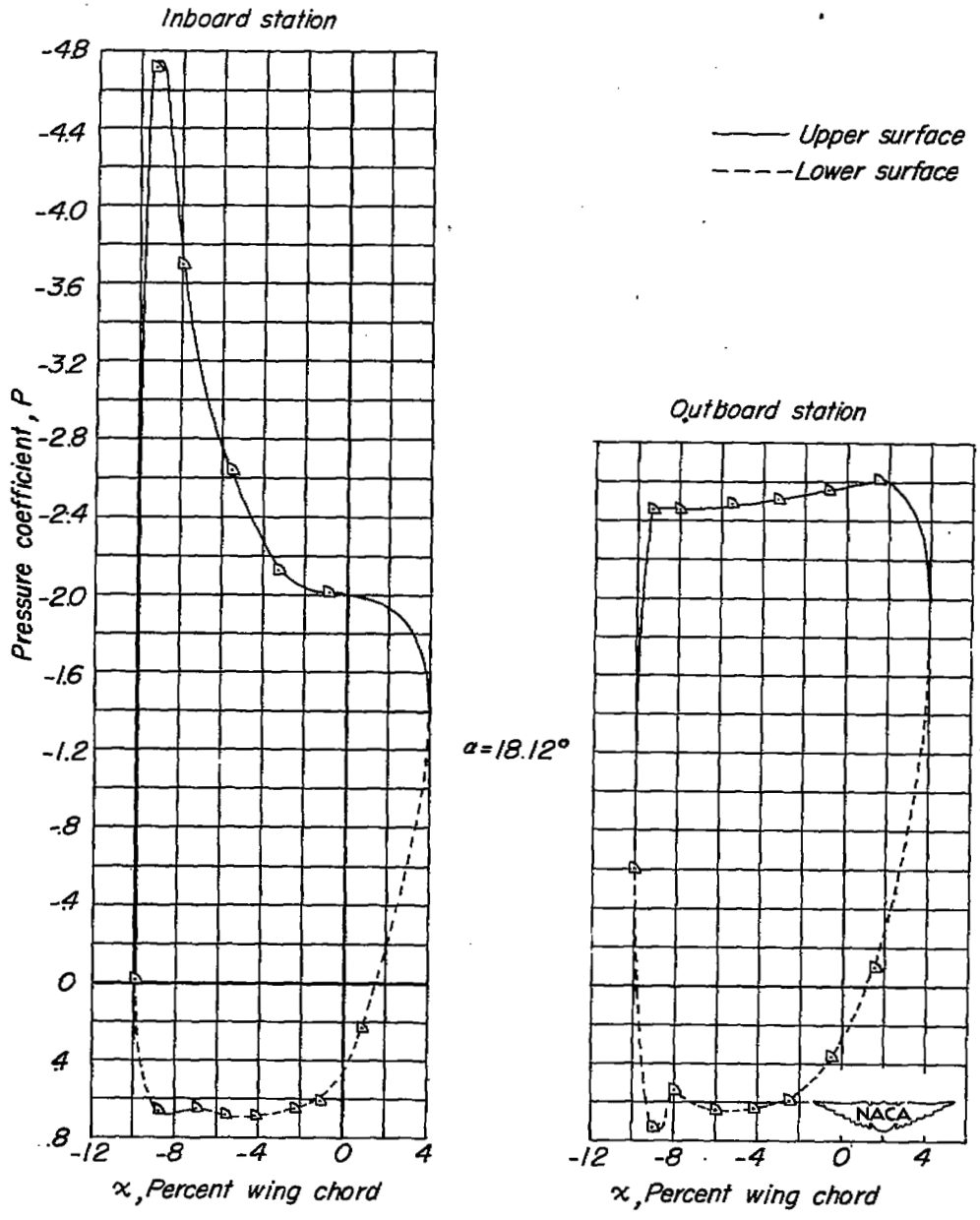

Figure 26.- Continued.

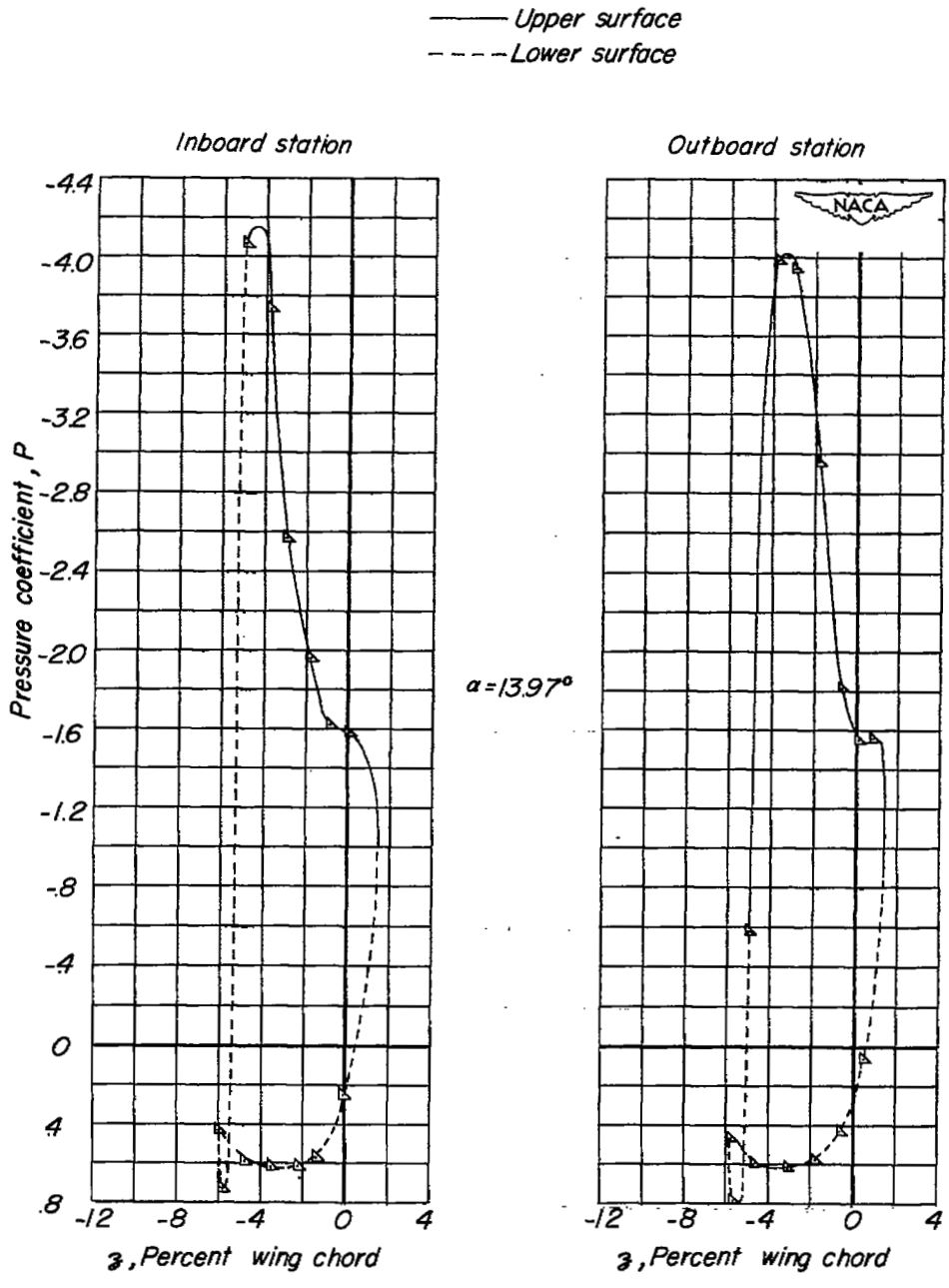

Figure 26.- Continued.

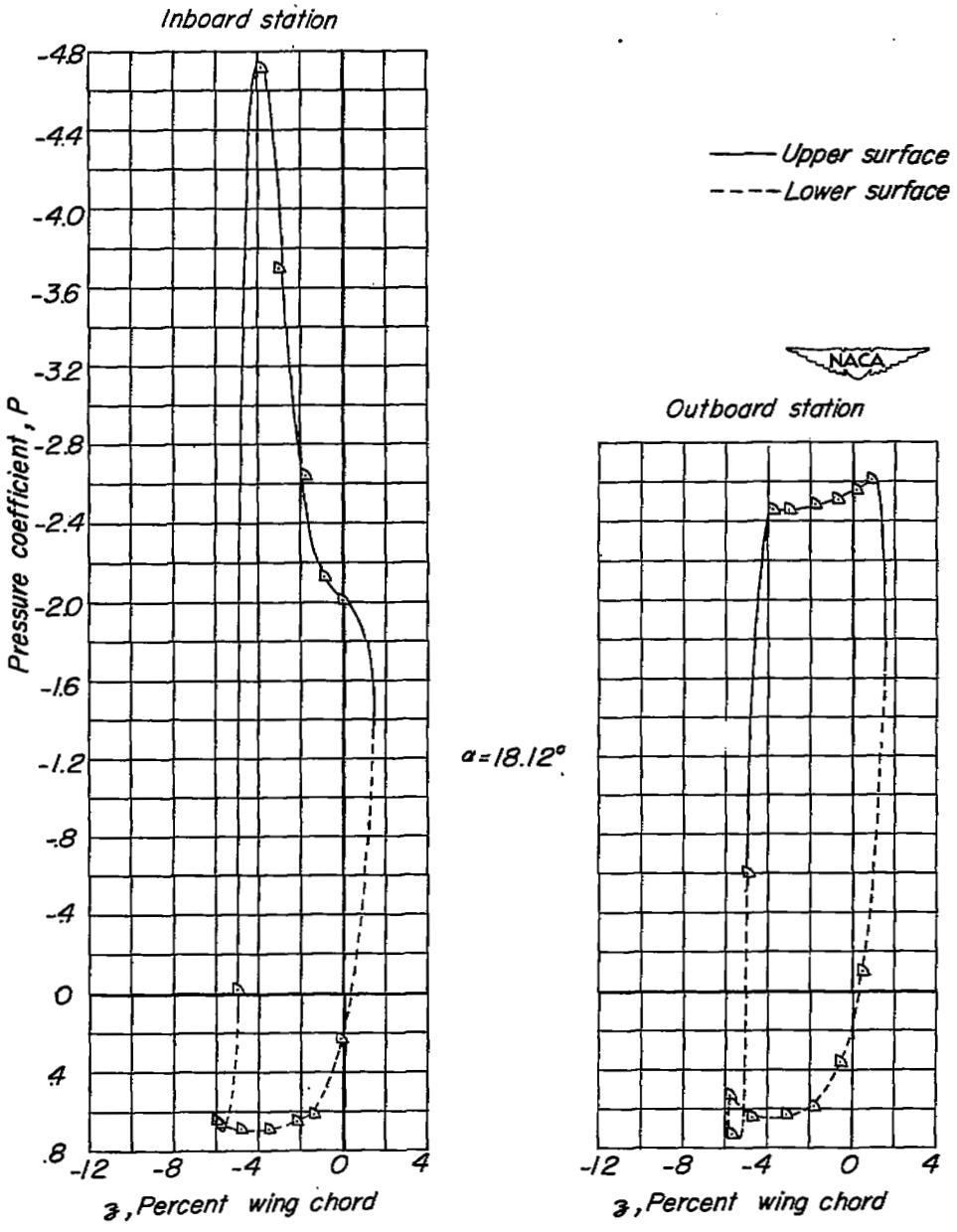

Figure 26.- Concluded.

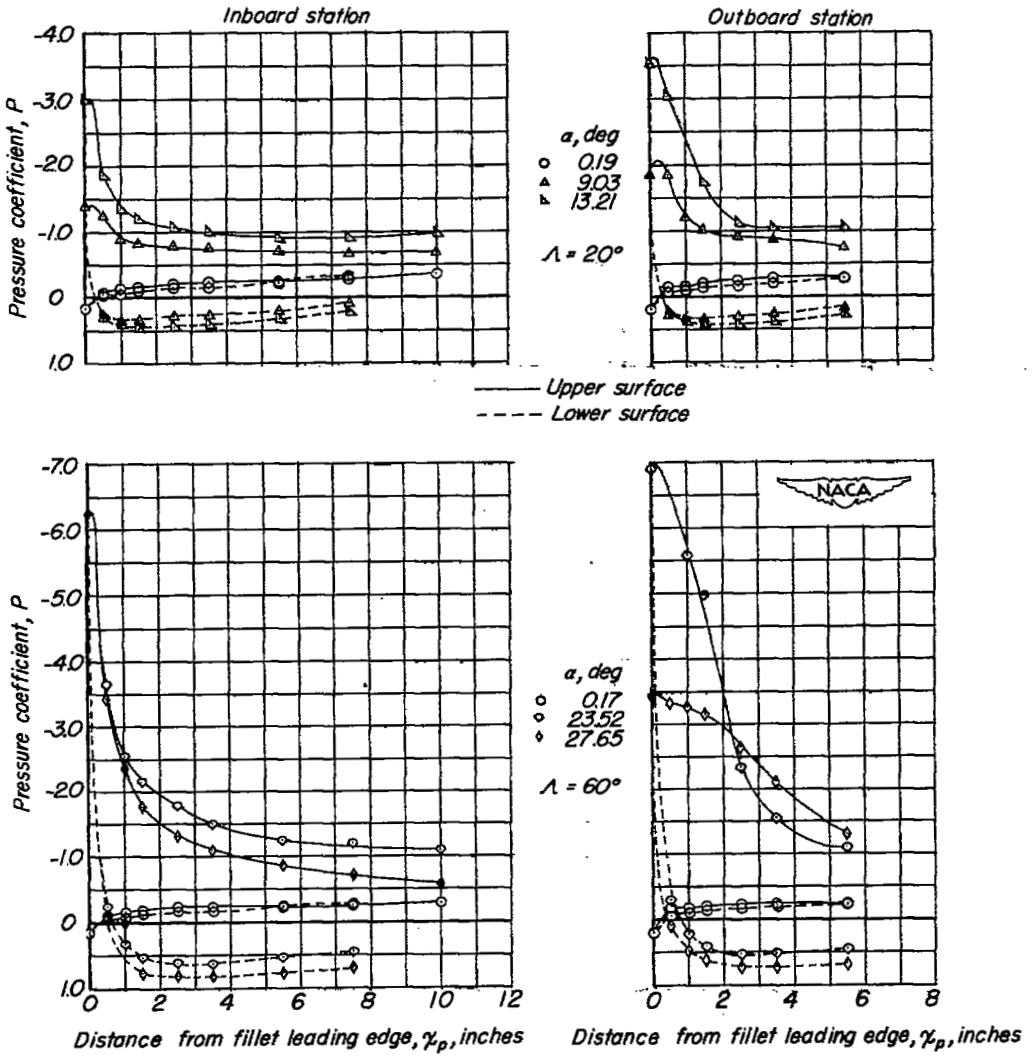

(a) Slats retracted.

Figure 27.- Pressure distribution on the fillet $\psi = 0^{\circ}$.

[redacted]

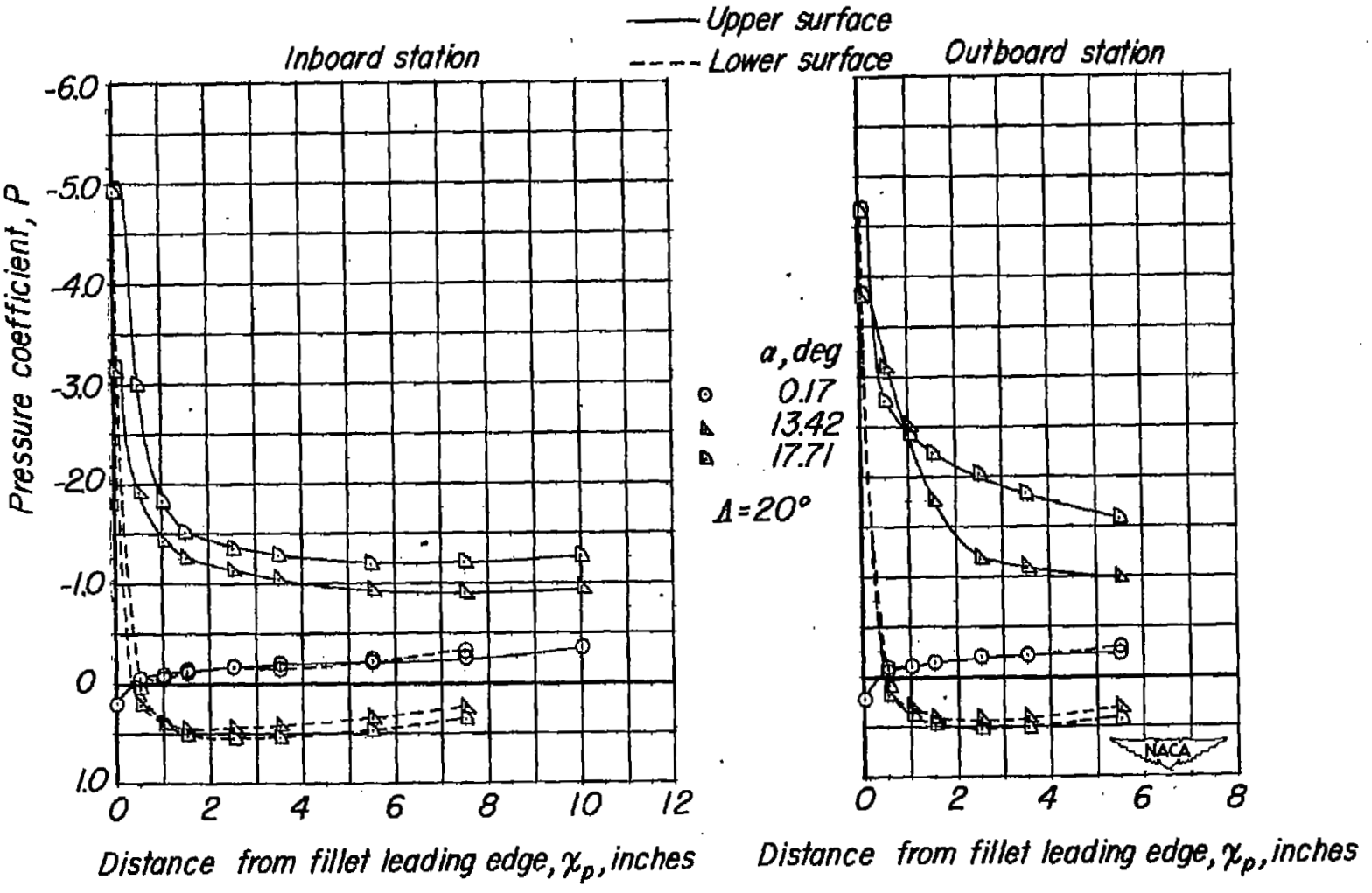

(b) Slats extended.

Figure 27.- Concluded.

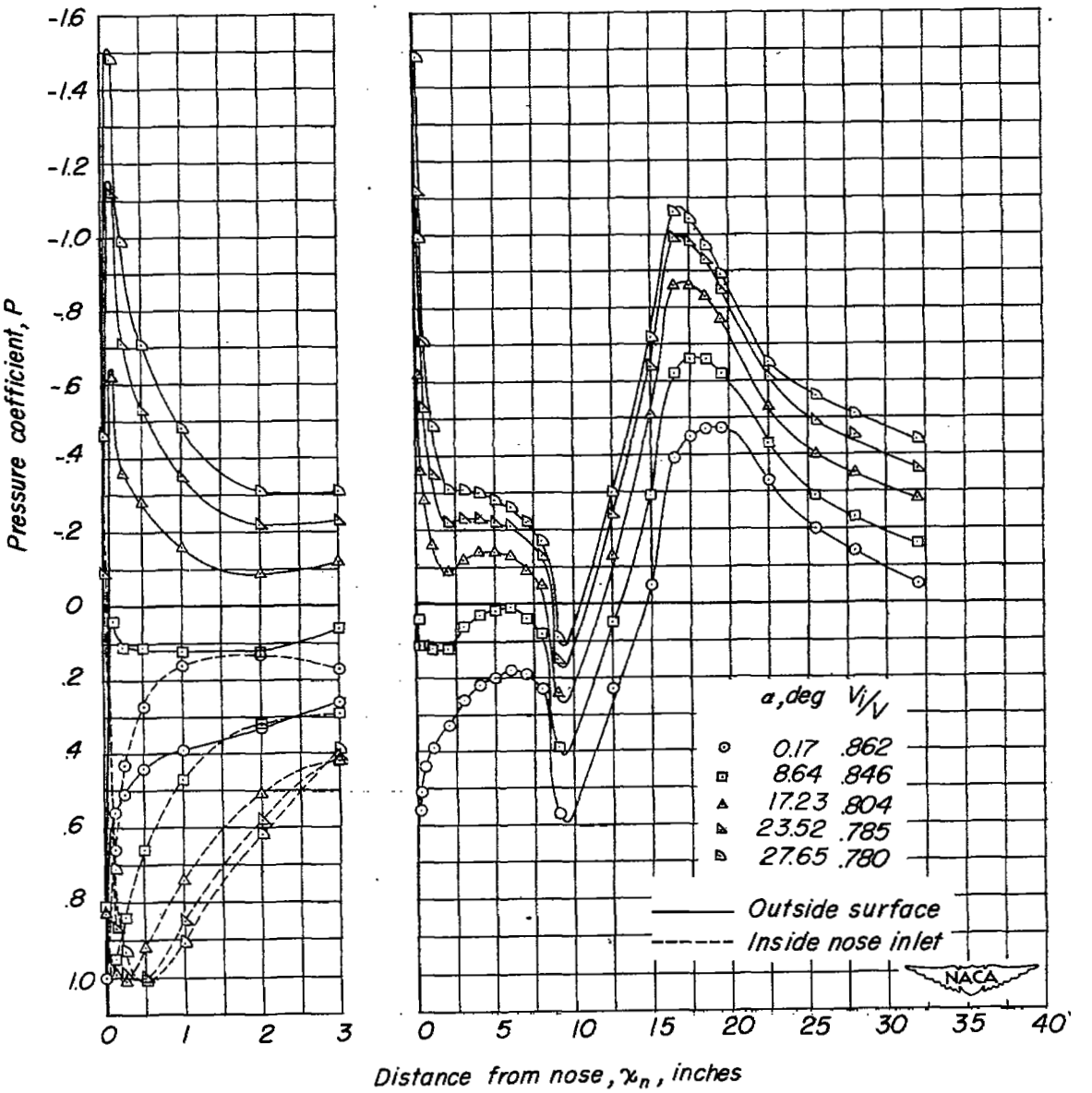

Figure 28.- Pressure distribution on fuselage upper surface. $\Lambda = 60°$; $\psi = 0°$. Jet exit full open.

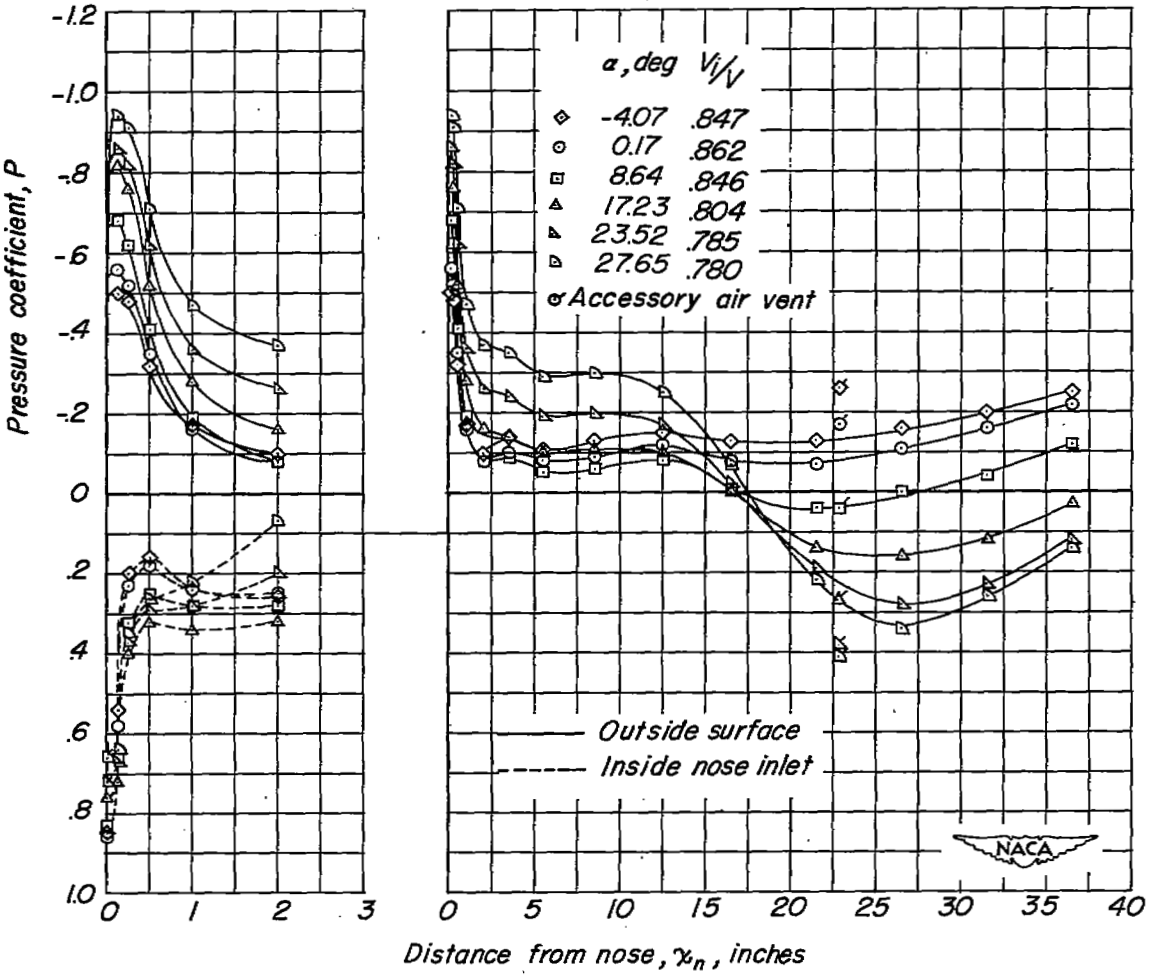

Figure 29.- Pressure distribution on fuselage side surface. $\Lambda = 60^\circ$; $\Psi = 0^\circ$. Jet exit full open.

[redacted]

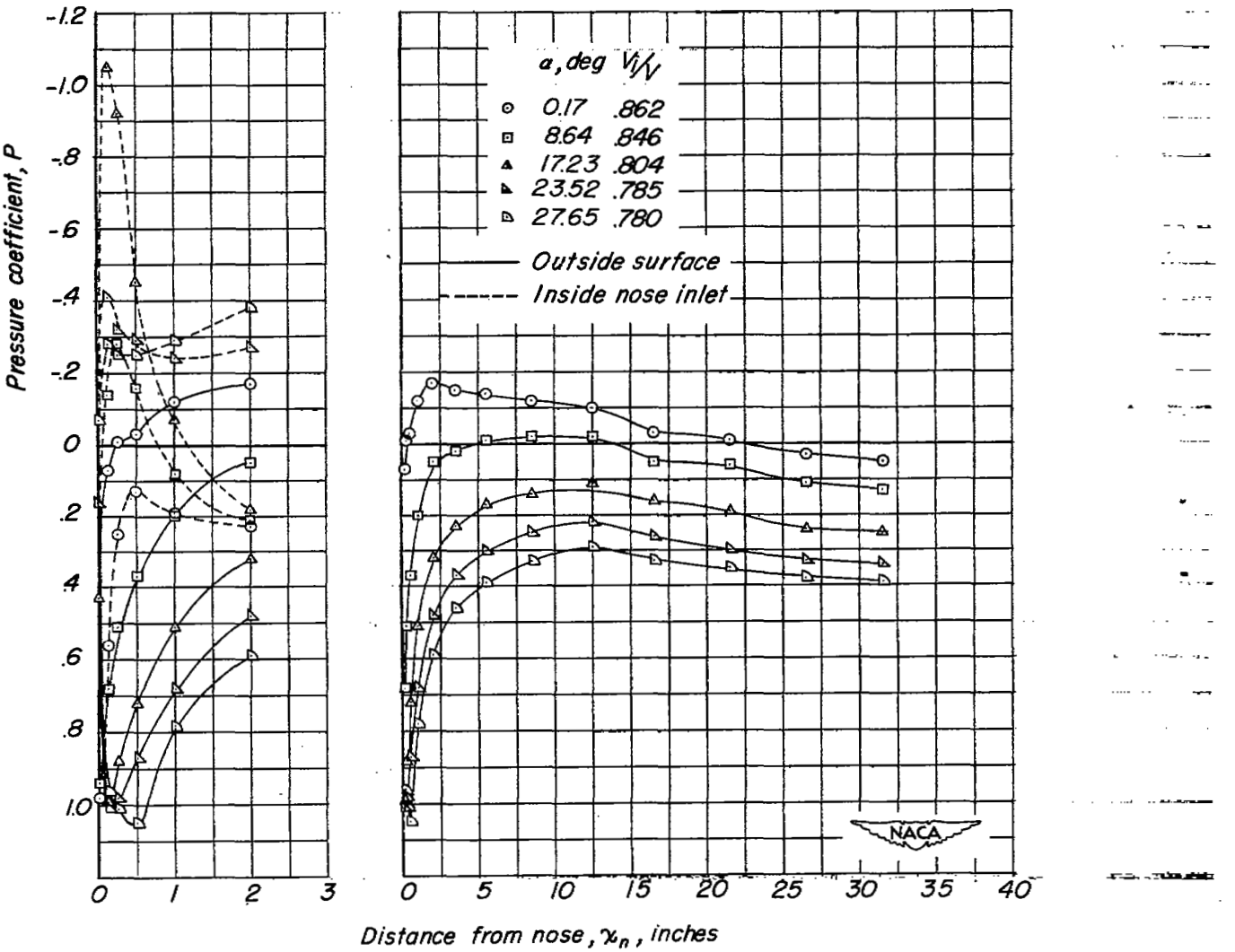

Figure 30.- Pressure distribution on fuselage lower surface. Λ = 60°; ψ = 0°. Jet exit full open.

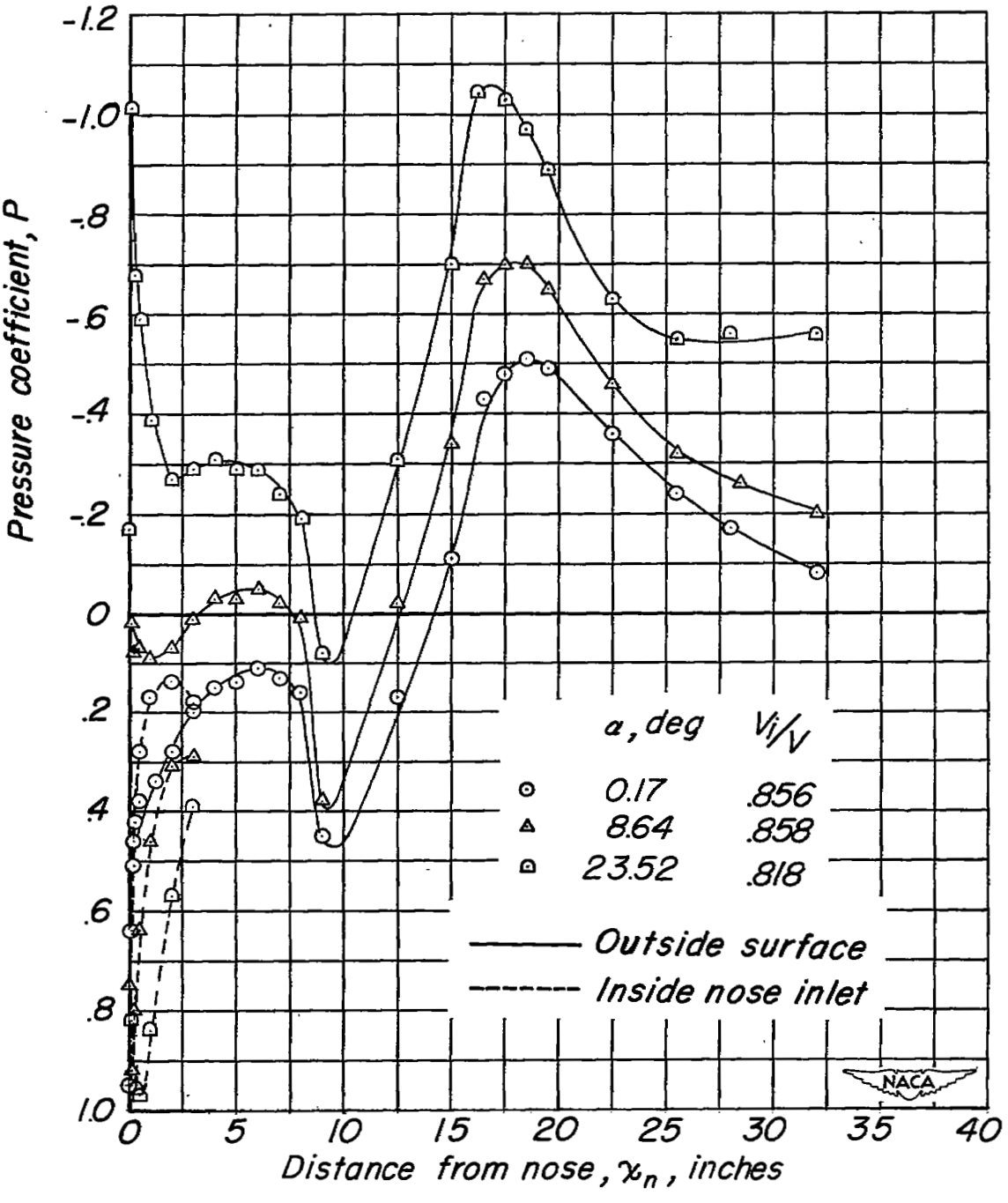

Figure 31.- Pressure distribution on fuselage upper surface. $\Lambda = 60^\circ$; $\psi = 5^\circ$. Jet exit full open.

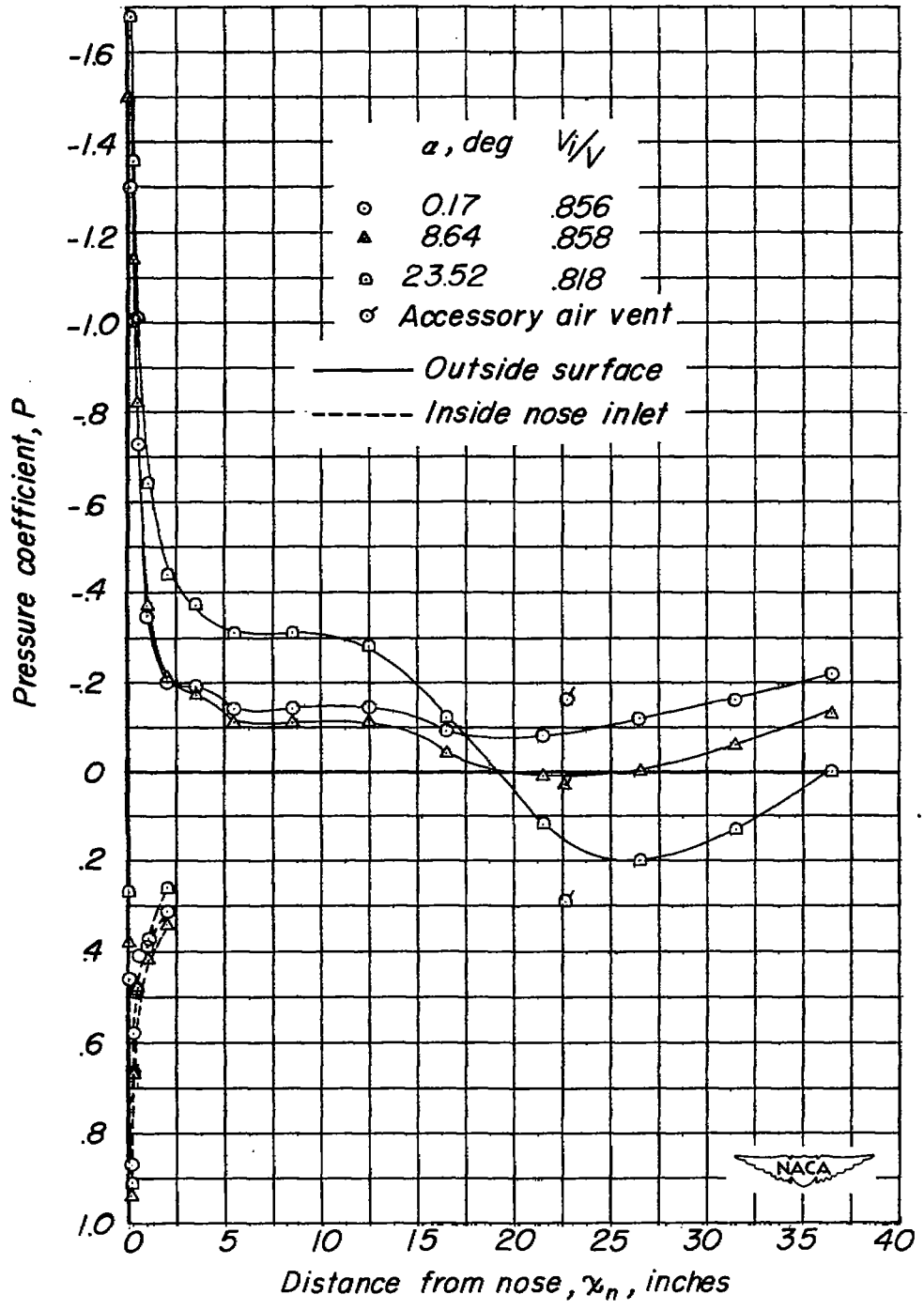

Figure 32.- Pressure distribution on fuselage side surface. $\Lambda = 60°$; $\psi = 5°$. Jet exit full open.

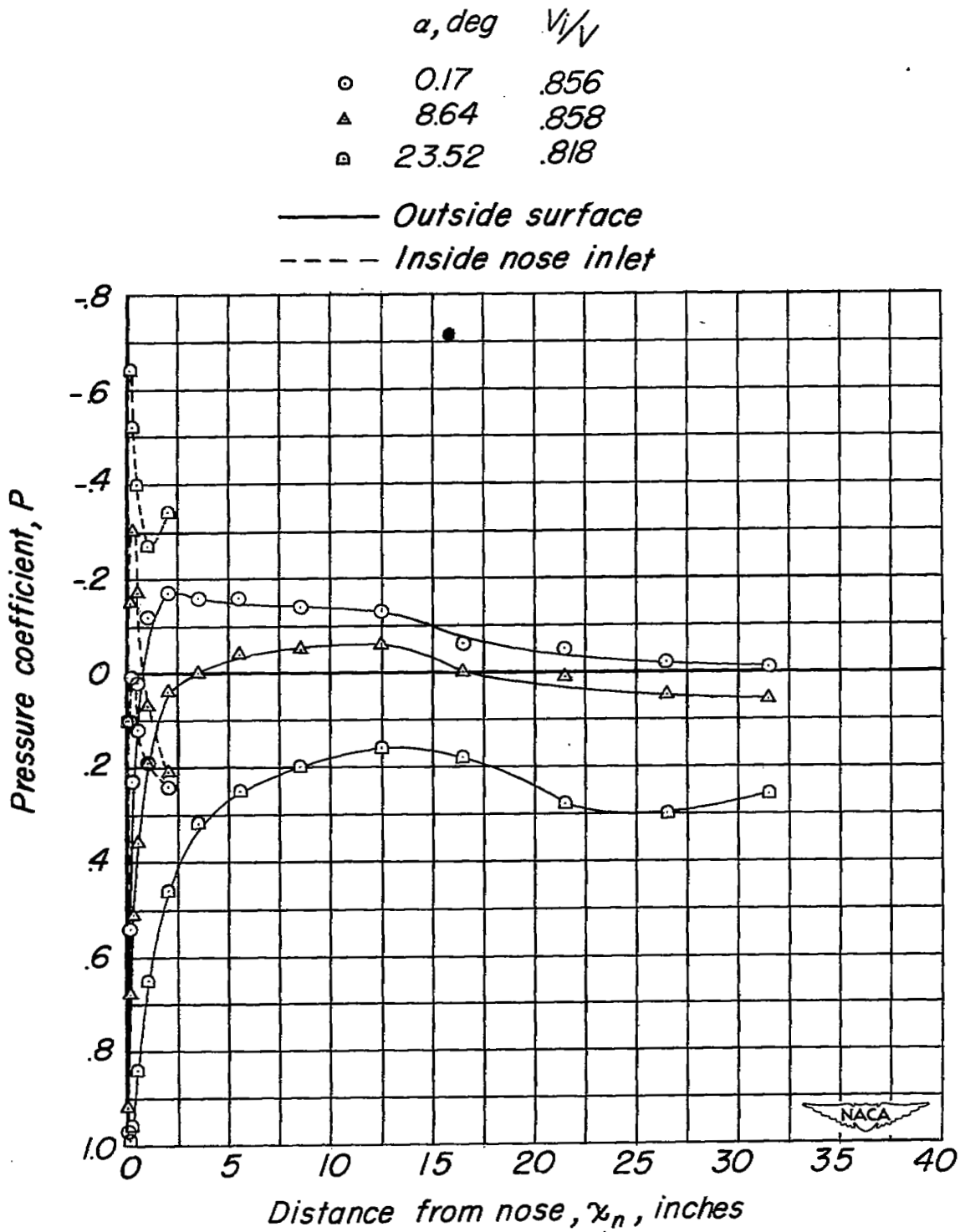

Figure 33.- Pressure distribution on fuselage lower surface. $\Lambda = 60°$; $\psi = 5°$. Jet exit full open.

[redacted]

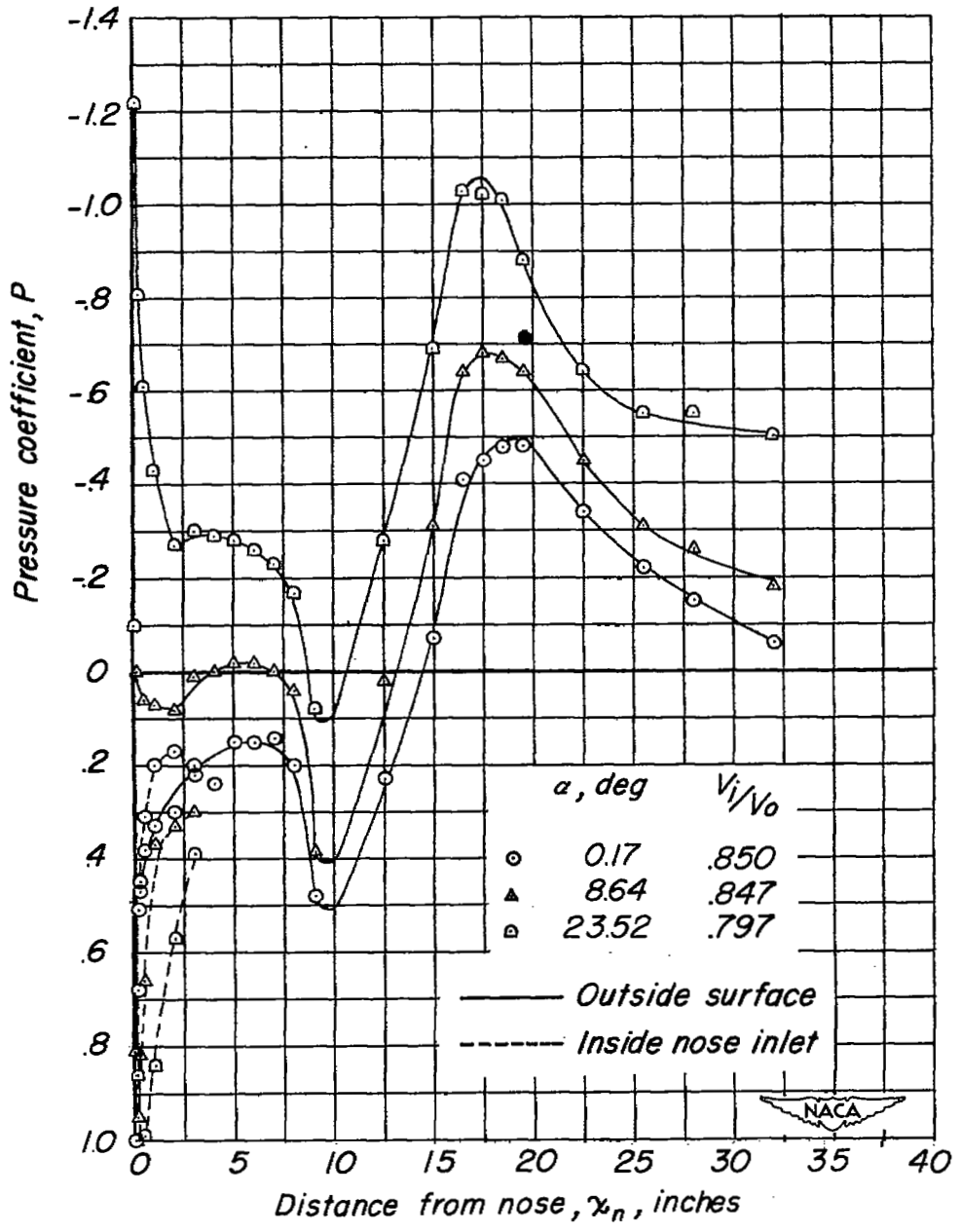

Figure 34.- Pressure distribution on fuselage upper surface. $\Lambda = 60^\circ$; $\psi = -5^\circ$. Jet exit full open.

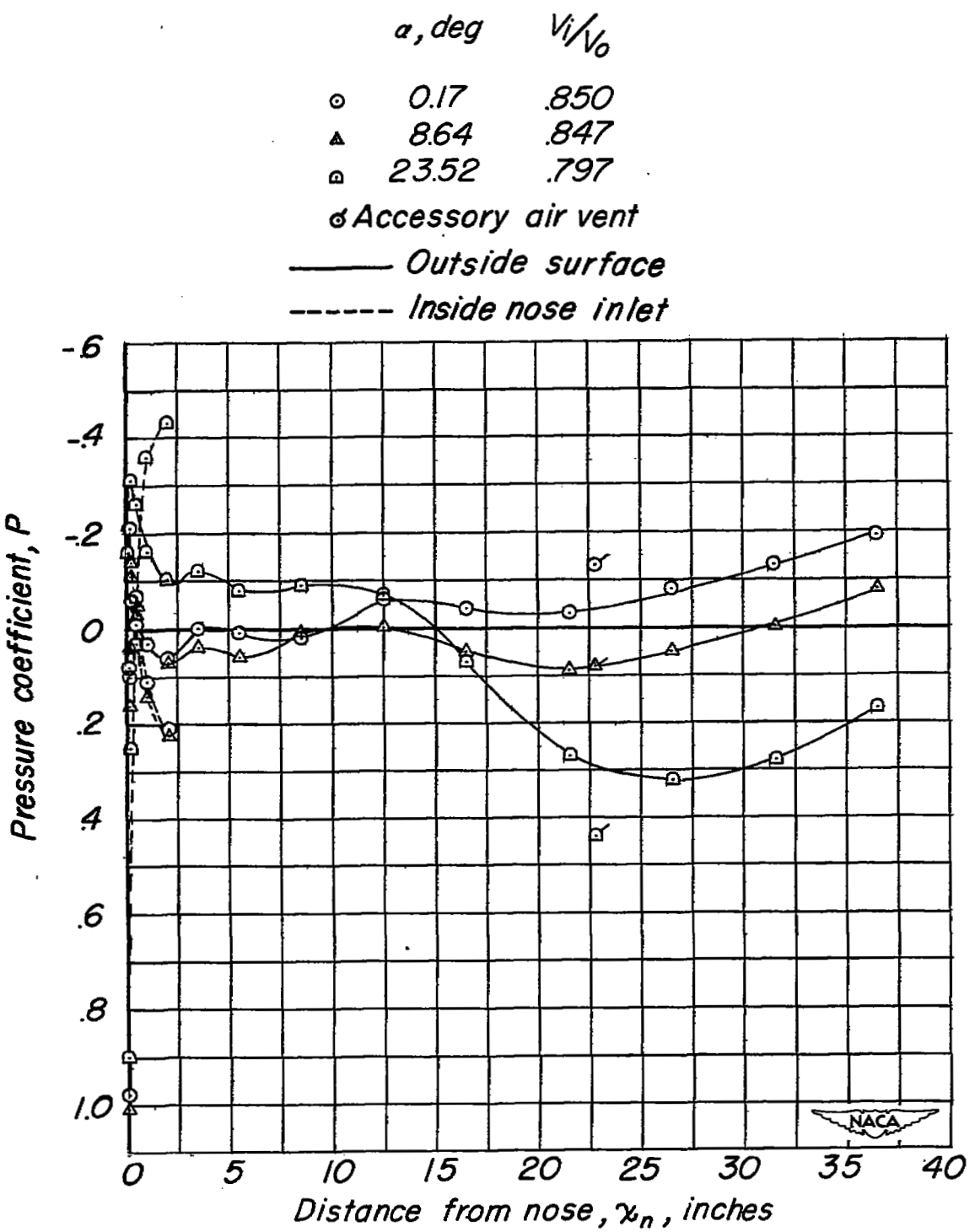

Figure 35.- Pressure distribution on fuselage side surface. $\Lambda = 60^\circ$; $\psi = -5^\circ$. Jet exit full open.

[redacted]

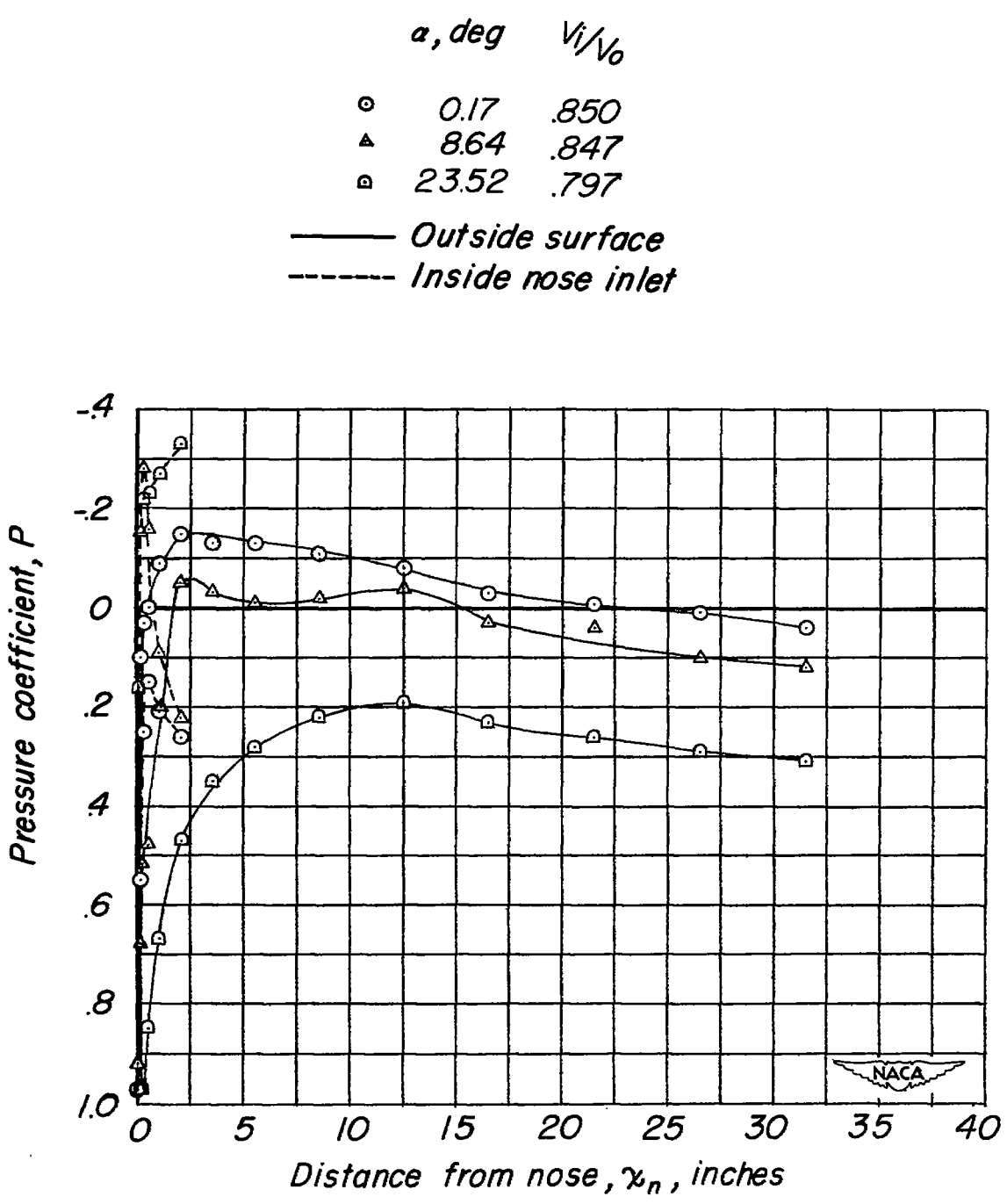

Figure 36.- Pressure distribution on fuselage lower surface. $\Lambda = 60°$; $\psi = -5°$. Jet exit full open.

[redacted]

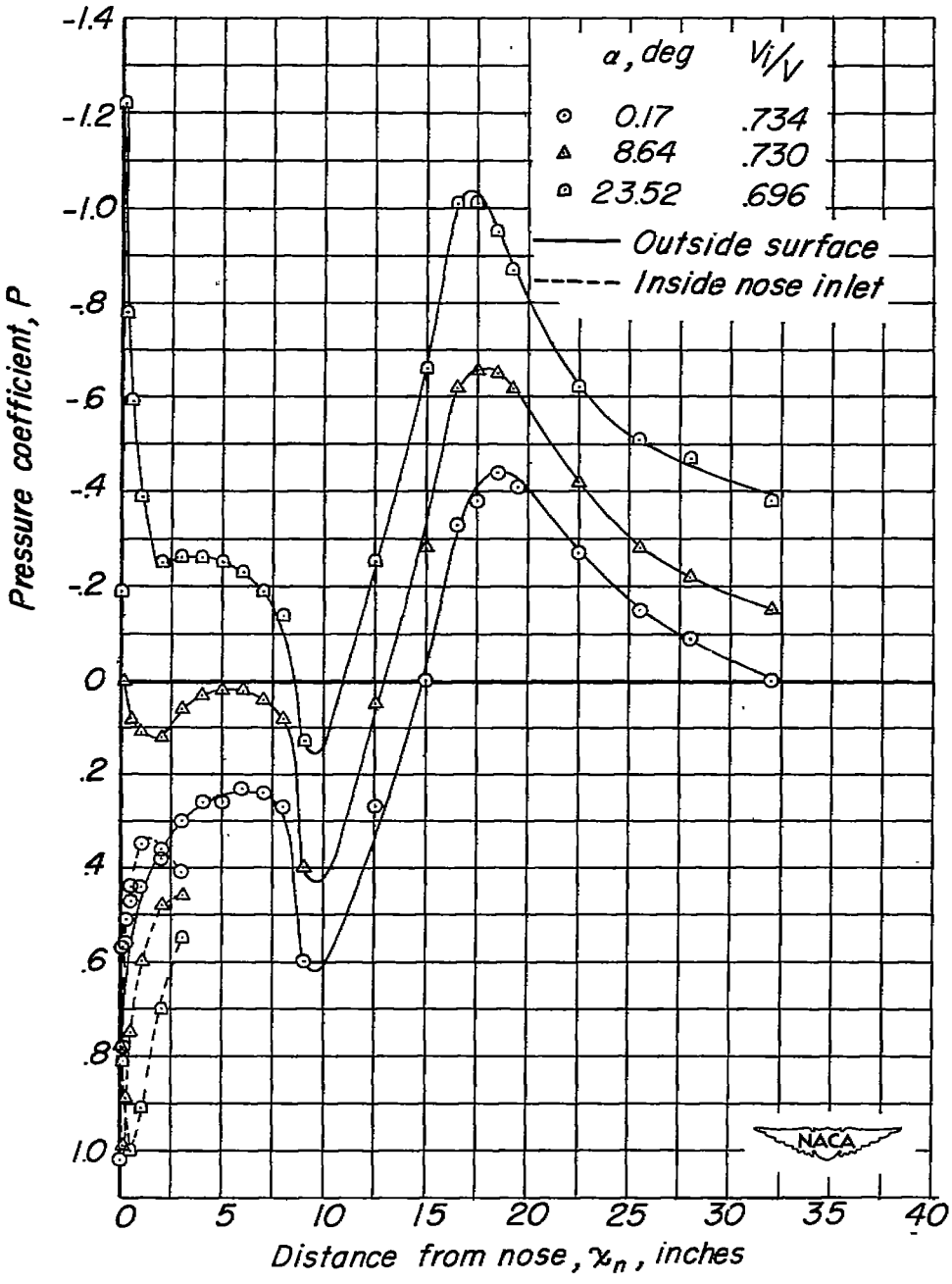

Figure 37.- Pressure distribution on fuselage upper surface. $\Lambda = 60^\circ$; $\psi = 0^\circ$. Jet exit one-third closed.

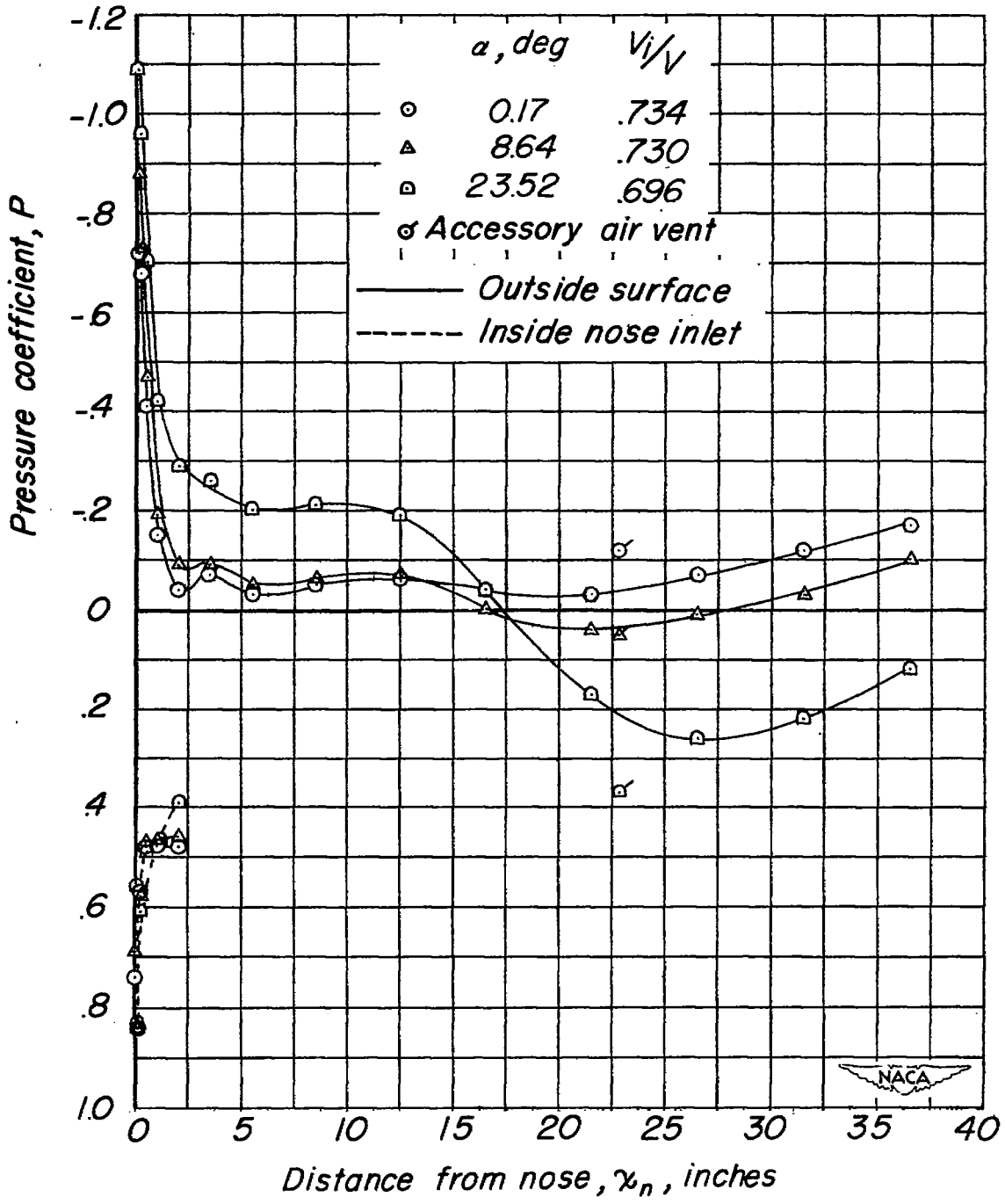

Figure 38.- Pressure distribution on fuselage side surface. $\Lambda = 60^\circ$; $\psi = 0^\circ$. Jet exit one-third closed.

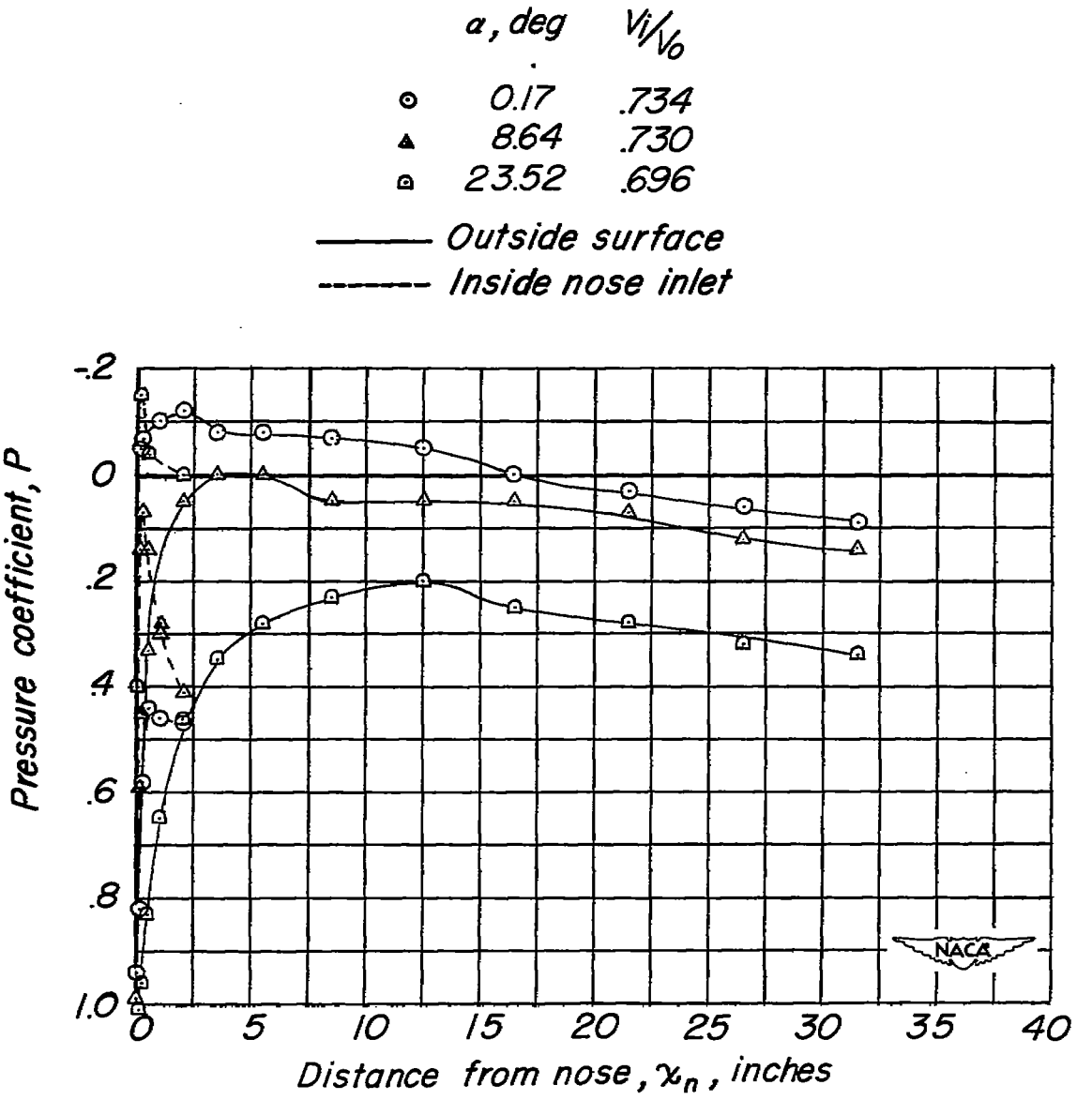

Figure 39.- Pressure distribution on fuselage lower surface. $\Lambda = 60^{\circ}$; $\psi = 0^{\circ}$. Jet exit one-third closed.

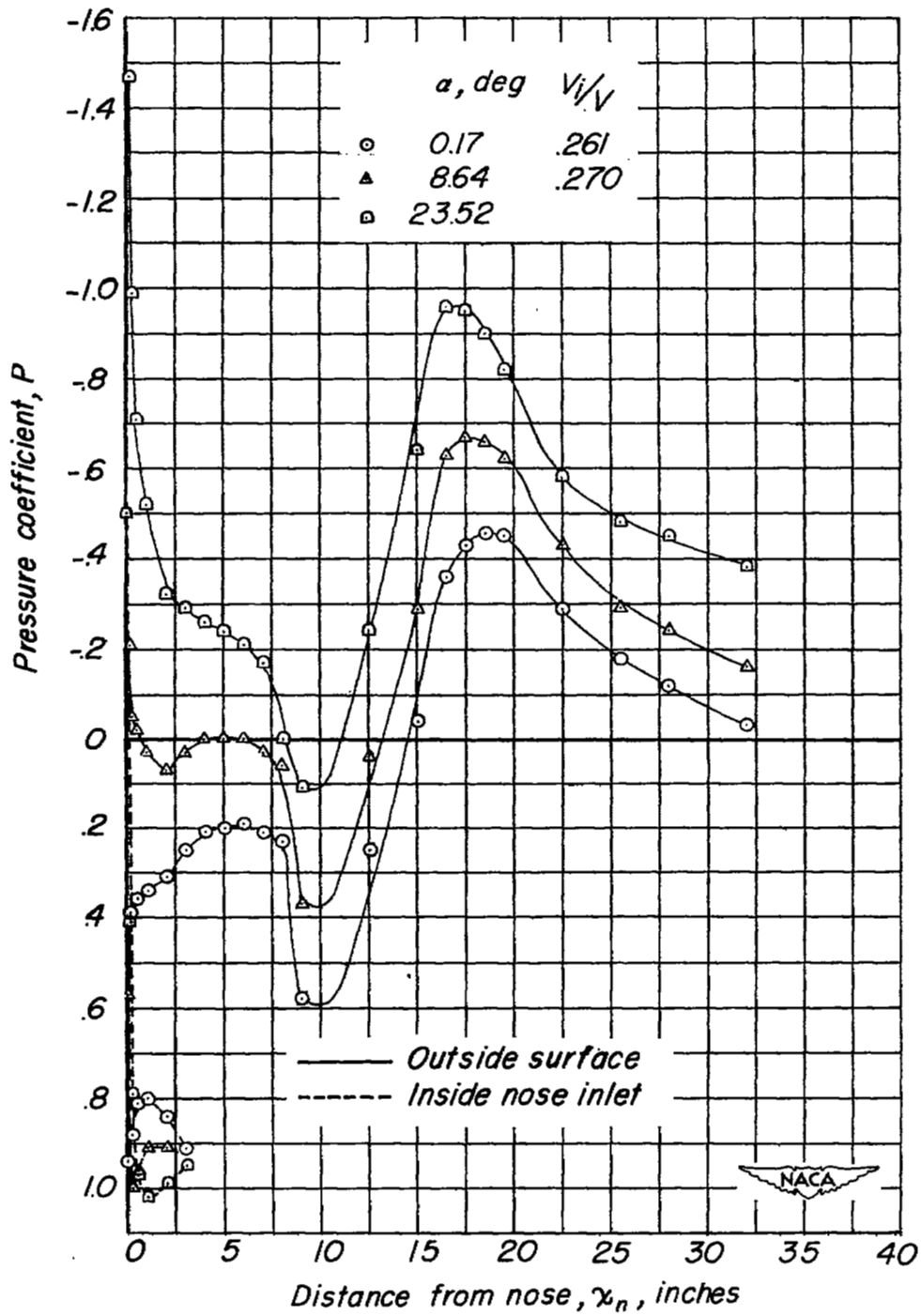

Figure 40.- Pressure distribution on fuselage upper surface. $\Lambda = 60^\circ$; $\psi = 0^\circ$. Jet exit two-thirds closed.

[redacted]

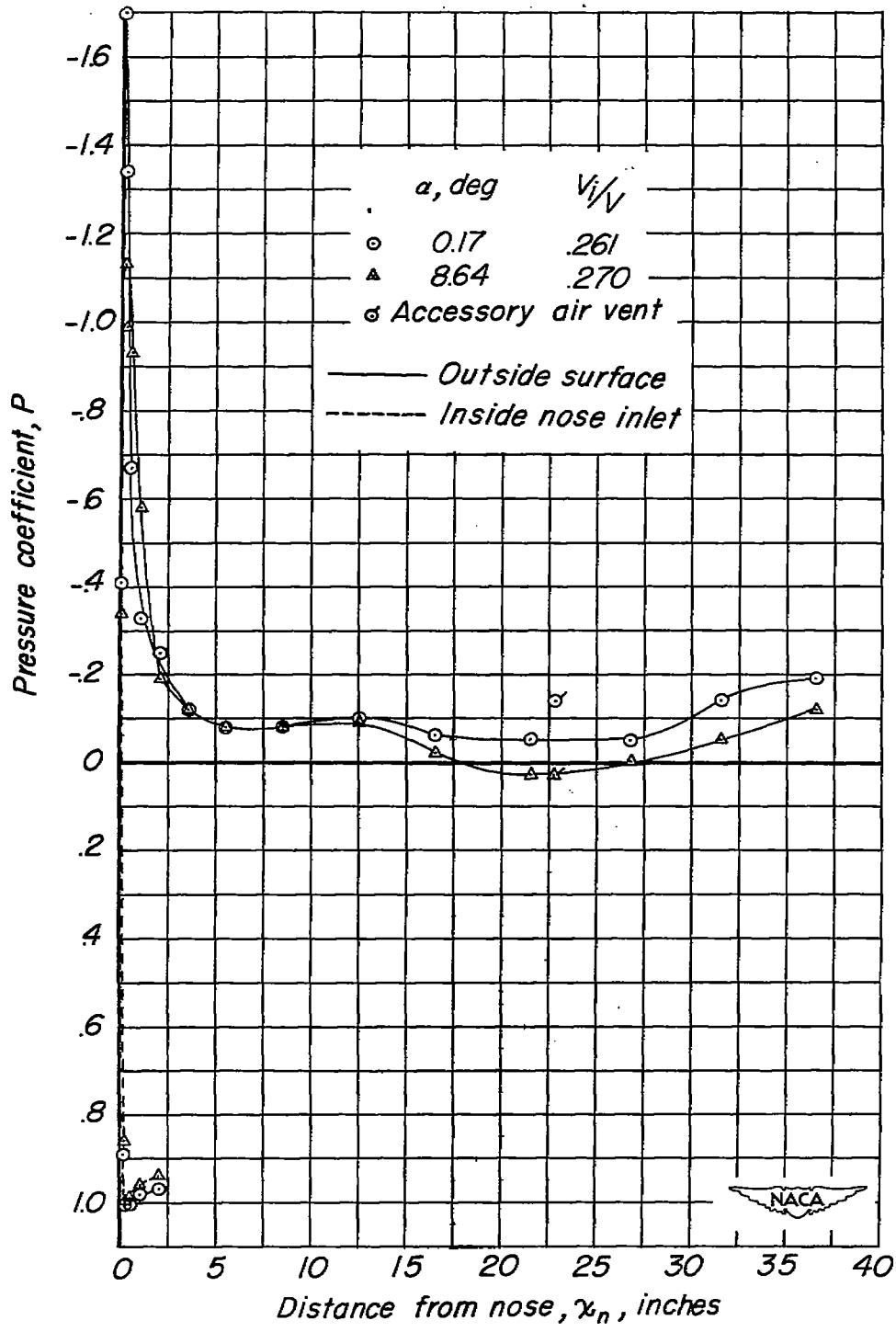

Figure 41.- Pressure distribution on fuselage side surface. $\Lambda = 60^\circ$; $\psi = 0^\circ$. Jet exit two-thirds closed.

[redacted]

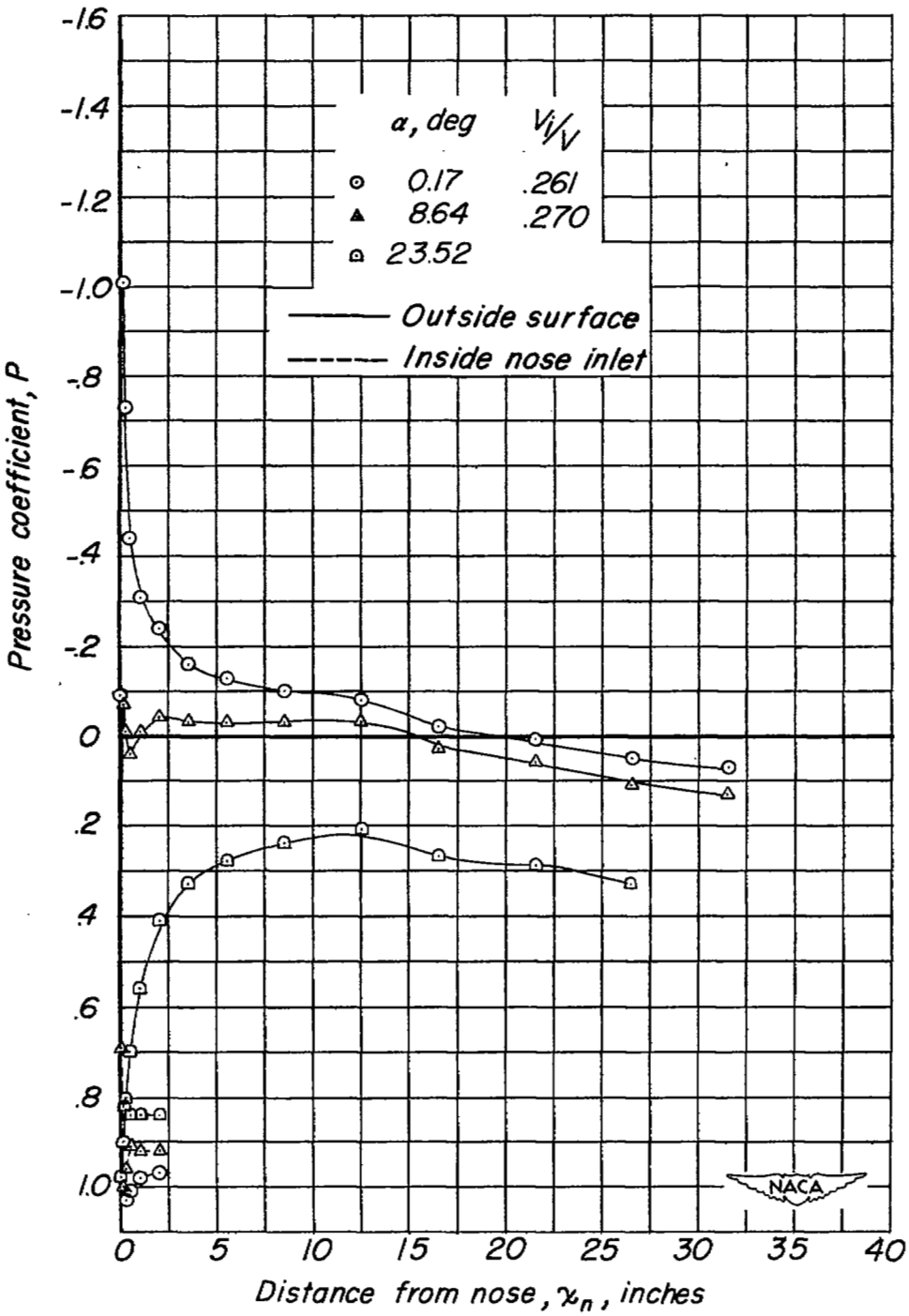

Figure 42.- Pressure distribution on fuselage lower surface. $\Lambda = 60^{\circ}$; $\Psi = 0^{\circ}$. Jet exit two-thirds closed.

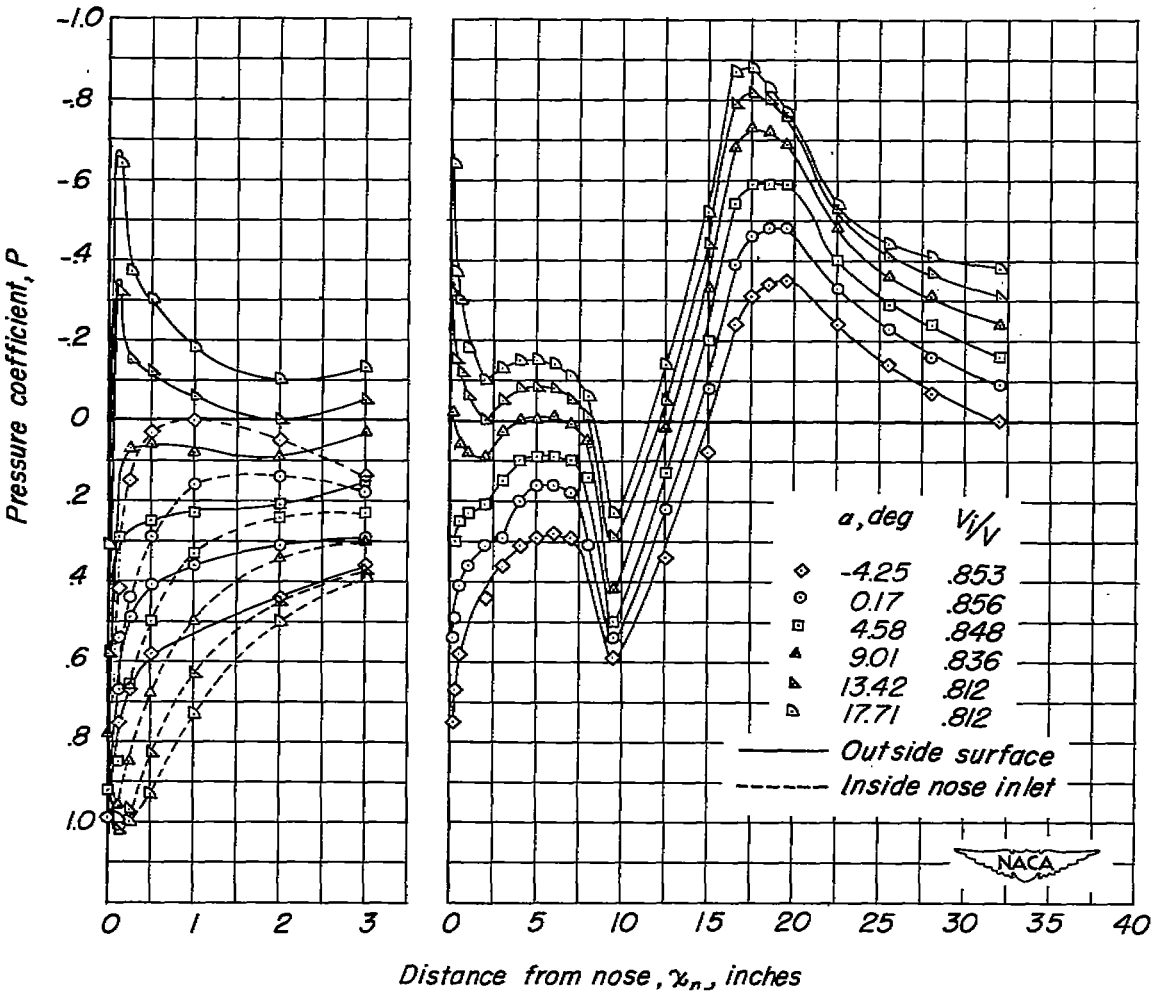

Figure 43.- Pressure distribution on fuselage upper surface. $\Lambda = 20^\circ$; $\psi = 0^\circ$. Jet exit full open.

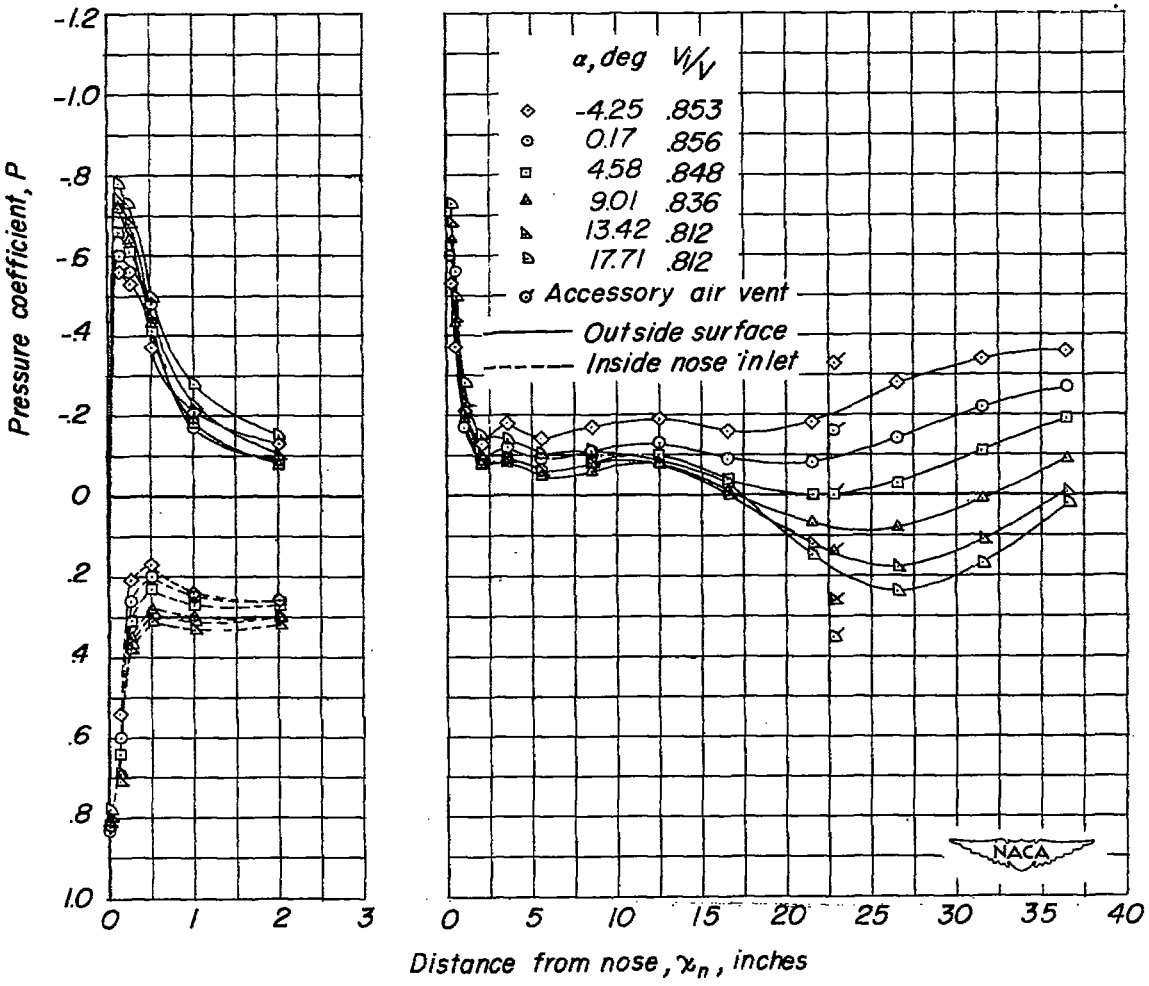

Figure 44.- Pressure distribution on fuselage side surface. $\Lambda = 20^{\circ}$; $\psi = 0^{\circ}$. Jet exit full open.

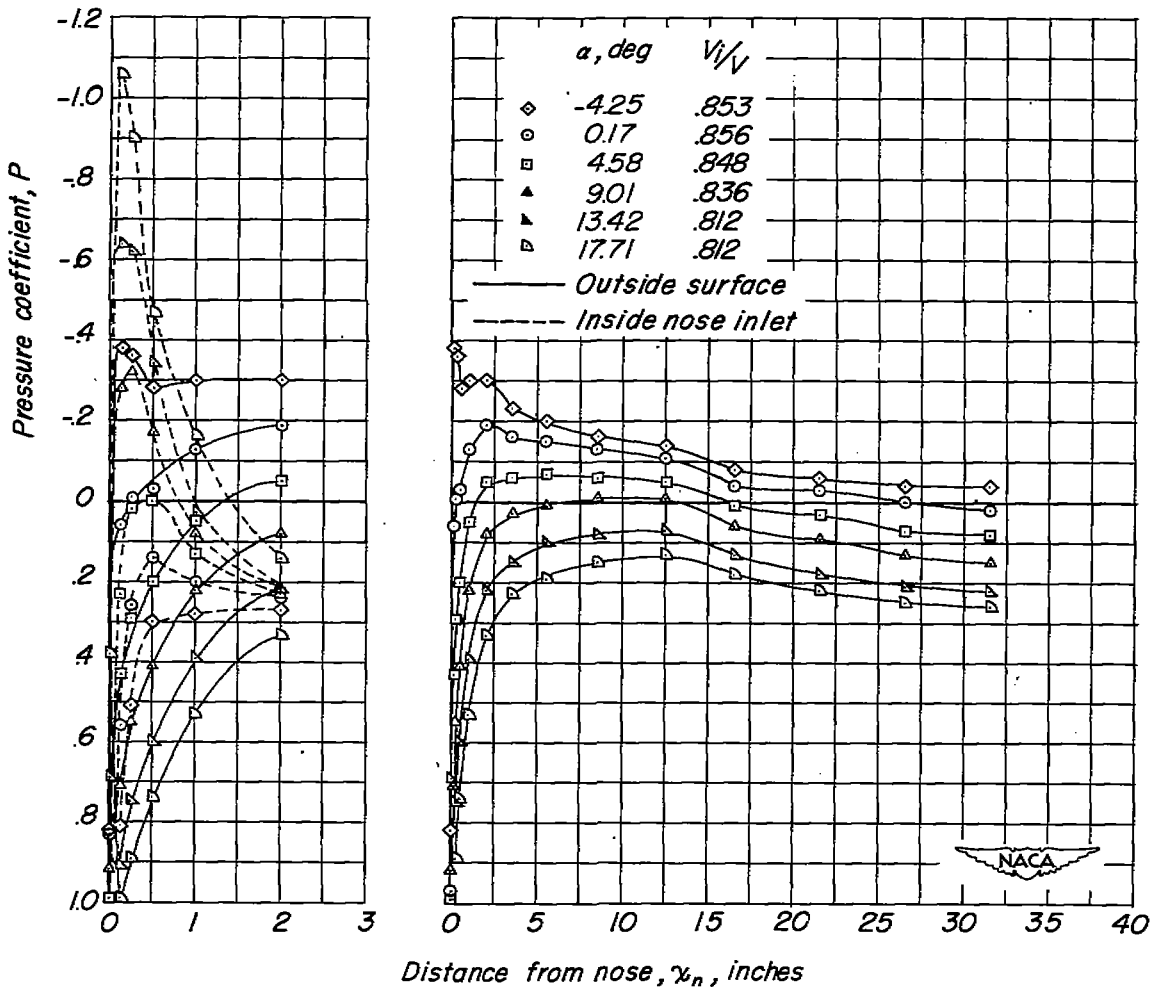

Figure 45.- Pressure distribution on fuselage lower surface. $\Lambda = 20^{\circ}$; $\psi = 0^{\circ}$. Jet exit full open.

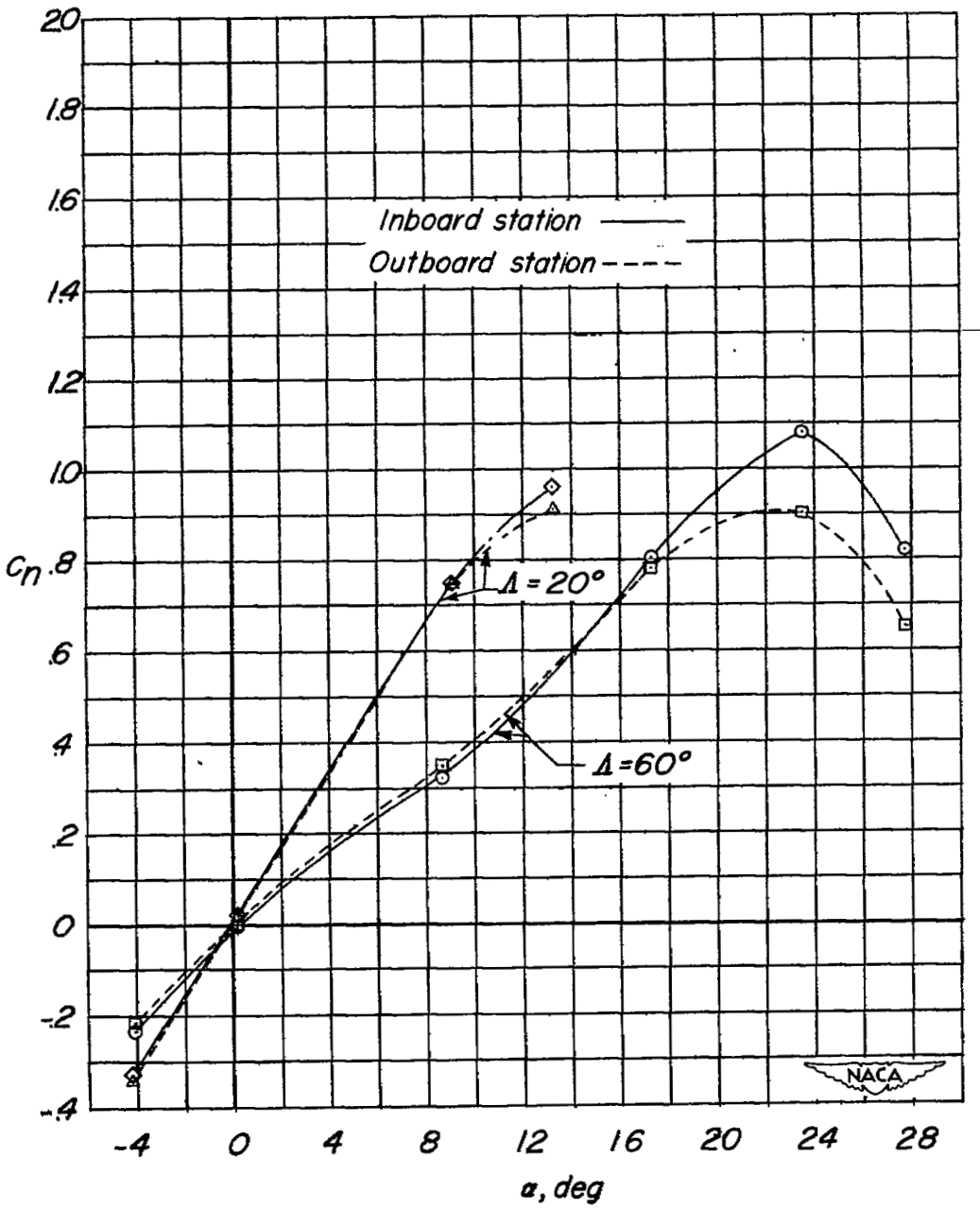

Figure 46.- Section characteristics of the wing with slats retracted. $\psi = 0^\circ$.

[redacted]

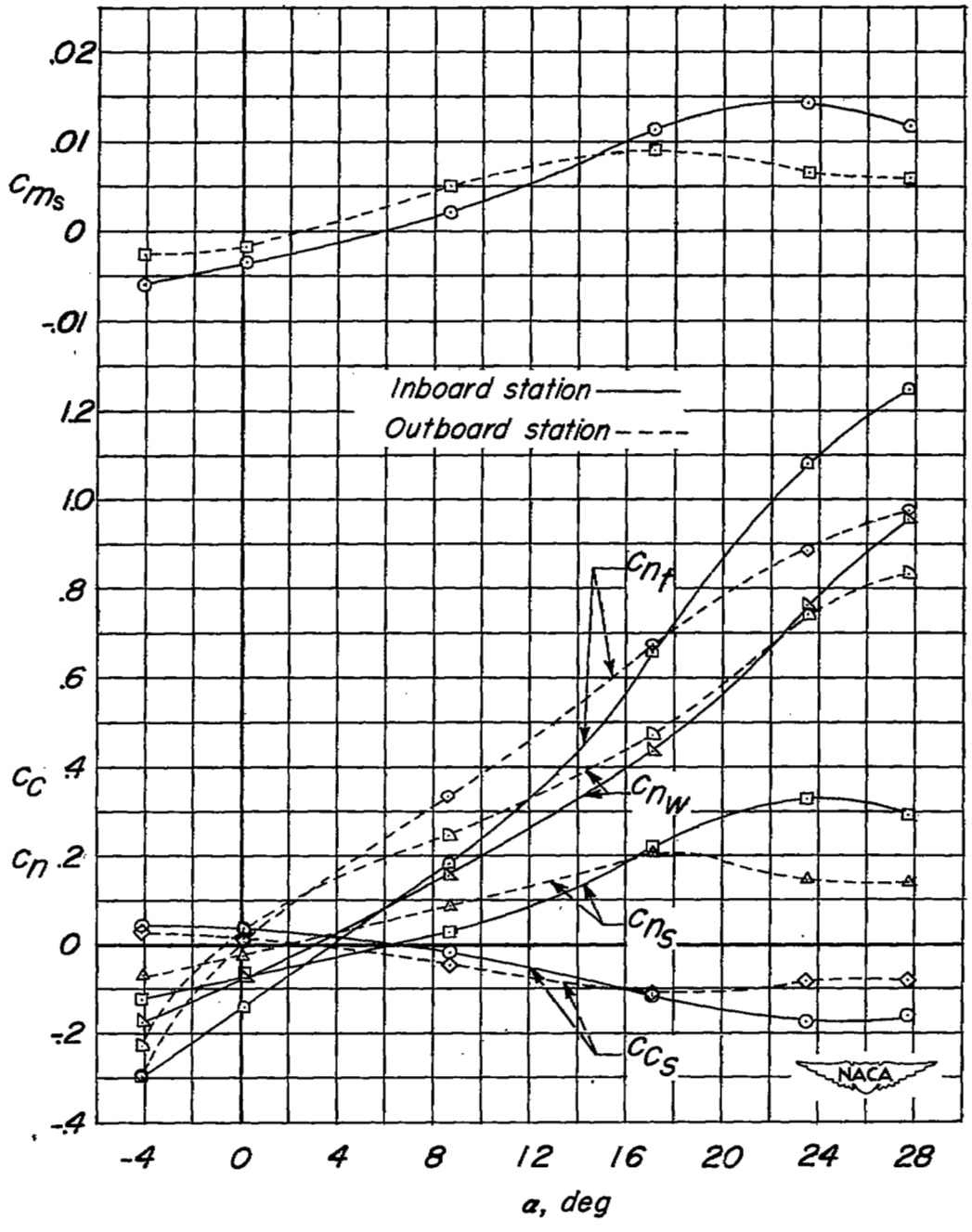

Figure 47.- Section characteristics of the wing with slats extended. $\Lambda = 60^\circ$; $\psi = 0^\circ$.

[redacted]

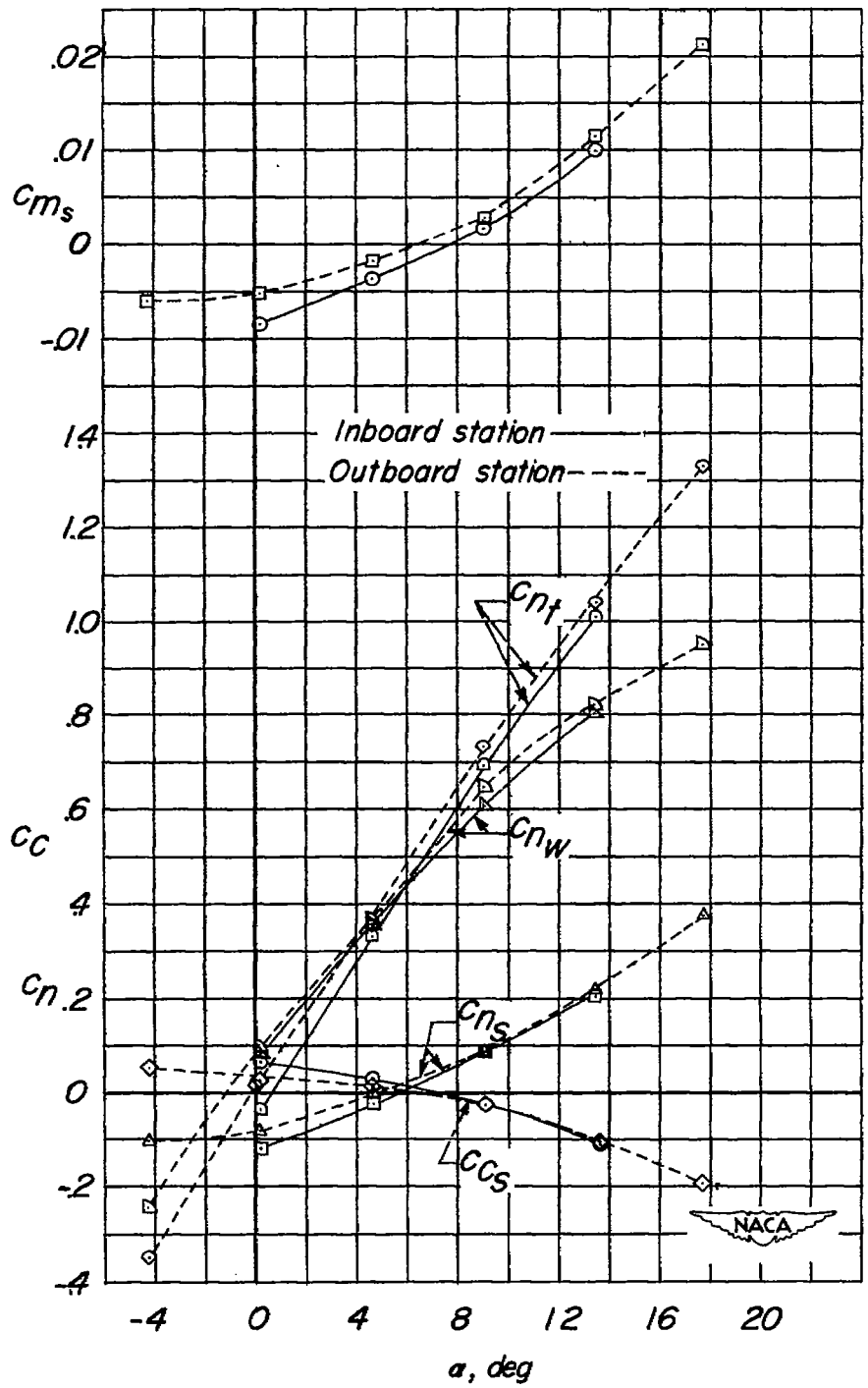

Figure 48.- Section characteristics of the wing with slats extended. $\Lambda = 20^\circ$; $\psi = 0^\circ$.

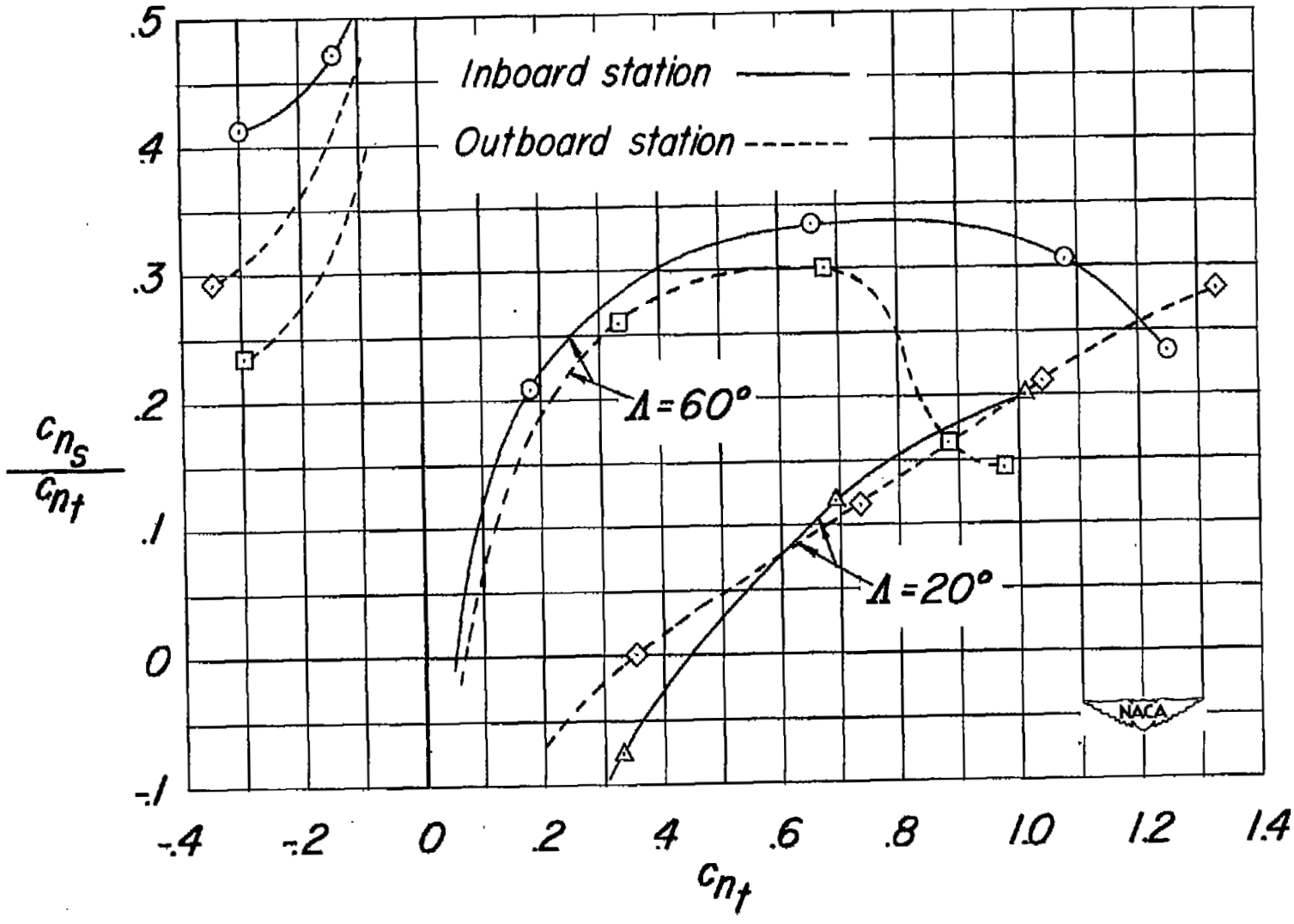

Figure 49.- Effect of sweep angle on division of load between slat and wing.

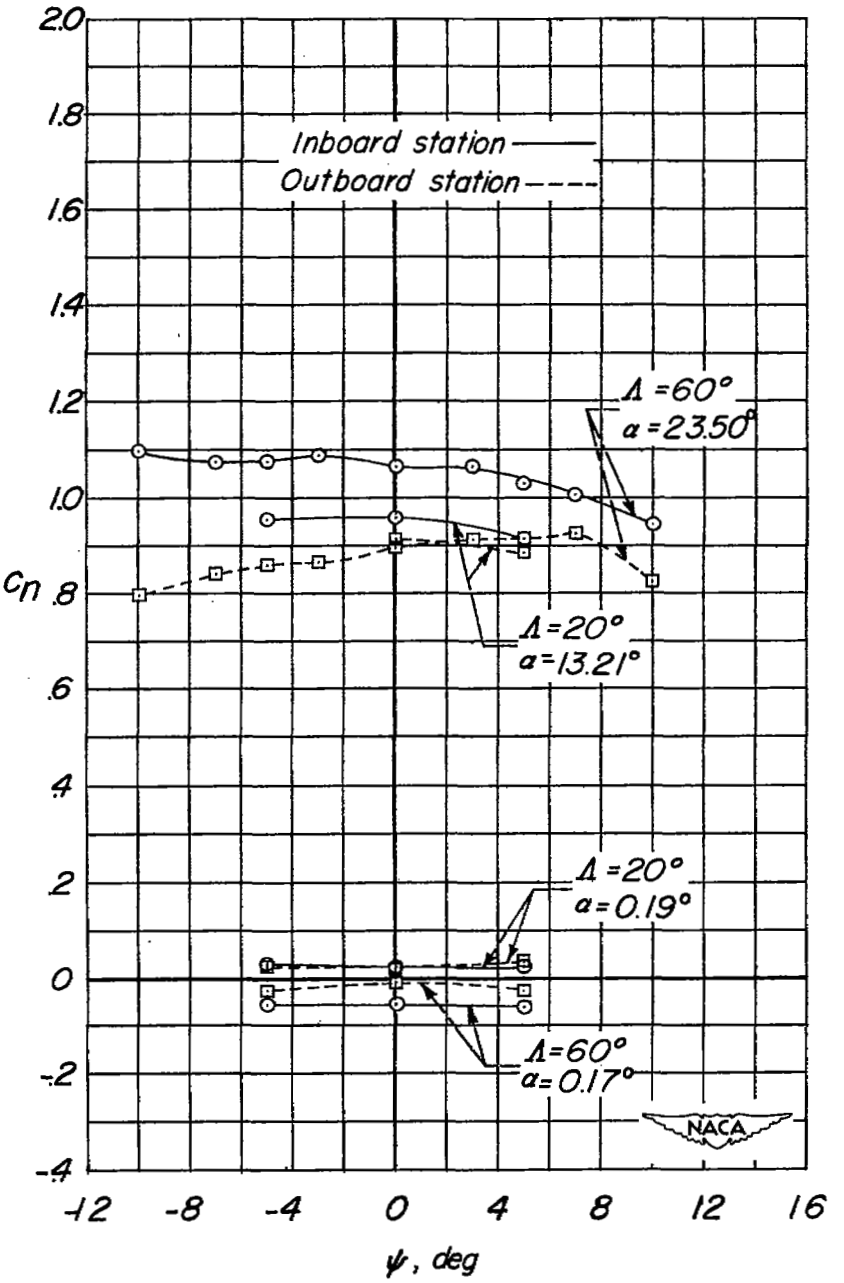

Figure 50.- Section characteristics of the wing with slats retracted.

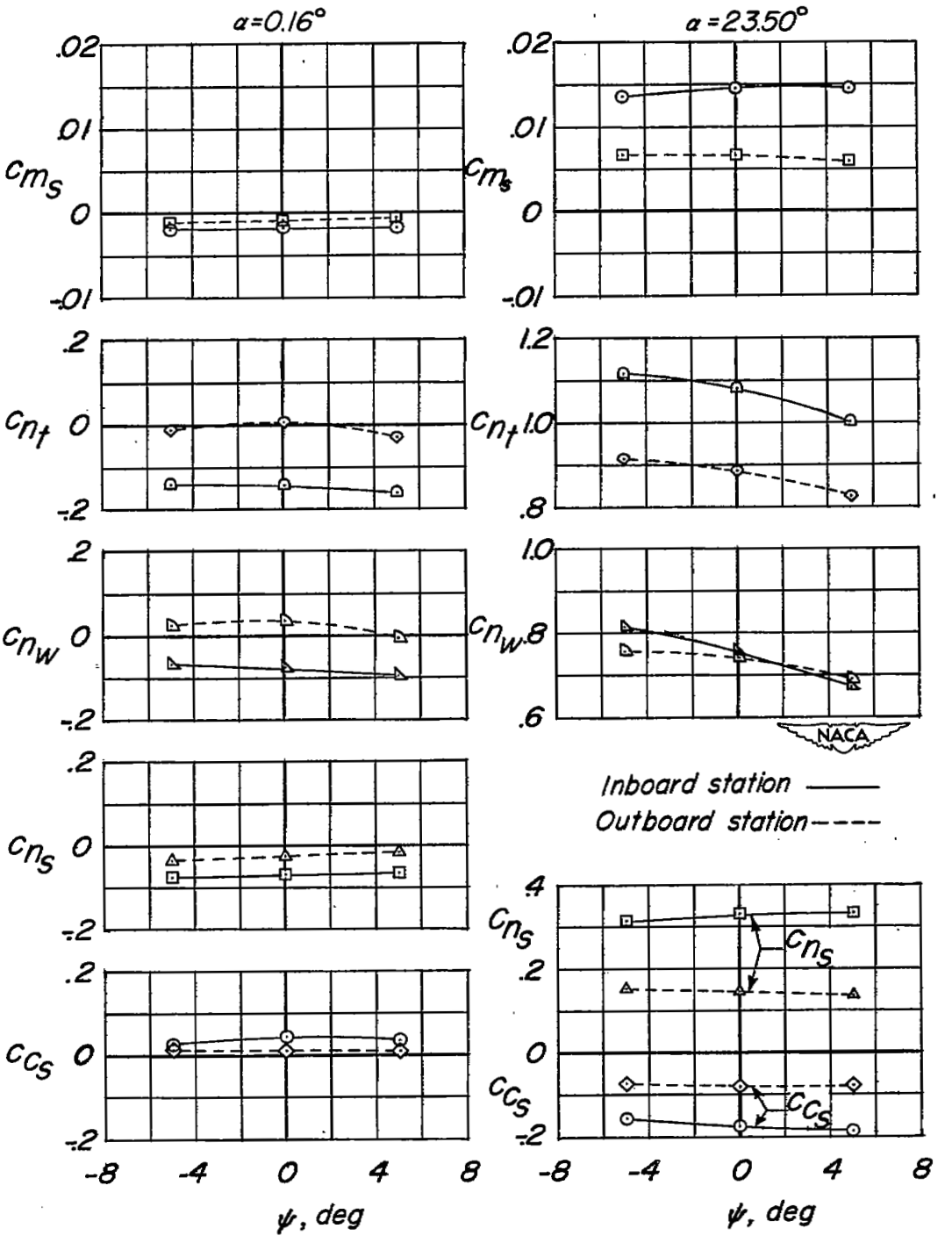

Figure 51.- Section characteristics of the wing with slats extended. $\Lambda = 60°$.

[redacted]

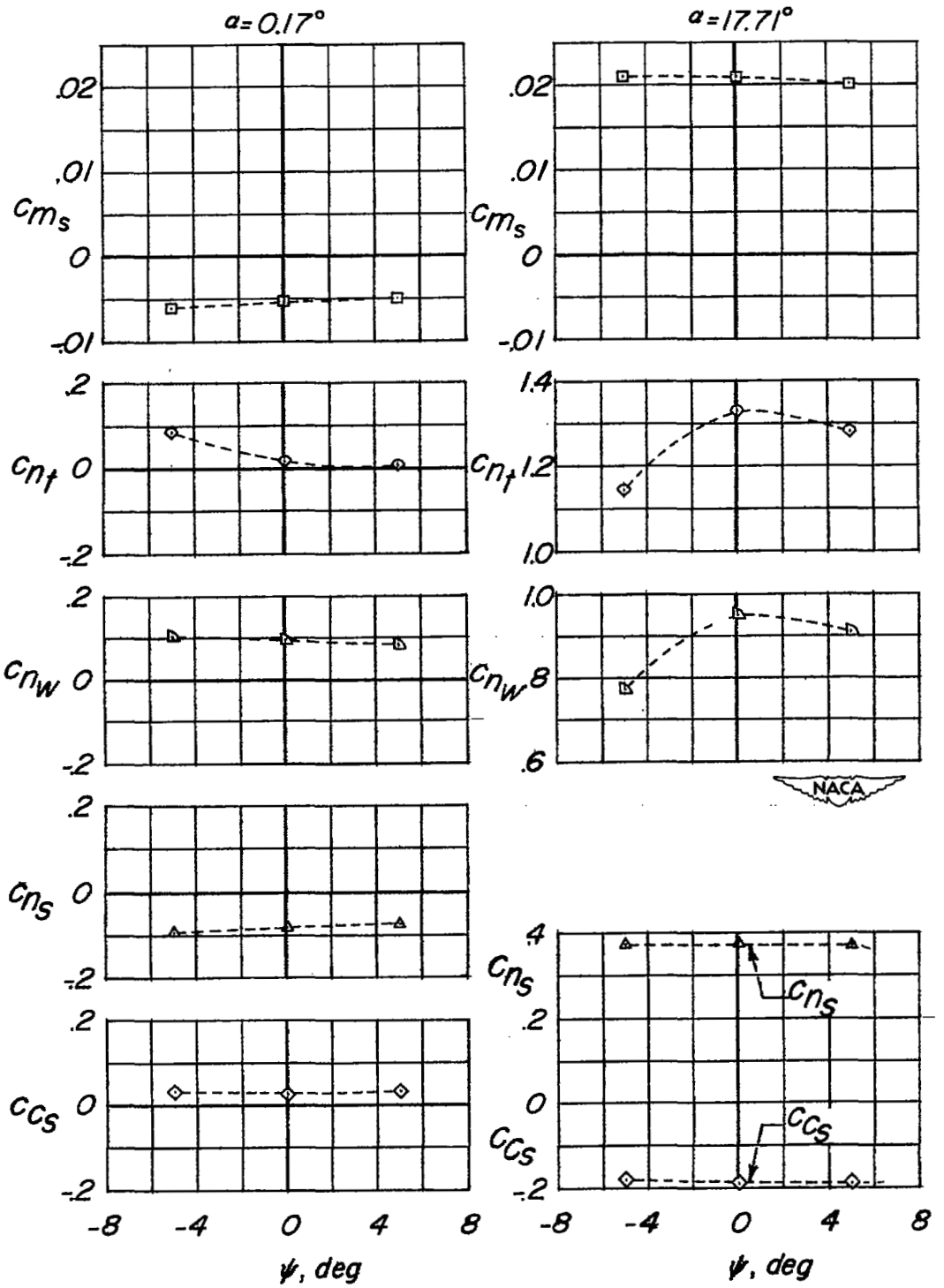

Figure 52.- Section characteristics of the outboard station of the wing with slats extended. $\Lambda = 20^{\circ}$.

[redacted]